ADVANCED DEFINITION STUDY FOR THE

DETERMINATION OF ATMOSPHERIC OZONE

USING THE SATELLITE ECLIPSE TECHNIQUE

FINAL REPORT

By R. Emmons, R. J. Preski, F. H. Kierstead, Jr.,
F. C. Doll, D. T. Wight, and D. C. Romick
Goodyear Aerospace Corporation

26 November 1973

Prepared under Contract No. NAS 1-12,685
by Goodyear Aerospace Corporation
Akron, Ohio 44315

for

NATIONAL AERONAUTICS AND SPACE ADMINISTRATION
LANGLEY RESEARCH CENTER, HAMPTON, VIRGINIA 23365

FOREWORD

This is the final report, prepared by Goodyear Aerospace
Corporation (GAC), covering the work performed and results
obtained under the "Advanced Definition Study for the
Determination of Atmospheric Ozone using the Satellite
Eclipse Technique."

The technical objectives and contract requirements are based
on the Scope of Work and other requirements set forth in the
contract schedule of NASA Contract NAS 1-12,685 issued by the
NASA Langley Research Center, Hampton, Virginia, and dated
August, 1973.

Work on this study was administered under the Environmental
and Space Sciences Division of the Langley Research Center,
Atmospherics Branch, Robert Tolson, Branch Chief; Aeronomy
Section headed by Gerald M. Keating, Section Head and Program
Manager. Robert B. Lee, III of the Aeronomy Section was
Technical Monitor and Administrator of the program for NASA LRC.

ABSTRACT

A study was made to evaluate the potential for remote ground-based measurement of upper atmospheric ozone by determining the absorption ratio of selected narrow bands of sunlight as reflected by satellites while passing into eclipse, using the NASA Mobile Satellite Photometric Observatory (MOSPO). Equipment modifications to provide optimum performance were analyzed and recommendations were made for improvements to the system to accomplish this. These included new sensor tubes, pulse counting detection circuitry, filters, beam-splitters and associated optical revision, along with an automatic tracking capability plus corresponding operational techniques which should extend the over-all measurement capability to include use of satellites down to 5th magnitude.

Utilization would be further extended through practical use of small 15 to 30 arc second field stops, versatile filter combinations and improved digital recording methods. Examination of available satellites, orbit distribution, tracking availability, weather, geographical and other factors indicate that, by making full use of the MOSPO mobility and these improvements, between 500 and 1000 vertical ozone profile measurements could be made per year over a wide geographical range with a 3-man field crew at a much lower cost than obtainable by any other known currently available method.

TABLE OF CONTENTS

Appendix

ILLUSTRATIONS

Figure

TABLES

LIST OF SYMBOLS

$\overset{\circ}{A}$	angstrom
λ	wave length
h	Planck's constant
γ	particle velocity
I	incident plane
B	observer point
S'u	sunset point
S'o	subsolar point
K	reflected ray
M	magnitude, star
s	gain factor
d	deflection
k	extinction coefficient
x	air mass
ζ	zero point term
O	atomic oxygen
O_2	oxygen
O_3	ozone
h	height of ozone concentration
UV	ultraviolet
V	satellite velocity
θ	angle between orbital plane and plane of sun-earth line and radius vector
X	unit vector
Y	unit vector
Z	unit vector
β	longitude of the sun
ϵ	obliquity of the ecliptic
Ω	angle of rotation about polar axis
P	component of sun vector directed toward node
S	component of sun in the equatorial plane
Q	component of sun vector in orbital plane
U	component of sun vector perpendicular to orbital plane
i	inclination of satellite orbit
δ'	spherical coordinate of the anti-sun point

δ	declination of sun
α'	angle between orbit and earth equator
Υ	aries
A	angle between the sun-earth line and the radius vector
V'	satellites true anomaly at shadow entry
R	radius of the earth
r	satellite radius vector
ϕ	latitude of shadow entry
ϕ_s	latitude of tangent point
E	elevation above horizon, satellite
W	radiant power received by the photocathode

ADVANCED DEFINITION STUDY FOR THE DETERMINATION
OF ATMOSPHERIC OZONE USING THE SATELLITE ECLIPSE TECHNIQUE

By R. Emmons, R. J. Preski, F. H. Kierstead, Jr.,
F. C. Doll, D. T. Wight, and D. C. Romick
Goodyear Aerospace Corporation

SUMMARY

This study has examined the nature of the ozone measurement problem
and the prospects for utilization of the satellite eclipse method
for effective measurement. The experimental measurements made with
the NASA MObile Satellite Photometric Observatory (MOSPO) over the
past few years constitutes a firm experience foundation on which to
base this definition study of the potential effectiveness that
should be obtainable.

The purpose of this study is to

    (1) Evaluate the potential of this method in relation
        to other practical or possible methods

    (2) Define the equipment requirements, principles,
        methods, and techniques that will provide the
        most effective measurement capability, and

    (3) Determine the optimum choices of alternate consid-
        erations that will give the best capability
        relative to cost.

Accordingly, this study undertook to first determine for each function
involved the alternate approaches which appeared reasonable, make a
comparative analysis to determine the best, and thus define the
optimum system, and its capability. This included all aspects of
the proposed ozone measurements: equipment requirements, mission
considerations, measurement techniques, data processing and analysis
methods.

The study of equipment requirements involved mainly the determination
of recommended modification and improvement to the existing MOSPO
equipment for most effective ozone measurement performance. The
resulting recommendations included use of smaller field stops by
adding automatic tracking, incorporation of added optical filtering,
a more sensitive photomultiplier, and pulse counting circuitry to
further improve sensitivity. These are expected to give a capability
for substantially improved measurement data from satellites ranging
down to about fifth magnitude. Additionally, digital IBM compatible
data recording with real-time monitoring is recommended so that the
data processing can also be fully automated - thus speeding up the
measurement cycle and substantially reducing costs.

The study of mission considerations, requirements and techniques led to a definition of the relationships between satellite orbits, observing site locations and resulting observing "windows." An investigation of available satellites and orbit characteristics down through sixth magnitude led to an understanding of the factors effecting mission planning and scheduling to make maximum use of these windows, and an indication that almost continuous useful measurement operations may be possible due to the increased sensitivity and magnitude of each of the recommended equipment improvements.

Additionally, an investigation of ephemeric data sources and methods led to recommended procedures that should prove practical and adequate, mainly involving utilization of the SPADATS satellite tracking system of NORAD. Implementation procedures have been defined both for satellite tracking data acquisition and for precise position determinations to meet the accuracy needs as indicated by the position sensitivity studies which were also conducted as a part of this investigation.

Finally, data processing procedures and techniques have been recommended, along with field calibration procedures and other observational methods and requirements designed to optimize measurement quality. It is expected that implementation of the recommendations of this study will result in a substantial new flow of needed ozone (and possibly some other) measurement data to answer urgent environmental and aeronomy questions at a very reasonable cost - - much lower than for other methods currently employed.

PRINCIPLES AND OBJECTIVES OF UPPER ATMOSPHERIC OZONE MEASUREMENT

Almost day by day, there has been a growing awareness of the real nature and importance of the role played by upper atmospheric ozone in shaping our environment. This growing awareness had resulted from several things - the better scientific understanding of the disciplines involved, the increasing (through still meager) bank of available data, the apprehension over such man-made contributors as jet aircraft and the supersonic transport, and growing general interest and understanding of all natural phenomena.

For ozone, all this is particularly true, since it apparently has a more powerful effect than previously realized. The nature of this effect and the mechanisms involved, and the need for, principles, objectives, and methods of ozone measurements are discussed below in this section.

The Importance of Ozone

While most atmospheric elements strongly affecting our surface environment are in the troposphere, where storms, climate, weather, etc., operate, ozone is a resident mainly of the stratosphere, that relatively tranquil region above the tropopause. Indeed, the importance of the stratosphere in several regards is seldom recognized, along with various aspects of ozone and other upper atmospheric

2

chemical and other associated physical effects. A discussion of these will form a better basis for consideration of measurement principles and objectives.

The Importance of the Stratosphere - The stratosphere is important both for the various functions that take place there, and for its regulating effect on the transmission (or blocking and filtering) of ultraviolet radiation from the sun.

Importance of Stratospheric Function: The high stratosphere lies like a giant translucent curtain over the much more active troposphere below. It is therefore able to effect a strong filtering function, despite its tenuous character, and can also do this somewhat selectively. For this reason, any significant alterations - even small ones - carry the potential possibility of subtle (or possibly even stronger) alterations in the behavior of the lower atmosphere beneath it, in addition to tis effects at the surface of the earth.

Pollution (either natural or artificial) is the most obvious such alteration of the stratosphere and its function, and is therefore worthy of serious considerationiin this regard.

Three properties of the stratosphere make natural and artificial pollution of this layer more critical than that of the troposphere.

   (1)   The thermal stability and virtual cloudlessness of the
         straosphere permit many pollutants to reside longer in the
         stratosphere (for a time measured in years) than in the
         troposphere (days or weeks). The equilibrium concentration
         produced by a continuous source can thus be 10 to 100 times
         greater in the stratosphere than in the troposphere for an
         equal source.

   (2)   Ultraviolet radiation creates ozone that is important, both
         in controlling stratospheric temperatures and in shielding
         life at the earth's surface from undesirable ultraviolet
         radiation. Even small changes of pollutants - e.g. (PPM)*
         for such pollutants as water vapor, or (PPB)** for nitric
         oxide can play a significant role in the ozone equilibrium.

   (3)   The lower stratosphere is close to radiative balance. That
         is, the individual heating and cooling rates due to water
         vapor, carbon dioxide and ozone very nearly cancel each
         other. Therefore, it is sensitive to relatively small
         changes which could alter this balance.

The sensitivity of the stratosphere to even small intrusions of man-made substances follows from the long residence time within the stratosphere and from the possible role of even small concentrations of certain substances in the ozone photochemistry and heat budget. The stratosphere contains the greater part of the ozone that shields

_____

*PPM Concentration factor in parts per million; i.e., parts of
       pollutants per million parts of atmosphere
**PPB Parts per billion (parts of pollutant per billion parts of
       atmospheric gas, etc.)

life from potentially damaging ultraviolet radiation; this service for the biosphere is performed by concentrations of the order of PPM. The ozone also plays a role in the stratospheric heat budget. For these two important reasons, it is vital to be able to explain the existing ozone concentrations and to predict future changes from either man's or nature's introduction of pollution into the stratosphere. It is not now possible to provide a comprehensive explanation for the observed ozone distribution for three reasons:

(1) Not all the constituents of the stratosphere are known.

(2) Some of the chemical reaction rates are still uncertain.

(3) Atmospheric transport of ozone and other ozone-producing and ozone-destroying trace gases have received too little attention.

No adequate forecast of future ozone changes due to man's activities can be expected until all three impediments are eliminated.

Trace gases other than ozone require new sampling techniques and instrumentation. The creation of a suitable model of atmospheric transport is far from trivial; it may be more difficult than sampling the high atmosphere.

The problem of stratospheric particles is primarily one of describing their numbers and characteristics. Since volcanoes inject massive amounts into the stratosphere, a program of monitoring following the next eruption will allow nature to perform an experiment that may help to assess atmospheric response to man's injection of particles into the stratosphere. Further, this together with routine monitoring during periods of low volcanic activity, will provide the background against which man's contribution can be judged.

Clouds in the stratosphere are rare. Without further information on their occurrence and character, it is impossible to assess the role that more or less atmospheric moisture can play in their modification. In particular, they should be sought in regions of the stratosphere with temperatures lower than about -75°C.

Stratospheric ozone is formed as a result of photodissociation of molecular oxygen. It is destroyed either by photodissociation or by recombination with atomic oxygen. Nitrogen oxides and hydrogen compounds may play a role in the stratospheric chemistry leading to the removal of ozone. Their photochemical influence in reducing ozone in the upper atmosphere is relatively direct. In the lower stratosphere, however, atmospheric transport, both vertical and horizontal, as well as the interaction between nitrogen oxides and hydrogen compounds, represents influencing factors in variations of the ozone distribution.

It is likely that significant modification by man of the existing natural composition of the lower stratosphere would be required to produce a decrease in stratospheric ozone. Because of the complexities of the problem, involving the interactions of stratospheric photochemistry and atmospheric dynamics, it is not possible to say how large this decrease would be or how this would affect the total ozone

4

in a vertical column. Because of its great potential importance,
considerable research effort should be undertaken to minimize this
uncertainty before man-made contamination of the stratosphere is
allowed to reach significant proportions.

Stratospheric Transmission of Ultraviolet Radiation: The UV
transparency of the upper atmosphere is substantially affected by
its composition, and particularly by the presence of ozone. Aircraft
engines emit water vapor and nitric oxide, both of which could quite
conceivably produce changes in the amount of stratospheric ozone.
Since ozone is also one of the radiatively active gases in the
atmosphere, particularly in the stratosphere, climatic modifications
may result. It appears likely that radiative effects due to possible
changes in ozone would be negligible. But another possible consequence
of the potential change by man of the stratospheric ozone content
would be the resulting variations in ultraviolet radiation reaching
the earth's surface, which could have serious consequences for the
biosphere in general and man in particular.

The intensity of incoming solar UV radiation received by the ground
depends on the intensity of the radiation at the top of the atmosphere,
then filtered out primarily through absorption by ozone but also by
scattering by air molecules and dust. Although the unattenuated solar
radiation contains decreasing energy with decreasing wavelength below
3400A, the large increase of absorptivity by ozone below 3400Å results
in even more pronounced decrease of the solar radiation received at
the ground, so that very little of the solar radiation below 3100Å
penetrates through the atmosphere to the surface.

It is well known that the human skin is very sensitive to various
wavelengths of ultraviolet light; the peak of this sensitivity is at
a wavelength of about 2950Å. Not much radiation at this wavelength
penetrates to the surface, but that which does penetrate depends on
the amount of ozone present in the path of the sun's rays. Large
amounts of the ozone present and/or long atmospheric paths (low sun)
would reduce the ultraviolet radiation transmitted to the ground.
Small amounts of ozone and/or short paths (high sun) increase the
ultraviolet transmitted to the ground.

It has been suggested that the apparent latitudinal increase in the
incidence of skin cancer toward the equator is because of the increase
of ultraviolet radiation received at the ground resulting from the
higher average solar elevation angle and decreased observed total
ozone toward the equator; for a fixed wavelength and solar zenith
angle a change in total ozone will result in a relative change in
ultraviolet radiation received at the surface.

The above subjects are discussed more fully in Reference 1.

Ozone Effects as a Heat Source - Photodissociation of oxygen is
produced by the more energetic photons with wavelengths between
1000 and 2000Å, and is more pronounced at about 100 km altitude.
The less energetic photons, with wavelengths of 2000 to 3000 Å,
penetrate even closer to the earth's surface into the lower strato-
sphere; there, they dissociate ozone which is less tightly bound than
oxygen. The temperature maximum at 50 km attests to the importance
of ozone photodissociation as a heat source. There is no corresponding
maximum in the temperature profile around 100 km where oxygen is

photodissociated. But while oxygen absorption is not particularly important as a heat source, it does have a profound effect on the chemical composition of both the upper and lower atmosphere.

One result of photodissociation of oxygen is that much of the atmospheric oxygen at high altitudes is in the atomic state. The actual concentration of atomic oxygen is determined by the balance between the rate at which it is produced by photodissociation and the rate at which it recombines to form molecular oxygen. Theoretical treatment has so far failed to provide quantitative information on the relative concentrations of atomic and molecular oxygen in the upper atmosphere.

Below 100 km in the lower stratosphere, the atomic oxygen produced by photodissociation combines with melecular oxygen to form ozone. Present only in trace amounts, ozone is only one hundred thousandth of the ambient density - - even in the 15 to 25 km range where ozone is at a maximum.

By absorbing strongly in the near ultraviolet (2000 to 3000Å), ozone not only shields the troposphere and the ground over this biologically harmful solar radiation wavelength range, but also provides the energy source responsible for the temperature maximum where the stratosphere and mesosphere meet at the stratopause (50 km altitude). The rate of radiation absorption at any altitude is proportional to the product of the concentration of absorbing constituents and the radiation flux. The altitude at which the rate of absorption reaches a maximum is called the absorption altitude for that wavelength.

Relationship with Other Constituents – Although the measurement and determination of amount of ozone is of prime importance in this study, it has been ascertained that the amount of ozone present in the stratosphere is affected by other trace constituents. For instance, nitrogen oxides participate in the chemical processes of stratospheric ozone. Excited atomic oxygen produced by photodissociation of ozone interacts with nitrous oxide (N_2O) to provide nitric oxide locally in the stratosphere.

Nitrogen dioxide can be photodissociated by near ultraviolet sunlight to give atomic oxygen and nitric oxide, or it can combine with atomic oxygen to produce nitric oxide and molecular oxygen. The nitric oxide combines with ozone, and in the ozone destruction, forms molecular oxygen and reforms nitrogen dioxide. Thus, in the stratosphere the photochemical effect of NO leads to a destruction of ozone through catalytic action.

Another example of interaction is the manner in which water vapor plays a role in the photochemistry of ozone. One of the products of photodissociation of ozone at wavelengths below 3100Å is excited atomic oxygen. Excited atoms react very rapidly with water vapor to produce 2 hydroxyl (OH) molecules. Of less importance in the stratosphere is the photodissociation of water vapor that also produces OH. Hydrogen, hydroxyl, and hydroperoxyl radicals and hydrogen peroxide molecules are linked in the catalytic destruction of atomic oxygen and ozone. The catalytic reaction of $OH + O_3 \longrightarrow HO_2 + O_2$ and $HO_2 + O_3 \longrightarrow OH + 2O_2$ have been suggested by many as representing a major destructive mechanism for ozone in the lower stratosphere.

6

This very brief qualitative description of the manner in which ozone interacts with other atmospheric constituents is described more extensively in the literature treating this subject. (See References 2 through 7.)

Mechanics of Ozone Production and Destruction - Ozone is formed in the earth's atmosphere as a result of the photodissociation of molecular oxygen by solar ultraviolet radiation. The most weakly absorbed ultraviolet radiation capable of dissociating oxygen is that absorbed in the Herzberg continuum (λ < 2420 Å); the amount of oxygen in the earth's atmosphere is such that even this radiation does not penetrate to the surface, but is absorbed at altitudes between 20 and 70 km. As a result, ozone is formed at high altitudes, and it occurs in greatest concentrations at altitudes in the vicinity of 20 to 30 km. The reactions leading to the formation of ozone are:

$$O_2 + h\nu \quad (\lambda < 2420 \text{ Å}) \rightarrow O + O \quad \text{and} \tag{1}$$

$$O + O_2 \rightarrow O_3 \tag{2}$$
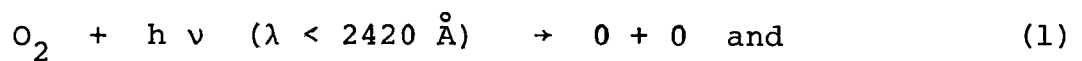
The rate of dissociation for (1) is determined by the intensity of solar ultraviolet radiation at the altitude in question and by the absorption cross section. Absorption in the Herzberg continuum is all that contributes to the rate of dissociation in the ozone region; absorption in the Schumann continuum (λ < 1760 Å) is more intense, and the ultraviolet radiation in this wavelength region is all absorbed at higher levels where the oxygen concentration is so low that ozone formation according to (2) is too slow to be of significance.

The reactions leading to the removal of ozone are:

$$O_3 + h\nu \rightarrow O_2 + O, \text{ and} \tag{3}$$

$$O_3 + O \rightarrow 2O_2 \tag{4}$$
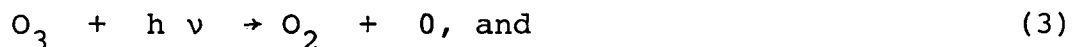
Direct photodestruction, (3), proceeds at a rate determined by the intensity of solar ultraviolet radiation (λ < 3000 Å) at the altitude in question and by the absorption cross section, which has its maximum value near 2550 Å. This removal of ozone is temporary, since atomic oxygen is released, which leads to ozone formation according to equation (2). Equation (4) is effective in removing ozone; also, atomic oxygen is removed by

$$O + O \rightarrow O_2 \tag{5}$$

Several other reactions also occur; however, those indicated by equations (1) through (5) are among the most important. At any altitude, the system proceeds to equilibrium in the presence of sunlight, giving rise to equilibrium concentration of ozone.

Although ozone is formed because of sunlight, it does not disappear at night. Instead, its concentration increases somewhat, especially above 40 km. This occurs because the equilibrium is displaced toward atomic oxygen and away from ozone by the ozone dissociating ultraviolet radiation. Since only a minor portion of the total atmospheric ozone is strongly influenced in this manner diurnal variations in total ozone content are usually small.

<u>Picture Obtained to Date</u> - From previous measurements of ozone by the various methods used to data, a generalized preliminary picture can be drawn as to the amount of ozone present at a given place on the earth with respect to such parameters as the total and vertical distribution with season, altitude, temperature, time-of-day, etc. Figures 1 and 2 (Reference 8) are contour maps which indicate the seasons of maximum (spring) and minimum (fall). It can be seen that total ozone in equatorial regions averages about 0.240 atmosphere-centimeters (atm-cm) and varies only slightly with season (atm-cm refers to the height of the resulting volume of ozone if all the ozone in the column of unit area were brought to normal surface pressure and temperature.) The amount of ozone increases poleward, reaching annual average values in excess of 0.380 atm-cm at high latitudes. North of the tropical zone, the variation with season is approximately sinusoidal, with a distinct maximum in early spring and a distinct minimum in the fall.

Average total ozone has a significant longitudinal variation. The general features of the ozone distribution conform roughly to the gross features of the mean circulation pattern of the lower strato-sphere. Larger amounts of ozone are associated with regions of low pressure and warm temperature above the tropopause, smaller amounts are found in the cold, anticyclonic circulation areas in the lower stratosphere. Average seasonal amounts in the northern regions range from 0.280 atm-cm over Norway in the fall to greater than 0.460 atm-cm over northern Canada and Greenland in the spring.

There are marked temporal and geographical variations in the vertical distribution of ozone. The maximum density of ozone is found in the lower stratosphere, usually between 15 and 30 km, ozone density above 30 km decreases rapidly with height (see Figure 3). Below the tropopause (∿10 km) the ozone density is small and relatively constant. Variations in the total amount of ozone are accounted for by varia-tions in the lower stratosphere. It has been found that the vertical distribution and their seasonal variations are qualitatively the same at high or low altitudes; the difference being that the seasonal variational in the lower stratosphere are smaller near the equator, there is little seasonal variation at any altitude and the maximum density occurs at a higher altitude (∿30 km).

The above statements indicate that there is a direct correlation between seasonal variability in the vertical distribution and in the total ozone amounts. This is due to the fact that changes in total ozone amounts are caused mainly by variations in the ozone concentra-tions in the lower stratosphere. The variability is governed by transport mechanisms involving large-scale atmosphere wind motions. A special feature of vertical ozone distribution is the occurrence of double maxima on days of large amounts of ozone. The primary maxima in concentration is observed between 20 and 35 km, and a secondary maxima between 10 and 20 km. The secondary maxima, if analyzed in
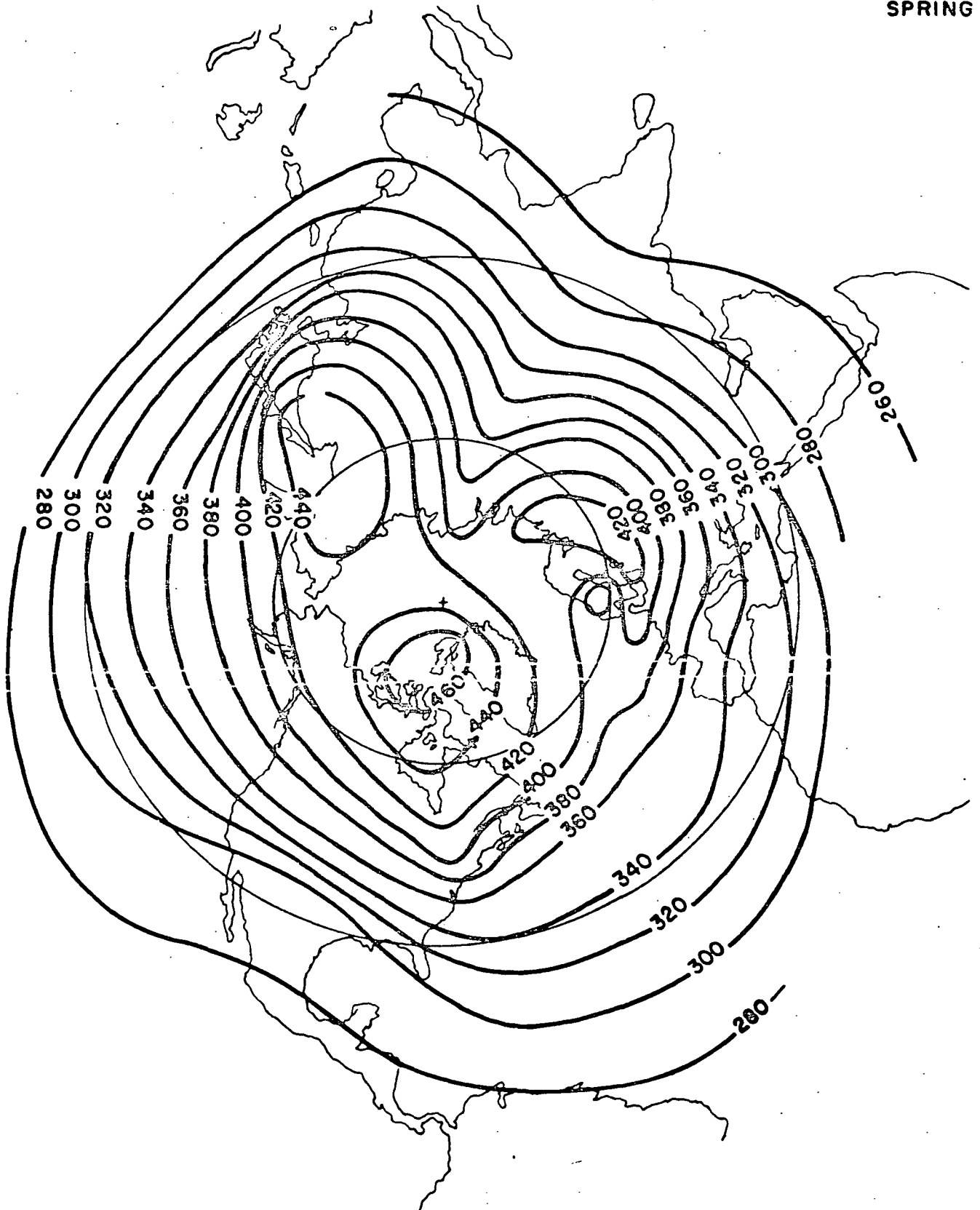
FIGURE 1   Average Distribution of Total Ozone Over the Northern
Hemisphere in the Spring
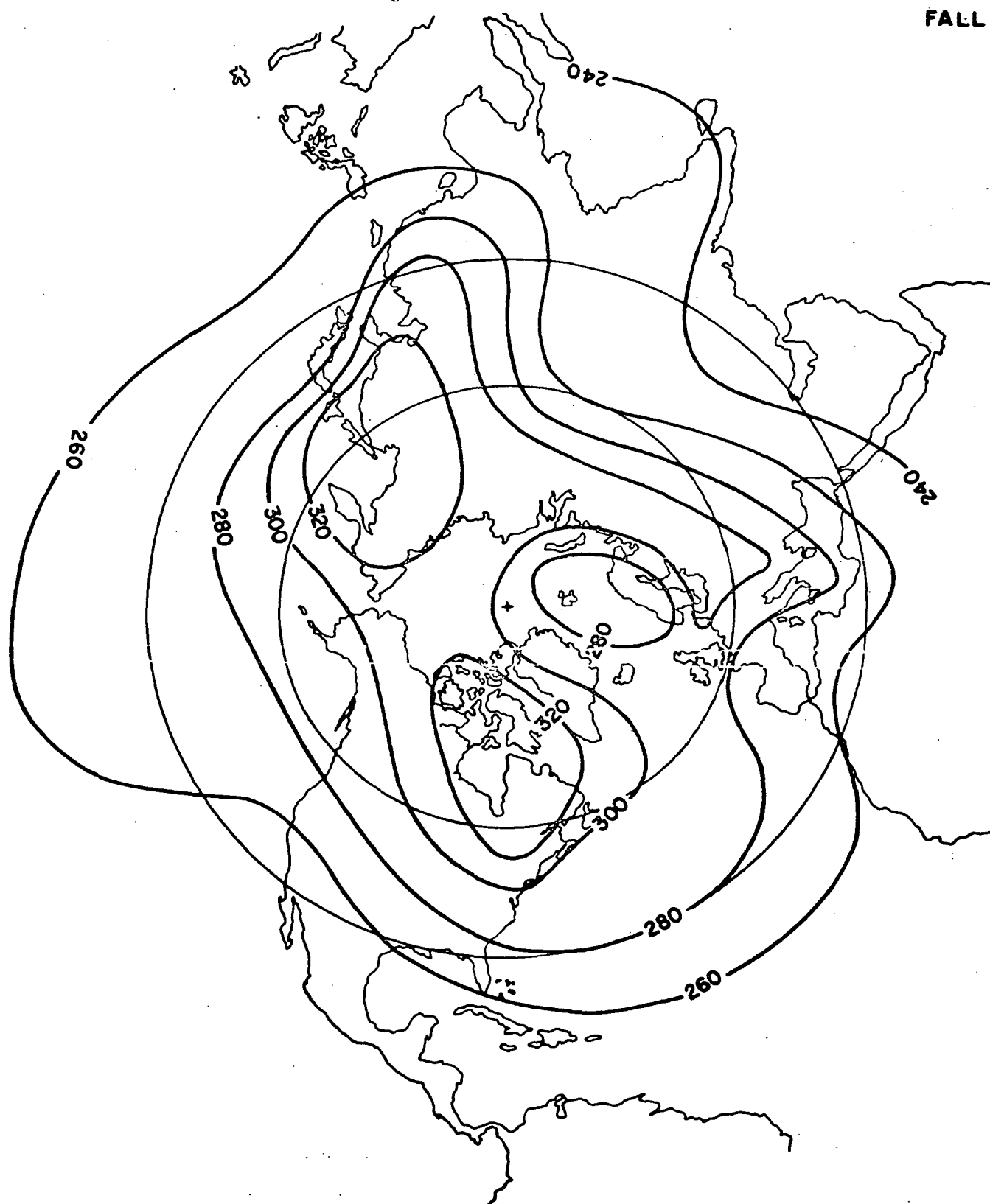
FIGURE 2   Average Distribution of Total Ozone Over the Northern
Hemisphere in the Fall
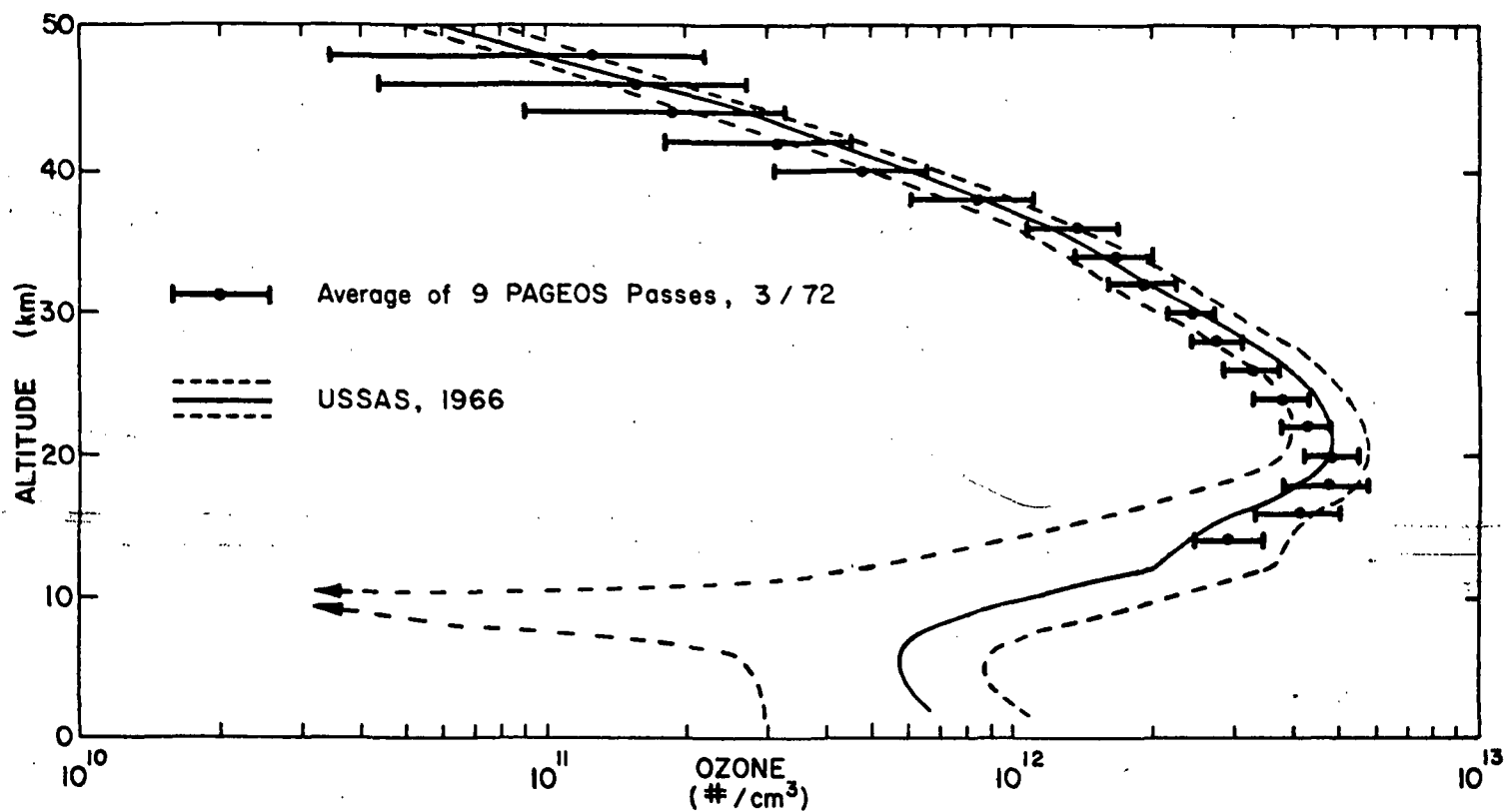
FIGURE 3   Ozone concentrations, molecules cm^{-3}, as a function of altitude, km, for the mean profile (solid circles) and standard deviation (error bars) of the PAGEOS measurements of March, 1972 compared with the USSAS, 1966 profile (solid line) and standard deviation (dashed lines) obtained from Reference 18.

terms of ozone-to-air mixing ratio, can provide information concerning the vertical component of stratospheric winds. Other pertinent information on the total and vertical distribution of ozone may be found in the literature, such as References 9 to 12.

Practical Concerns - It is possible to indicate here some of the more important concerns and objectives for determining the total amount and the vertical distribution of ozone in the atmosphere. A very large number could be mentioned, some of which have already been briefly discussed in previous sections. However, the following in outline form are considered to be among the more important at this time. As time passes and more is understood of the stratosphere and its constituents, this list will undoubtedly grow to include many more items.

Characteristics of the ozone model:

   (1) Space and time distribution of ozone

        (a) Seasonal and latitudinal variation of total amount of ozone.

        (b) Longitudinal and geographical variation of total amount of ozone.

        (c) The distribution of ozone with height.

        (d) Year-to-year variation.

        (e) Causes of seasonal and latitudinal variation with height..

   (2) Mechanism of Ozone Changes and Atmospheric Circulation

        (a) Day-to-day variation of the total amount of ozone and its relation to pressure changes.

        (b) Amount of ozone in the lower layers of the atmosphere.

        (c) Correlation between the total amount of ozone and meteorological parameters such as tropopause height, temperature, etc.

   (3) The Vertical Transport of Ozone

        (a) Importance of day-to-day changes.

        (b) Importance of advection and vertical motion.

        (c) Mechanism of vertical transport of ozone.

   (4) Inter-effects between ozone and other gases, such as oxygen, water vapor, nitrogen oxides, etc.

Effect of Ozone on Communications in the Polar Regions

Effect of Ozone on the Thermal Balance in the Atmosphere

Reasons for Upward Trends of Ozone in Recent Years

Physiological Effects of Changes in Ozone Amount

As was previously stated this brief list is not meant to be all inclusive but is merely put forth as a justification for further and more accurate ozone measurements by any and all possible means. It is indeed fortunate that sufficient measurements of ozone and other trace gases have been made in the past so that a partial understanding of the interactions of the gases is now known. However, great numbers of measurements and analyses are still needed before it can be said that the understanding of these interactions is complete or even adequate.

If, in view of the picture presented here that has developed to data, sufficient additional measurement data could be obtained over a sufficient range of geographical, seasonal and other variations in the region above that where current jet aircraft are regularly operating (where in situ measurements could easily be made by them); that is above 10 to 15 kilometers – – then it would be possible to develop a sufficient picture, correlate it with proposed supersonic and regular jet airways, industrial regions, land masses, etc. and thereby devise means to derive a viable future policy affecting these matters.

ALTERNATE METHODS OF MEASUREMENT

Choices of Approach – Since discovery of the ozone layer over 60 years ago, many optical and chemical techniques have been utilized to determine the total ozone content and the vertical distribution. These techniques may be divided further into methods which measure ozone directly and indirectly. The direct methods of measurement include measurement by instrumented aircraft already operating in the areas (very economical, but mainly limited to below 10 to 15 km), instrumented rockets (very satisfactory, but very expensive and localized to launch sites), and supersonic jets (military and commercial transports in the CIAP Program, but as yet of limited and somewhat doubtful widespread availability, and good only to perhaps 20 km). So for the really widespread, extensive, and inexpensive measurements needed, the indirect methods which can make measurements at substantial distances (both vertically and horizontally) from the actual instruments will have to be employed. And since (mainly for these reasons) only indirect techniques are of interest here, only these techniques will be discussed.

Indirect Methods Used to Date – The indirect methods which have been used extensively are those associated with the various ozone absorption bands at 2000 to 3300 Å, 6000 Å, 9.6 μm, and 8 cm. The most used techniques are the Umkehr method, differential attenuation of sunlight by eclipsing of articifial satellites, backscattering from satellites, and a new technique utilizing Raman spectroscopy. The satellite eclipse method, which is the prime subject of this study, will be reviewed first.

The Satellite Eclipse Method - A method of ozone determination
which has been utilized recently is the satellite eclipse method
(differential attenuation of solar radiation). This method provides
the opportunity of remotely determining ozone concentrations over
geographic locations inaccessible to other methods in an inexpensive
fashion. Early investigators using ground-based instrumentation
included Venkateswaran, Moore, Link, Fesenkov, and Preski of GAC
(References 13 through 17). More recent investigations by Lee and
McDougal of NASA-Langley (Reference 18) have provided stratospheric
ozone concentrations over the North Atlantic Ocean and the continental
United States from measurements performed at Yuma, Arizona. The
ozone reduction technique used by Lee and McDougal incorporates an
improved method to define the corresponding altitude of the ozone
determination. The reduction technique includes the effects of
solar limb dardening, finite size of the sun, and atmospheric
refraction. The measurements are made simultaneously in narrow-band
filters centered at 6000 Å and 7000 Å (regions of high and low ozone
absorption). This combination of wavelengths maximizes the attenuation
due to ozone with respect to the attenuation due to air and aerosols.

From early investigations and from those recently performed by NASA-
Langley, it is now possible to analyze the data with a high degree of
confidence and to specify further improvements to the data taking,
reduction, and analysis techniques. The satellite eclipse method is
described in the following paragraphs, and possible improvements to
the NASA-Langley method are discussed in later sections of this report.

The principles involved in the differential attenuation technique are
illustrated in Figure 4. The solar ray illuminating the satellite
and being reflected to the observer at (O) at a given instant is
shown. The point of nearest approach of this ray on the earth's
surface is actuated at the intersection of the terminator and the
incident plane, I. This is called the sunset point (S_U'), while the
subsolar point is marked (S_O'). The reflected ray (K) lies in a
different plane than the incident plant (I). These planes rotate
continuously with the satellite motion, but the effect of rotation
may be neglected during the brief period of the eclipse. The hori-
zontal path is much greater than the more vertical reflected ray path,
and thus, the attenuation takes place mainly in the I-plane. Also,
the attenuation in the R-plane changes little during the period of
importance during the observation, because the satellite zenith
distance does not alter appreciably during that period. During the
eclipse portion of the pass, the satellite measurements contain the
horizontal and vertical attenuation of the atmosphere. The measure-
ments are normalized by division with a pre-eclipse measurement
(obtained previously in the pass when the sun-satellite line passed
just above the atmosphere). This enables the ozone distribution to
be determined over the sunset point without the need to know the
total ozone between the ground-based photometer and the satellite.

14
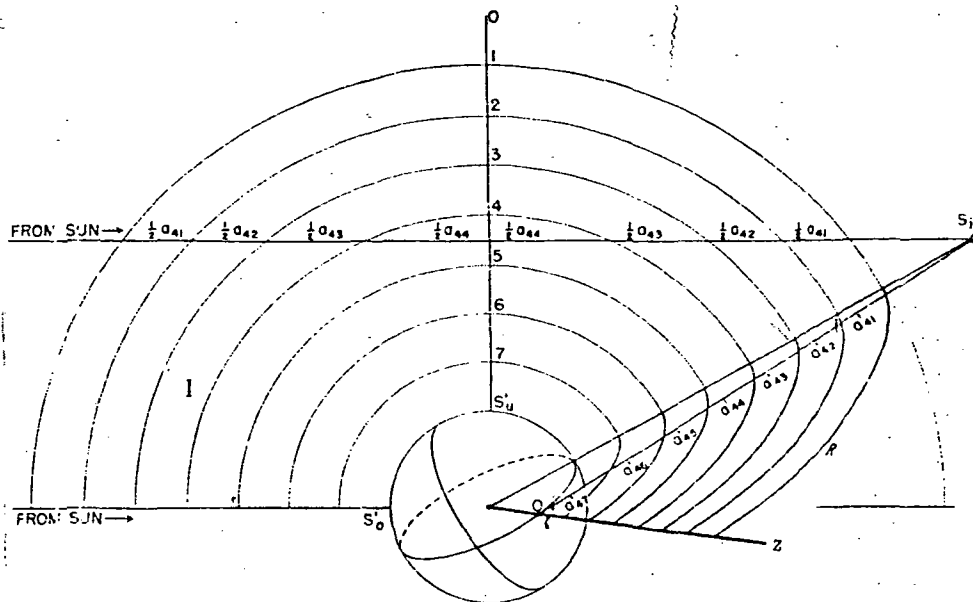
FIGURE 4   The Geometry of the Satellite Illumination Prior to
            Its Eclipse

The attenuation is due to two physical processes: ozone absorption
and scattering by air and aerosols. The ozone absorption peaks in
the visible region at about 6000 Å (Chappius band). Since this band
is somewhat weaker than the ultraviolet band at 2000 to 3500 Å
(Hartley-Huggins band), the attenuation of solar radiation by the
horizontal portion of the atmosphere occurs in an altitude range
from 50 to 10 km. Scattering by air molecules follows the Rayleigh
(λ^{-4}) Law, decreasing with increasing wavelength. Figure 5
(Reference 19) shows the strong wavelength dependence of the absorption
cross section of ozone and the decreasing wavelength dependence of
the scattering cross section of air molecules in the visible region.

In order to minimize the air and aerosol scattering correction to
the total attenuation to deduce ozone concentrations, the NASA-Langley/
GAC method makes measurements in the 6000 Å and 7000 Å bands simultan-
eously. For these two bands, the relative difference in the absorption
coefficient for ozone (5:1) is much greater than the relative difference
in the scattering coefficient for air (2:1) (see Figure 5). The
attenuation of the 6000 Å /7000 Å intensity ratio is predominately
due to ozone absorption with a small correction for air and aerosol
scattering. For example, at 25 km approximately 95% of the attenua-
tion is due to ozone and only 8% is due to air and aerosols.

It should be noted that ozone measurements performed by the Umkehr
method and the method of differential attenuation of solar radiation
from artificial satellites have utilized the strong absorbing wave-
lengths in the UV, while the ground-based measurements using the
differential technique have been performed using the Chappius wave-
length region. Consideration has also been given to measuring the
ozone absorption in the UV using the differential attenuation method
from the ground, a short discussion of which follows.

ABSORPTION CROSS SECTION OF OZONE (cm² × 10⁻²¹)

SCATTERING CROSS SECTION OF AIR (cm² × 10⁻²⁷)

— ABSORPTION CROSS
    SECTION
--- SCATTERING CROSS
    SECTION

WAVELENGTH λ(Å)
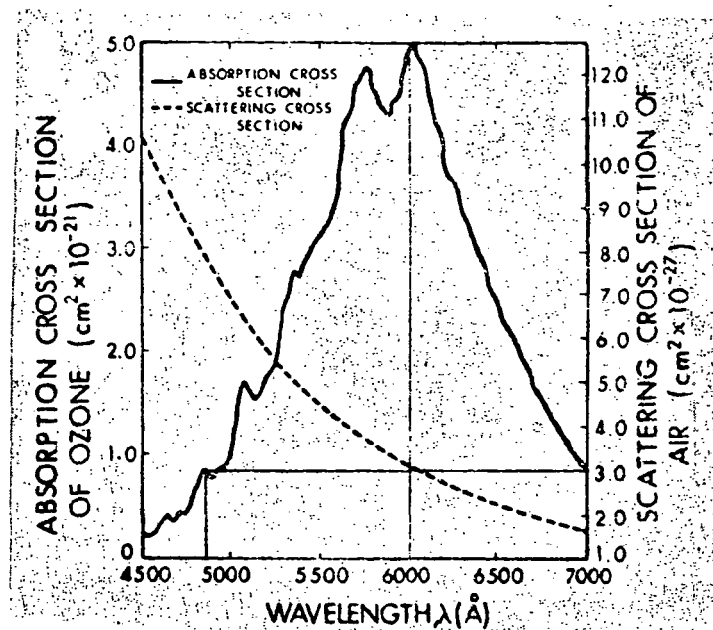
FIGURE 5   Absorption Cross Sections of Ozone and
            Scattering Cross Sections of Air (cm² per
            Molecule) in the Region of the Cahppius Bands

As has been stated previously, the atmospheric absorption due to
ozone in the 2000 to 3500 Å, UV-region, is many magnitudes stronger
than that in the Chappius region. For instance, the ozone absorption
coefficient in the 1963 U.S. Standard Atmosphere at 3000 Å is 2.00 x
10^{-1}/km, as compared with 2.61 x 10^{-3}/km at 6000 Å. The former value
is far less than the maximum absorption in the UV, which is located
at approximately 2500 Å, while the value at 6000 Å is the maximum in
the Cahppius region. A possible combination of ozone/nonabsorption
wavelengths would be 3300 Å and 4500 Å; the 4500 Å region being the
same measurement as that used for the nonabsorption measurement with
the 6000 and 7000 Å filters. The higher ozone absorption coefficient
at 3300 Å results in the horizontal attenuation occurring at higher
altitudes, from 70 to about 30 km. As is well known the extinction
coefficient at 3300 Å is quite high; Johnson and Mitchell obtained
average values of primary extinction coefficients of 0.692 at 3300 Å
as opposed to 0.237 at 4500 Å for 100 observation nights at Catalina
Observatory near Tucson, Arizona, which is known for its excellent
clarity and seeing conditions. If this spectral region is to
determine ozone, it is probable that observations should be made from
high altitudes (Mt. Palomar height) where UV extinction is relatively
low. There are substantial advantages in using the 3300 Å as opposed
to the 6000 Å region for ozone determination, especially with respect
to determining at heights above 50 km, if suitable measurement sites
can be used.

Umkehr (Inversion) Method   -   Perhaps, the most extensively used
indirect method to date is the so-called Umkehr method (literally
inversion). The Umkehr effect is observed when measurements are
made of the ratio of the zenith sky light intensities of two wave-
lengths (3114 and 3324 Å) in the solar ultraviolet with the sun near

the horizon. If the logarithm of the ratio of the intensity of the short (strongly absorbed) wavelength to the intensity of the long (weakly absorbed) wavelength is plotted against the sun's zenith angle, this log-intensity ratio decreases as the zenith angle increases until a minimum is reached for a zenith angle of approximately 85°. As the zenith angle increases further, the log-intensity ratio increases again. This reversal of the curve was first observed and named by Gotz in 1931, who realized also that information about the vertical distribution of ozone could be obtained from the Umkehr curve.

It is not necessarily suggested that the Umkehr method be utilized as a supplement to the satellite eclipse photometry technique (although this is not beyond the realm of possiblity), but it is suggested that the Umkehr method be examined from the literature and information be obtained by visits, correspondence, and/or phone calls to various investigators who have used this technique. Persons and/or places where measurements and/or data reduction have been performed extensively include; (1) Mateer, University of Michigan, (2) Meteorological Branch, Department of Transport, Toronto, (3) Dutsch, National Center for Atmospheric Research, Boulder, Colorado, etc. This technique is extensively referenced in the literature; see for instance, Reference 20 to 23.

It might be noted that Umkehr reductions are made extensively for investigators by the Meteorological Branch, Department of Transport, Canada, using the technique devised by Mateer and Dutsch (see Reference 24).

Narrow-Band Filter Requirements

Chappius Band - Since the NASA-MOSPO already contains narrow-band filters centered at approximately 6000 and 7000 Å (Figure 6), it is not necessary to place new filters in these wavelength regions. Slight consideration might be given to replacing the 7000 Å filter with one centered near 7200 Å, coincidental with the Johnson-Mitchell stellar photometric bnad at 7200 A for extinction measurements. It is also recommended that a new nonabsorption narrow-band filter be placed near the 4500 Å region as has been used by other investigators. This filter should have a half-band width of about 15 to 20 Å as do the other two filters. It is felt that the addition of this filter will aid in more accurately determining the amount of ozone present bacause there will be two independent calculations performed; i.e., from the 4500 to 6000 Å pair and from the 6000 to 7000 Å pair. Another advantage from use of the band at 4500 and 7000 Å is the possibility of obtaining independent values of the aerosol contribution at these wavelengths. It should be stated that the nonabsorption wavelengths should have nearly identical absorption coefficients, such a as is true at approximately 4500 and 7200 Å, which is also coincidental with Johnson narrow-band wavelengths.

Near UV-Band - As has been stated elsewhere in this report, the previous attempts at obtaining ozone data by ground-based instrumentation utilizing the differential attenuation technique have all been performed in the Chappius band region.

It is here recommended that an additional filter be placed at 3300 Å along with the ones at 4500, 6000 and 7000 Å. Since the extinction coefficient at 3300 Å is approximately 3 times that at 4500 Å (or approximately one stellar magnitude), it is possible that the filter at 3300 Å will have to be wider than the one at 4500 Å. A filter of approximately 30 to 40 Å half band width is thought to be adequate for this purpose.

Observational Techniques and Requirements

Calibration Requirements and Techniques - Previous determinations of ozone utilizing the method of immersion of an artificial satellite into the earth's shadow have not taken into consideration extinction as a function of zenith distance, wavelength, etc. A short preliminary discussion and calculations are given here outlining a possible method for determining these corrections to the equations for determination of ozone.

The equations for determination of second-order coefficients, scale factors, and primary extinction coefficients and zero-point terms are well known and have been used in the past by GAC to determinate stellar and artificial satellite magnitude levels. The standard stars used in these determinations are those as published by Johnson, et al, at the University of Arizona for the UBVRI spectral regions. Since these spectral regions are broad-band ($\sim$600 to 1000 Å wide at the half-band width), and since the "effective" wavelengths are at different places in the electromagnetic spectrum than are those for the ozone measurements (although the R-band wavelength is very close to the wavelength for the nonabsorption region used in the ozone measurements), it is thought that the narrow-band values should be used for the extinction determinations in the ozone measurements. Such calibration measurements are thought to be advisable for best accuracy because of some possible variation of extinction with wavelength.

If this method is utilized, the narrow-band stellar magnitudes as determined and published by Johnson in their 13-color medium-narrow-band photometry system could be used. The effective wavelengths for this system are at 3300, 3500, 3700, 4000, 4500, 5200, 5800, 6300, 7200, 8000, 8600, 9900 and 11000 Å. Since the published catalog listing the results of these measurements (see References 25 and 26) includes star values at or near the wavelengths of interest (e.g. 3300 Å, 4500 Å, 5800 Å, 6300 Å, and 7200 Å) they can be used in a fashion analogous to the way in which the broad-band stellar catalogs are used for conventional satellite photometry. Typical response curves used in these bands are shown in Figure 7. It is noticed that these wavelengths are not coincidental with the ozone wavelengths and thus an interpolation for the effective magnitudes at 6000 and 7000 Å would have to be made. However, because of the simplified equations used in the determination of narrow-band stellar magnitudes, it appears that this method might prove superior (for this application) to the method used in broad-band photometry.

Figure 6. Calibration Charts for GAC Procured Narrow Band Chappius Filters

Type 811   Date 10/18/68
Peak λ   6022A
½ pt. Bandwidth   14A
% Transmission   43½%
BAIRD ATOMIC, INC.

Type 811   Date 10/18/68
Peak λ   7029.4A
½ pt. Bandwidth   18A
% Transmission   50½%
BAIRD ATOMIC, INC.

5920 Transmittal λ Calibration = 5919A
6020A
6120-1 = 6119A
6920 plus 7A λ Calibration = 6927A
7020A
7120+7A = 7127A

19

(a)
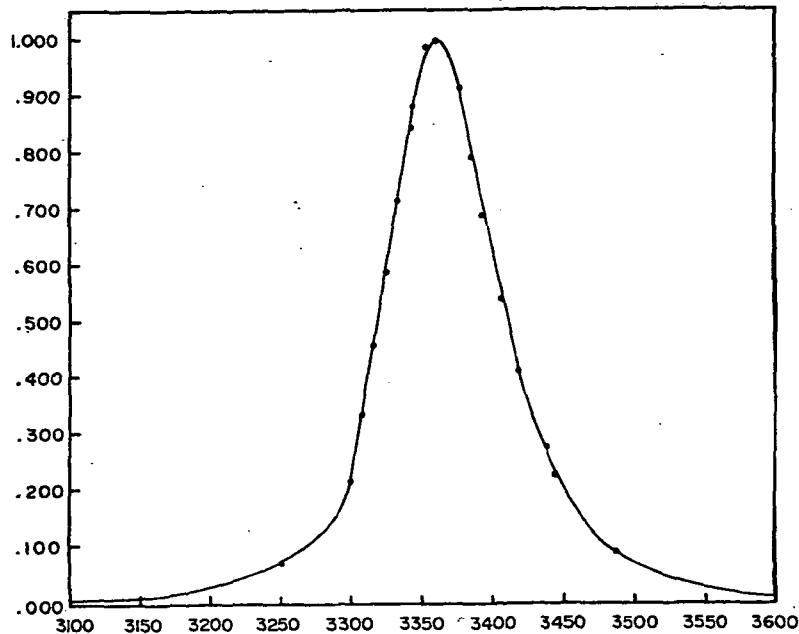
Wavelength ∿ Å
Normalized response function for filter 33

(b)
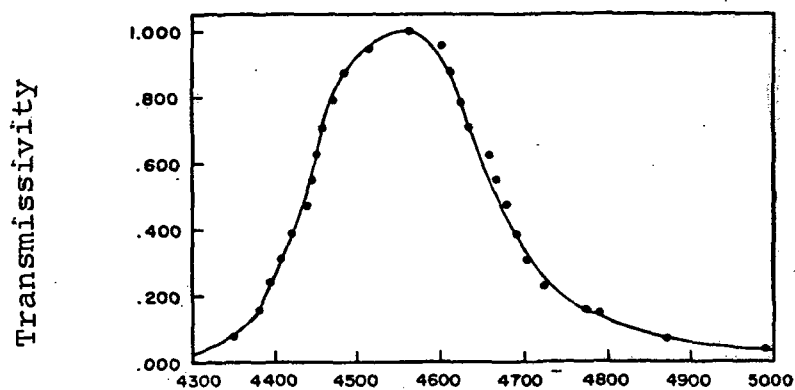
Wavelength ∿ Å
Normalized response function for filter 45

(c)
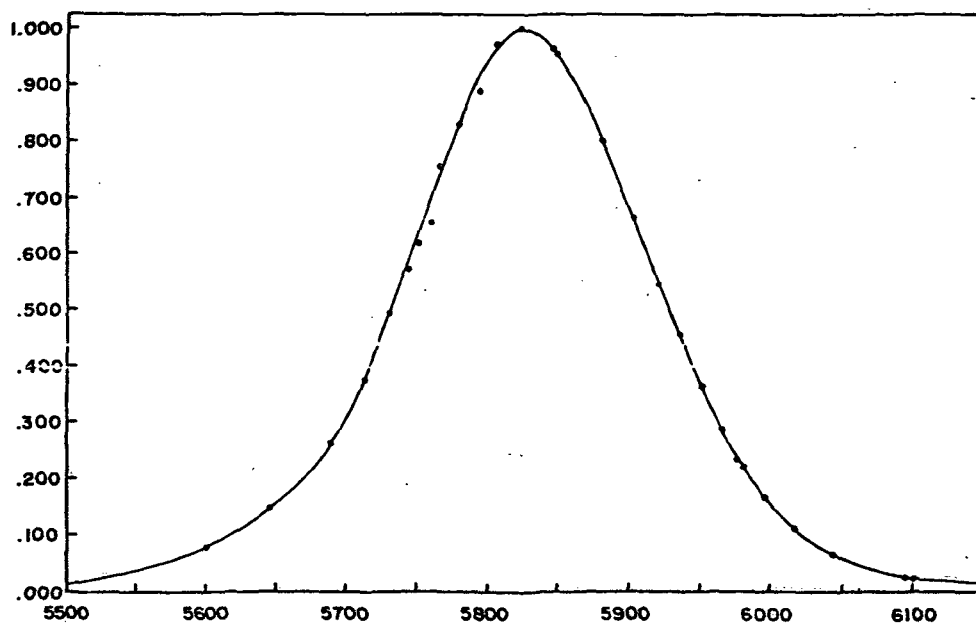
Wavelength ∿ Å
Normalized response function for filter 58

FIGURE 7

20

(d)

Wavelength ∿ Å
Normalized response function for filter 63

(e)

Wavelength ∿ Å
Normalized response function for filter 72
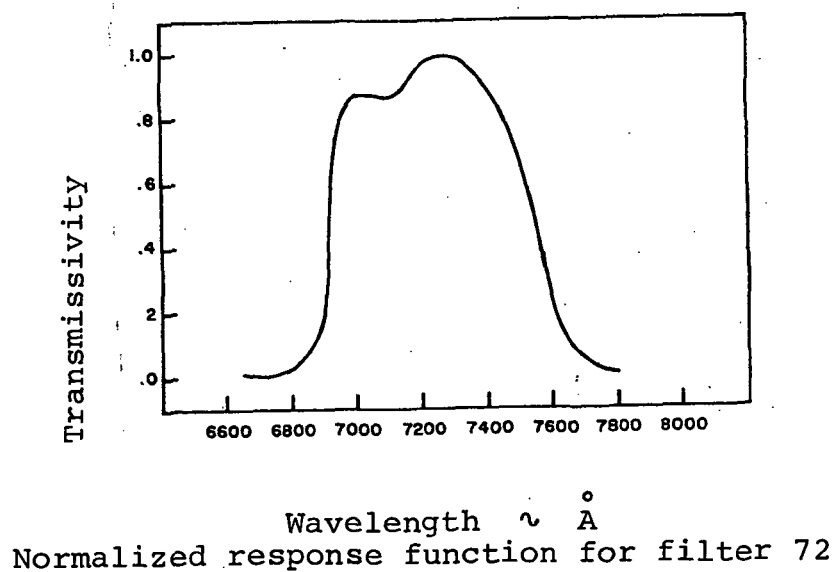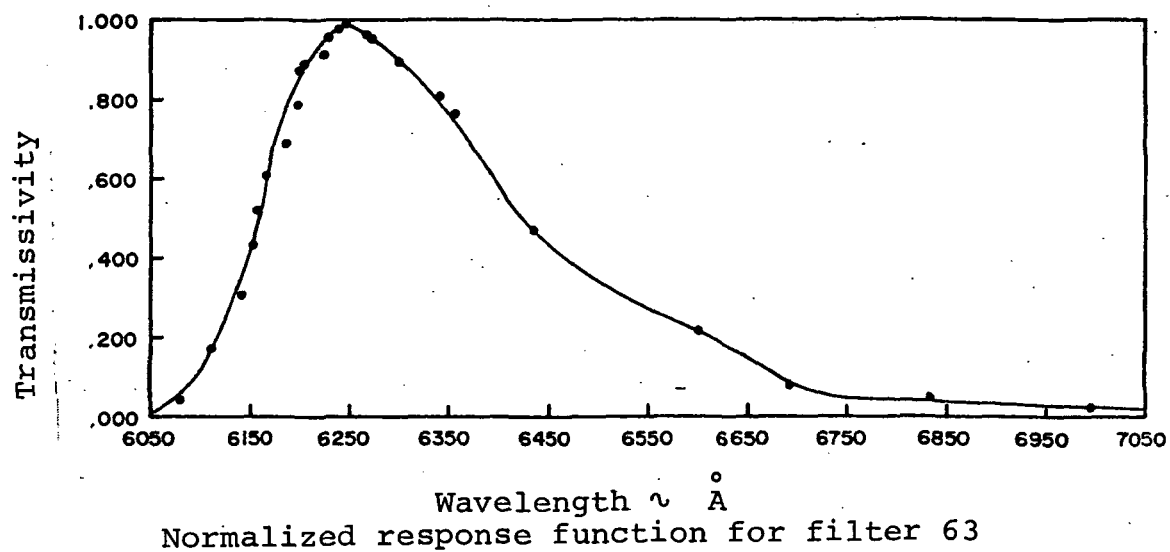
FIGURE 7   (continued)

21

The equation for magnitude determinations as utilized by Johnson is as follows:

$$M = s - 2.5 \log d - k_1 x + \zeta \tag{6}$$

where M is the magnitude, s is the gain factor, d is the galvanometer deflection, k is the extinction coefficient, x is the air mass, and ζ is the zero point term.

It is to be noticed that there are no second-order terms or scale factors in this equation.

F-G-K spectral class standard stars in the 6000 and 7000 $\overset{\circ}{A}$ regions would be measured to determine these extinction coefficients. These star calibration measurements would be made before and after the pass through the same narrow band filters used during the pass to photometer the satellite eclipse. (See Reference 27.)

In practice, determinations made in this way should be compared with measurements derived without use of calibration star reading to verify the degree and worthwhileness of accuracy improvement by their uses.

Data Taking Techniques — Sky Background Requirements and Methods

The present four-channel photometric system allows simultaneous, continuous sky background and satellite monitoring. This method is ideal for ordinary UBV-VRI satellite photometry in which the satellite sky background signal is taken throughout the satellite pass. As the satellite approaches the earth's shadow, the signal becomes dimmer and thus the gain must be raised in order to keep the signal at a satisfactory level. Since the time of duration of eclipse photometry is short ($\sim$ 10 to 60 seconds), it is imperative that random or inadvertent signal dropout not occur or be minimized. It has been recommended elsewhere in this report that all four channels be used to obtainddata such as the ozone absorption region, nonabsorption region, aerosols, etc., simultaneously. If this method is utilized in the future, the sky background signal cannot be monitored continuously during the period of eclipse. A different method of determining the differential (satellite + sky - sky) signal will have to be developed. Several possibilities exist as to these methods:

(1)   Before and after the pass, the 4-axis settings could be set at the predicted positions and the sky levels be registered along the satellite path.

(2)   The sky levels might be determined during the observation by the following technique. Acquire the satellite several minutes before eclipse, drop off to acquire the sky background and then reacquire just prior to eclipse. The background level at the end of the eclipse will commence when the satellite signal merges into the sky background. This technique may require some interpolation during the eclipse period if the satellite altitude is 30° or less.

(3) A third possible method is to continuously track the
     satellite during the eclipse, but drop out periodically
     (automatically) using a magnetic switch or an optical wedge.
     The dropouts should be limited to no more than 1/10 second
     if this integration time is adequate.

It is possible that the difference in sky background level between
first and last contact will be small with regard to pulse-count
discrimination. The differential zenith angle in the worst case will
probably not be much more than 10 to 15 degrees (and more probably
5 degrees) during the course of an eclipse; thus, the pulse count
differential should be small. If this indeed is true, sky background
should not be a major problem during an eclipse; the best method to
use to obtain the background will depend on whether the very short
integration time is adequate and/or whether the differential sky
background is significant.

Data Processing and Instrumentation Requirements

It is recommended that the over-all reduction and analysis program be
examined and appropriate modifications be made to the various computer
programs. Since the inputs to different sections will be discussed
in more detail elsewhere, only an outline plus a brief discussion of
each subject will be given here.

Sunset Point - The present program for calculation of sunset points
should be examined to determine whether the treatment of atmospheric
refraction and finite sun size affects the accuracy of the latitude
and longitude of the sunset points or the assumed measurement
altitude. (Fesenkov's method can be considered for this - Reference
16). The program can then be refined as deemed advisable. Reference
28 also explains methods of incorporation of several parameters into
the ozone determination equations.

Accurate Orbit Determination - Definitive orbits of the satellites
with position determination accuracies of approximately 330 m (1000
feet) are required to be compatible with automatic data reduction,
integration times on the order of 1/10 second, and shell sizes on
the order of 1 kilometer or less. Definitive orbits may be obtained
from Ent AFB. This question is more fully treated in the next
section.

Extinction Coefficients - Primary extinction coefficients are
definitely required in each wavelength band used. A program should
be developed as to how many stars should be used, types of stars
(F-G-K spectral class) and a revised computer program written to
calculate the extinction coefficients. This program will probably
not be as complex as the program now used for conventional stellar
and satellite photometry as it may not require second-order
coefficients or scale factors.

Over-all Computer Programming - The fundamental equations for calculation of ozone should be examined and corrections placed into the equations for extinction, solar limb darkening, atmospheric refraction, finite size of the sun, Rayleigh scattering, etc. The model must include the shell size, the definitive orbit positions and other parameters. It is recommended that NASA-Langley send its present computer program to GAC for analysis and incorporation of improved features. Plot programs and layout of important data on printout sheets should be part of the over-all development. The layout should include satellite position, relative brightnesses of the various bands, vertical ozone determinations at the various altitudes in atm-cm/km and numbers of molecules/cm, total ozone in atm-cm and total number of molecules, etc.

Independent Determination of Scattering Coefficients - As was stated previously, it is possible to obtain independent values of scattering coefficients from the measurements at approximately 4500 Å and 7200 Å. Since the ozone amounts are equal and the Rayleigh scattering known, the remainder of the extinction is due to scattering. There are details to be worked out with relation to particle size and numbers of particles versus wavelength, however, this type of consideration has been studied extensively and should not be considered as a major roadblock. It should be stated that independent measurements of atmospheric particles are important as a function of time due to such events as possible stratospheric contamination by SST's or volcanic eruptions.

Data Point Interval Integration Time - Data point readings should be at least once every 1/10 second for compatibility with the shell size/ altitude resolution and accuracy objectives. (This is also treated in the next section.)

Data Format - Because of the tremendous potential for data reduction cost saveing, increased data yield, and speed-up in obtaining results, it is strongly recommended that the data be recorded in IBM compatible. format, and that software and processing procedures be developed so that the full data processing can be automated.

MISSION CONSIDERATIONS AND REQUIREMENTS

Introduction

In order to meet the ozone measurement objectives described in the preceding section, there are several measurement mission considerations that need to be treated. A primary consideration is the number of observational opportunities that will be available, and what site locations will provide such observational opportunities. This in turn specifies the requirements in terms of time at various sites and satellites to be observed to meet a given ozone measurement data acquisition objective.

The other major mission requirements involve the obtaining of associated satellite position data to meet measurement accuracy objectives, and the mission planning and preparation requirements, including observing windows for each site, satellite eclipse observing schedules, acquisition and tracking data, etc. These considerations and requirements are treated in this section.

Observational Opportunity Aspects

The observational opportunities for satellite ozone measurements will depend on the geometry of the satellite orbit, which will in turn determine the frequency of eclipse occurrence, and upon the number of available satellites meeting brightness and reflectivity requirements. In addition, other factors, such as locale, weather, contingencies, etc., will play a role.

The basic operational geometry will involve the location - - mainly the latitude - - of the observing sites, inclination of the orbit plane, orbit height, etc. These geometry relationship parameters must be defined, and the average eclipse frequency established.

Determination of Shadow Entry Latitude

The latitude at which shadow entry occurs is determined by the position of the sun* and the orientation of the satellite orbit. For any specific satellite, both are functions of time and therefore interrelated. However, for the general assessment of observational opportunities they will be considered to be independent.

A closed solution for the shadow entry point is not possible for an elliptical orbit, so the investigation was confined to circular orbits. The general conclusions, however, should be valid for moderately eccentric orbits. Also, for convenience it has been assumed that the earth's orbit about the sun is circular - i.e. the sun's longitude is a linear function of time.

In order to find the latitude of shadow entry, the position of the sun with respect to the orbit plane of the satellite is first determined through a series of axis transformations (see Figure 8).

The rectangular equatorial components of a unit vector pointing toward the sun are

$$X = \cos \beta \qquad\qquad (7)$$

$$Y = \sin \beta \cos \varepsilon \qquad\qquad (8)$$

$$Z = \sin \beta \sin \varepsilon \qquad\qquad (9)$$

*Position of the sun fixes the position of the antisun location.

where β is the longitude of the sun and ε is the obliquity of the ecliptic. Rotation about the polar axis through the angle Ω , the right ascension of the node of the satellite, gives

$$P = X \cos \Omega + Y \sin \Omega \qquad (10)$$

$$S = -X \sin \Omega + Y \cos \Omega \qquad (11)$$

where P is the component of the sun vector directed toward the node and S is the component in the equatorial plane and orthogonal to P. Rotation into the orbital plane gives

$$Q = S \cos i + Z \sin i \qquad (12)$$

$$U = -S \sin i + Z \cos i \qquad (13)$$

where i is the inclination of the satellite orbit, Q is the component of the sun vector in the orbital plane orthogonal to P, and U is the component perpendicular to the orbital plane.

The spherical coordinates of the sun vector with respect to the orbital plane are
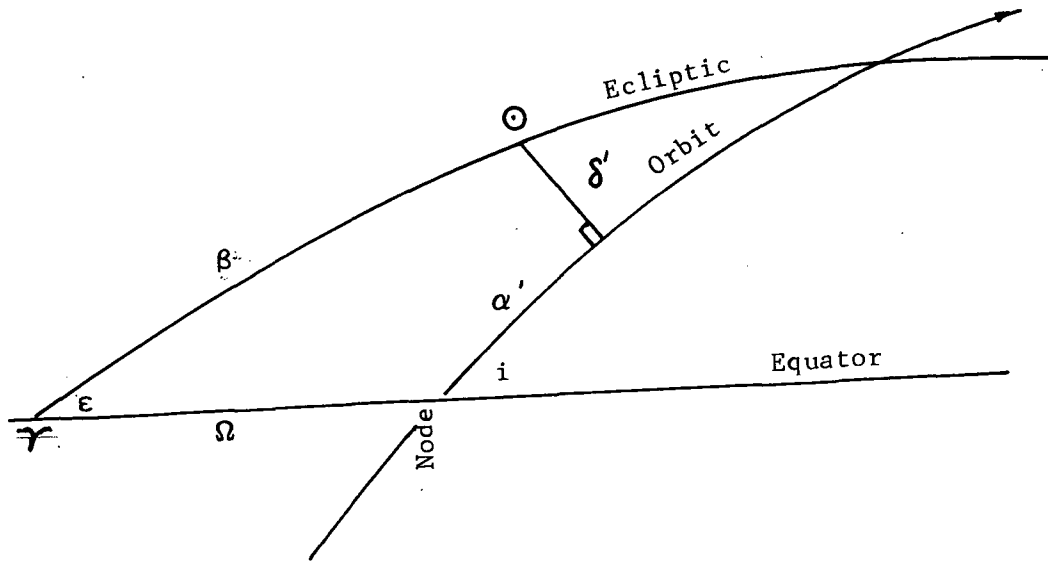
FIGURE 8   Axis Transformation Geometry and Symbols
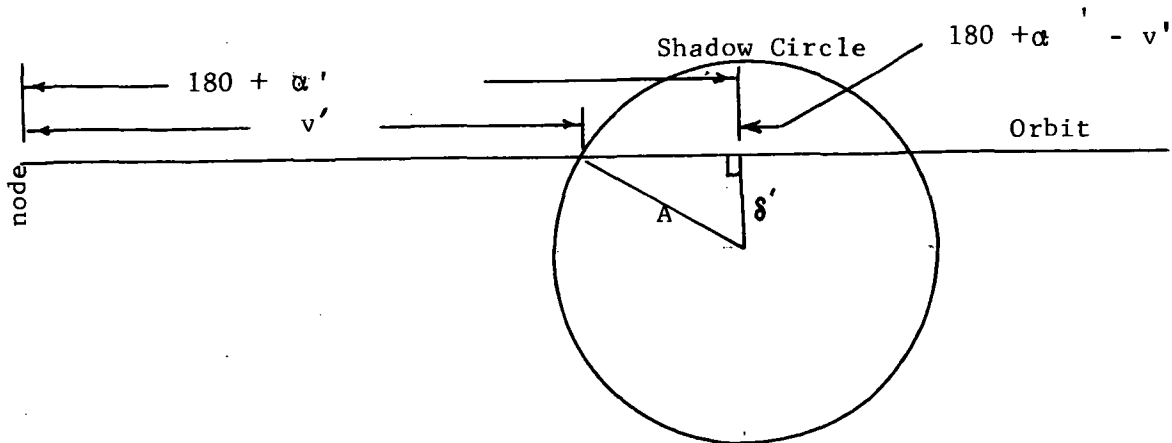
FIGURE 9   Shadow Geometry

$$\alpha' = \tan^{-1} Q/P \tag{14}$$

$$\delta = \sin^{-1} R = \cos^{-1} \sqrt{P^2 + Q^2} \tag{15}$$

The spherical coordinates of the antisun point are, of course, $\alpha' + 180$ and $- \delta'$.

The intersection of the shadow cylinder with a sphere of radius equal to the satellite radius vector projects onto the celestial sphere as a small circle whose center is at $(\alpha' + 180, - \delta')$ and whose radius is

$$A = \sin^{-1} \frac{R}{r} \tag{16}$$

where R is the radius of the earth and r is the satellite radius vector. Figure 9 shows the geometry of the intersection of the satellite orbit with the shadow circle. v' is the satellite's true anomaly at shadow entry, measured from the node. If $|\delta'|$ is greater than A, there is no shadow entry.

From Napiers laws it is apparent that

$$\cos A = \cos \delta' \cos (180 + \alpha' - v') \tag{17}$$

$$= \cos \delta' \cos (v' - \alpha')$$

whence

$$v' = \alpha' + \cos^{-1} (-\cos A/\cos \delta') \tag{18}$$

Note that there are two solutions to this equation, depending on the quadrant assigned to the arc cosine. The second quadrant solution represents the shadow entry; the third quadrant solution is the shadow exit. The latitude of the shadow entry is then

$$\phi = \sin^{-1} (\sin v' \sin i) \tag{19}$$

and the latitude of the tangent point (where the ozone absorption occurs) is

$$\phi_s - \sin^{-1} \frac{\sin \phi + Z \cos A}{\sin A} \tag{20}$$

The great-circle distance between an observer and a satellite which appears to the observer to be at an elevation E above the horizon is

$$\Delta\phi = \cos^{-1} \left[(R \cos E)/r \right] - E \tag{21}$$

27

Eclipse Frequency

A computer program was written to evaluate the probability of observing a shadow entry of a single satellite from a fixed observing station, as a function of station latitude. For a fixed satellite orbit inclination and height, the longitude of the sun is varied in equal increments from 0° to 180° and the right ascension of the node of the satellite is varied from 0° to 360°. Tallies are kept, for stations at equal intervals of latitude from 0° to 90°, of each shadow entry thus generated whose latitude is within $\Delta\phi$ of each station. At the completion of the program each tally is divided by the number of shadow entries attempted and multiplied by the factor $\Delta\phi/(360 \cos \phi)$. This factor represents the probability that the longitude of the shadow is close enough to that of the station. It is accurate at lower latitudes, but it fails near the pole where $\cos \phi$ becomes very small.

Note that it is assumed that all eclipse entries whose latitude and longitude differ by less than $\Delta\phi$ and $\Delta\phi / \cos \phi$ respectively from those of the observer will be seen. This somewhat overstates the probabilities by substituting a square window for a circular window. A better formulation which avoids this problem is now available and will be used in any future studies.

The probability of observing a shadow entry on a given day is obtained by multiplying the probability per orbit by the number of orbits per day.

The probability of having the tangent point at a specified latitude is obtained similarly by tallying against the tangent point latitude and dividing each tally by the number of shadow entries attempted.

The computer program and the input data format are included in Appendix A.

Computer Results - Figures 10 through 17 present the unsmoothed results of the computerized statistical studies of selected orbits that were performed to determine

    (1)   the relative frequencies of shadow entries versus the observer's latitude (Figures 10 through 13), and

    (2)   the relative frequencies at which the point of tangency of the incident solar ray (sunset) occurred at a given latitude (Figures 14 through 17).

In the first instance the results show a complex dependency of frequency upon orbital height, inclination, and observer latitude which prevents making simple all-inclusive generalizations.

At a given site at low or moderate latitude, Figures 10 through 13 show that the relative frequency of observable shadow entries increases with increased orbital height to at least 1600 km. For all but low inclination orbits the results show decreasing sensitivity of frequency to observer latitude as orbital height is increased.

450 KM

Figure 10

RELATIVE FREQUENCY OF SHADOW ENTRIES PER DAY
OBSERVABLE ABOVE 30 DEGREES ELEVATION
AT A GIVEN LATITUDE (N. OR S.)
ORBITAL HEIGHT: 450 KM.
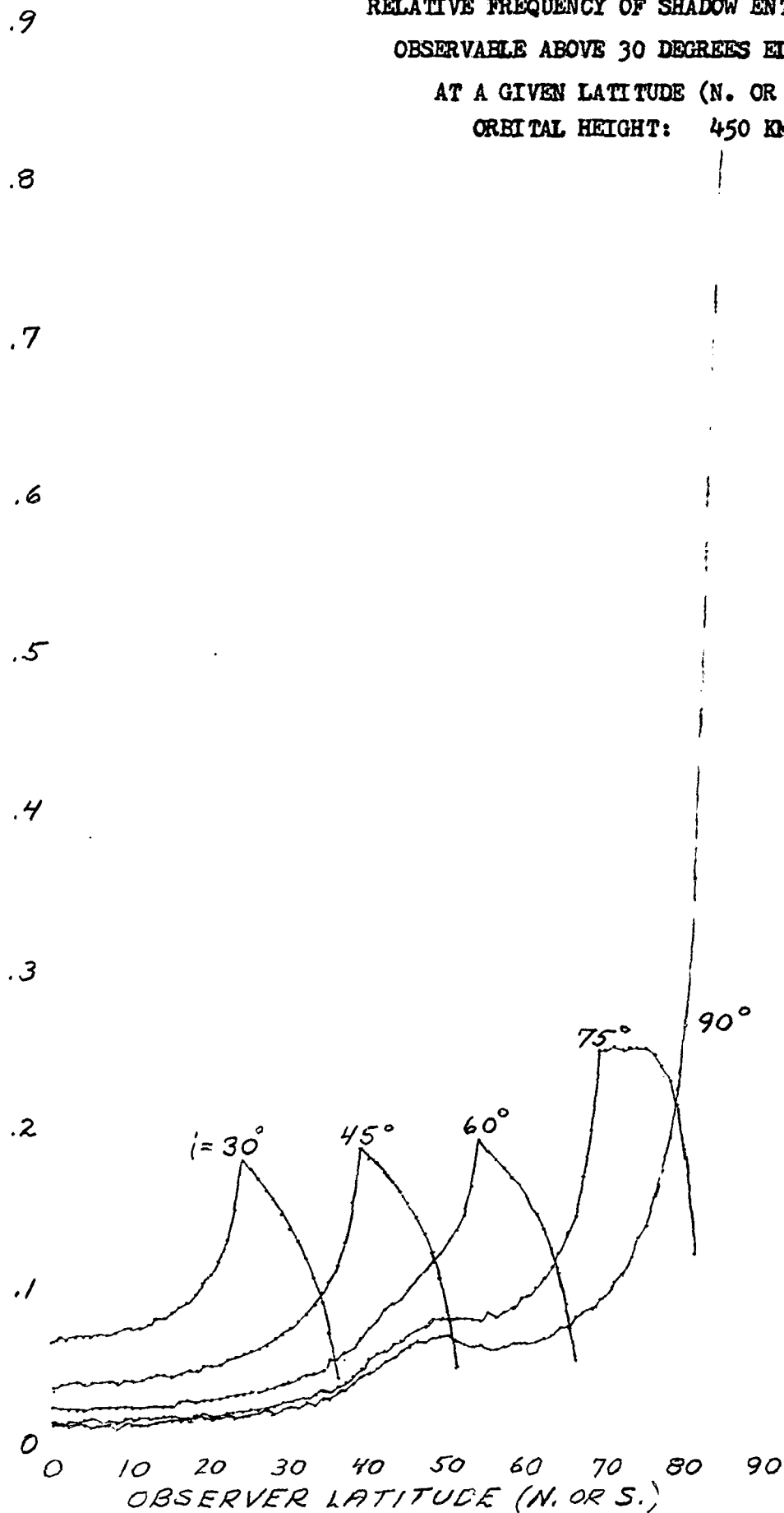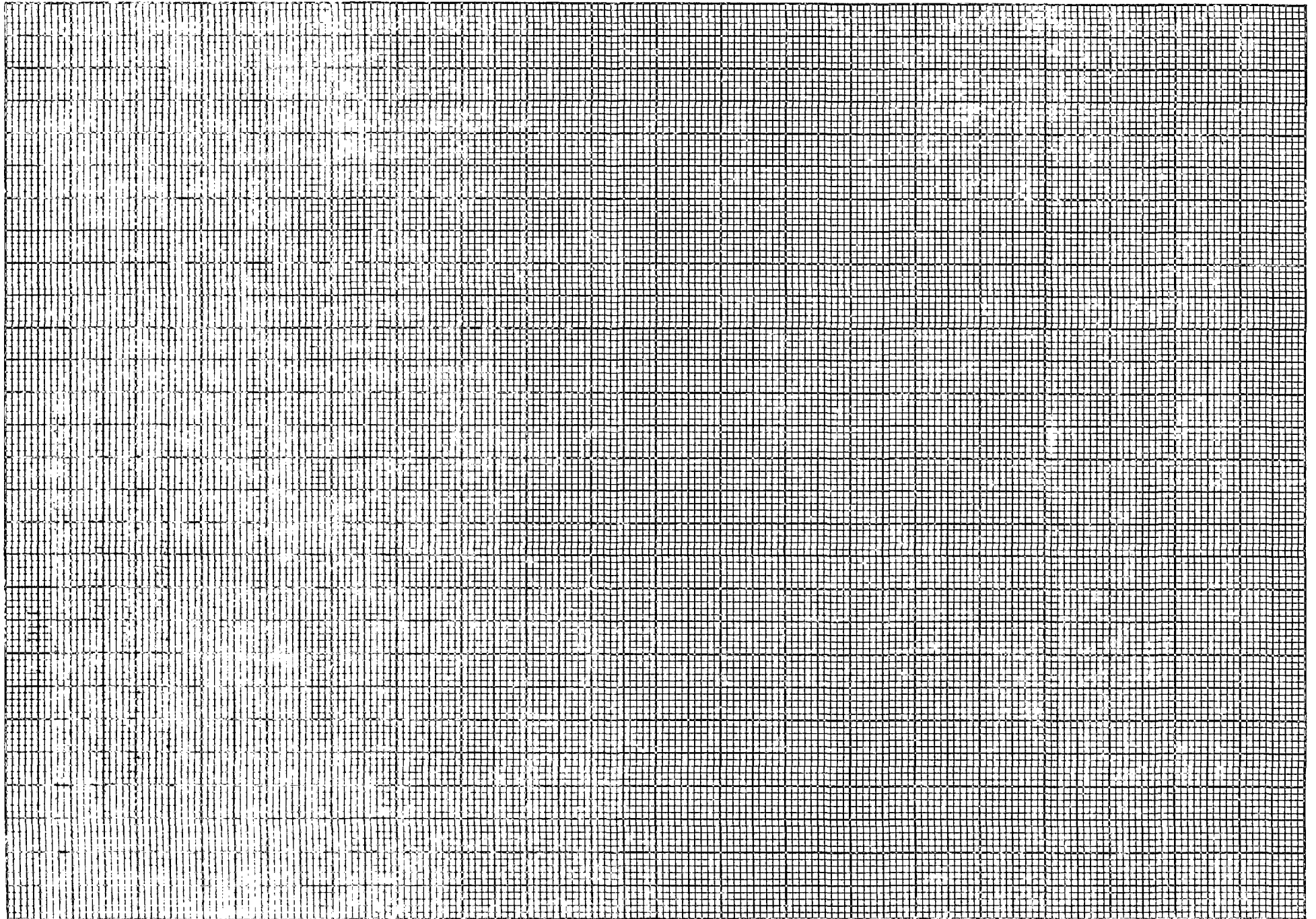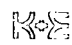
1000 Km

Figure 11

RELATIVE FREQUENCY OF SHADOW ENTRIES PER DAY
OBSERVABLE ABOVE 30 DEGREES ELEVATION
AT A GIVEN LATITUDE (N. OR S.)
ORBITAL HEIGHT: 1000 KM.

KEUFFEL & ESSER CO.
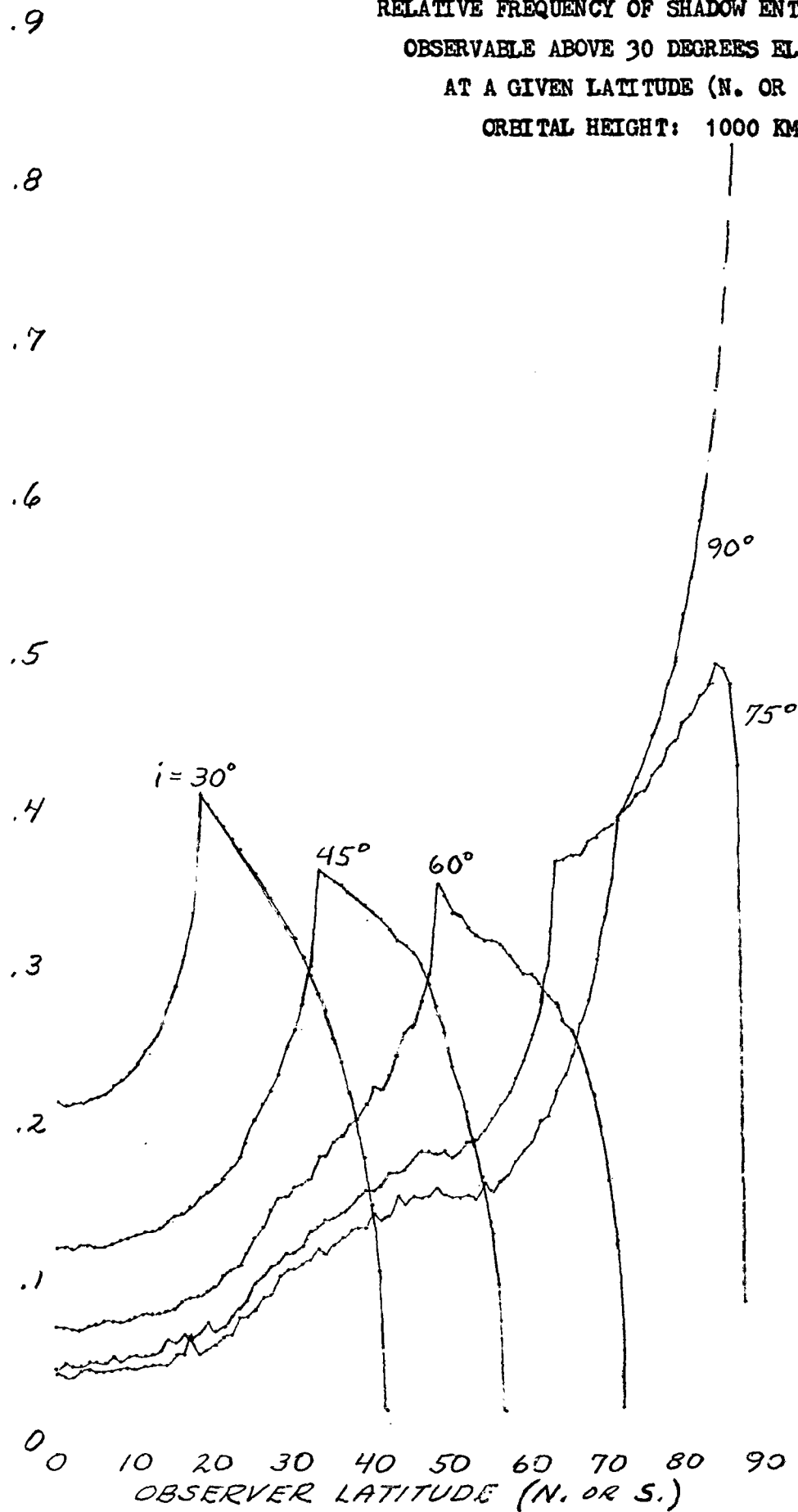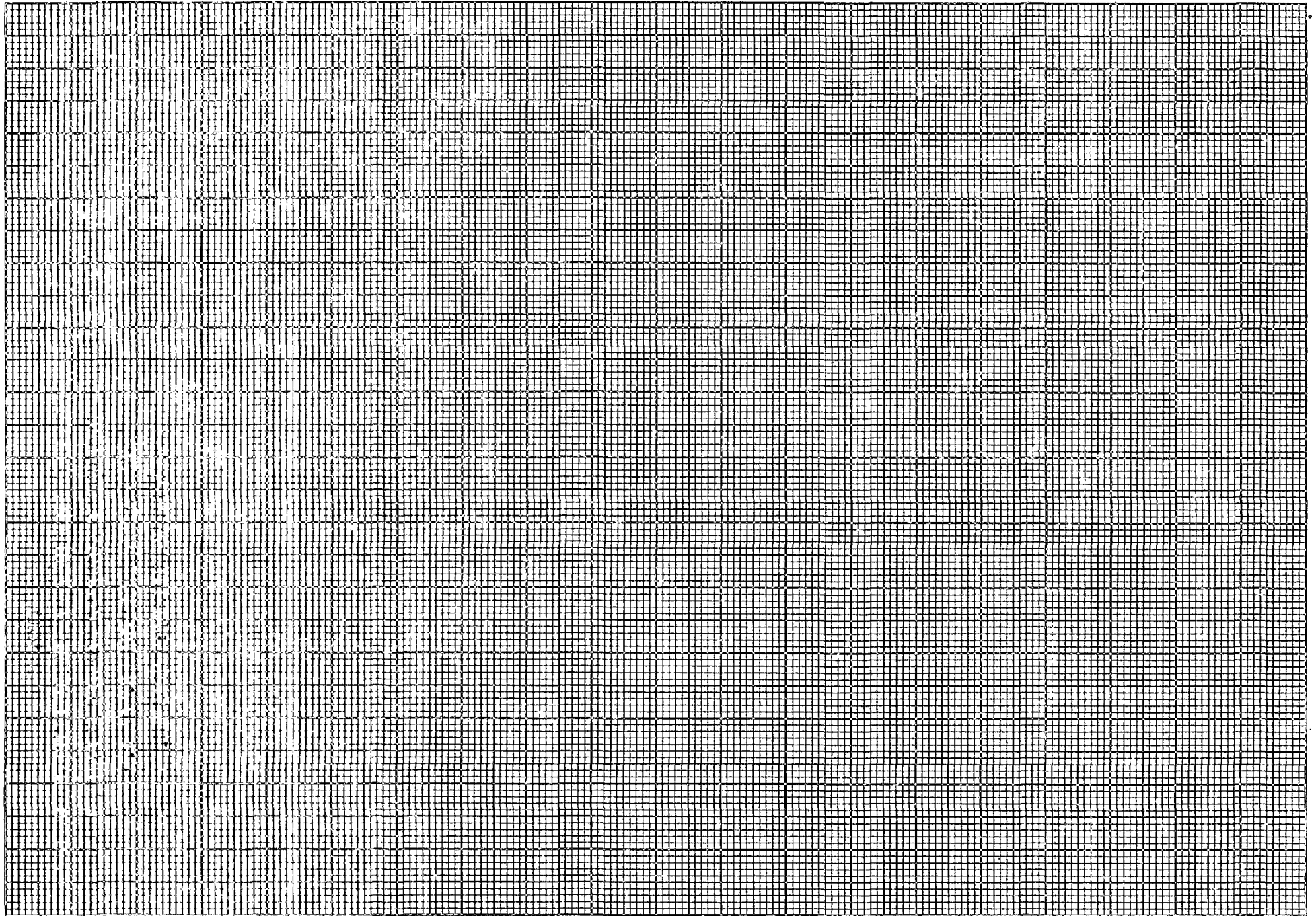
1600 KM

Figure 12

RELATIVE FREQUENCY OF SHADOW ENTRIES PER DAY
OBSERVABLE ABOVE 30 DEGREES ELEVATION
AT A GIVEN LATITUDE (N. OR S.)
ORBITAL HEIGHT: 1600 KM.

RELATIVE DAILY FREQUENCY OF SHADOW ENTRIES ABOVE 30° ELEVATION

$i = 30°$

45°

60°

75°   90°

OBSERVER LATITUDE (N. OR S.)

31
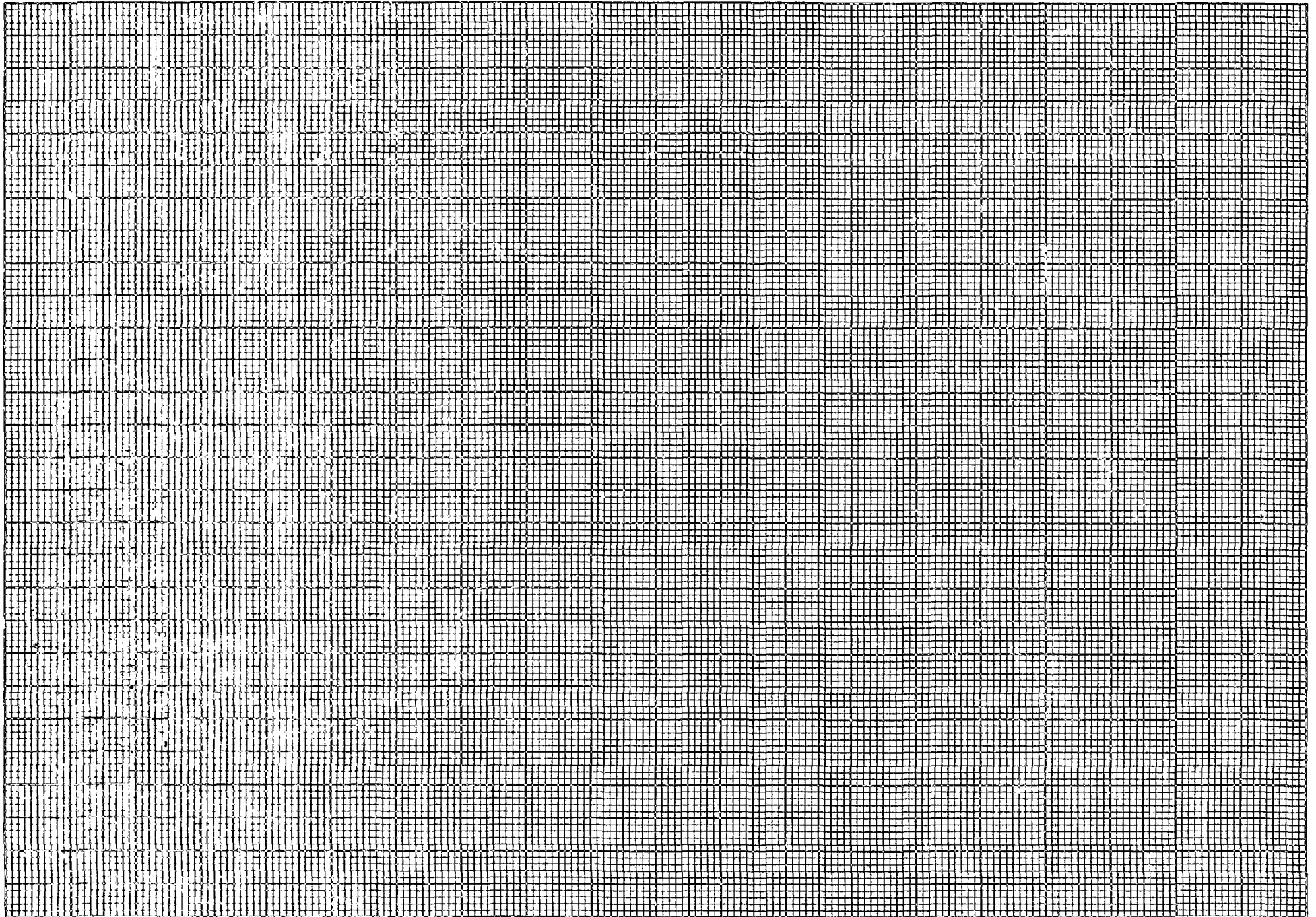
4200 KM

Figure 13

RELATIVE FREQUENCY OF SHADOW ENTRIES PER DAY
OBSERVABLE ABOVE 30 DEGREES ELEVATION
AT A GIVEN LATITUDE (N. OR S.)
ORBITAL HEIGHT: 4200 KM.

RELATIVE DAILY FREQUENCY OF SHADOW ENTRIES ABOVE 30° ELEVATION

OBSERVER LATITUDE (N. OR S.)

32
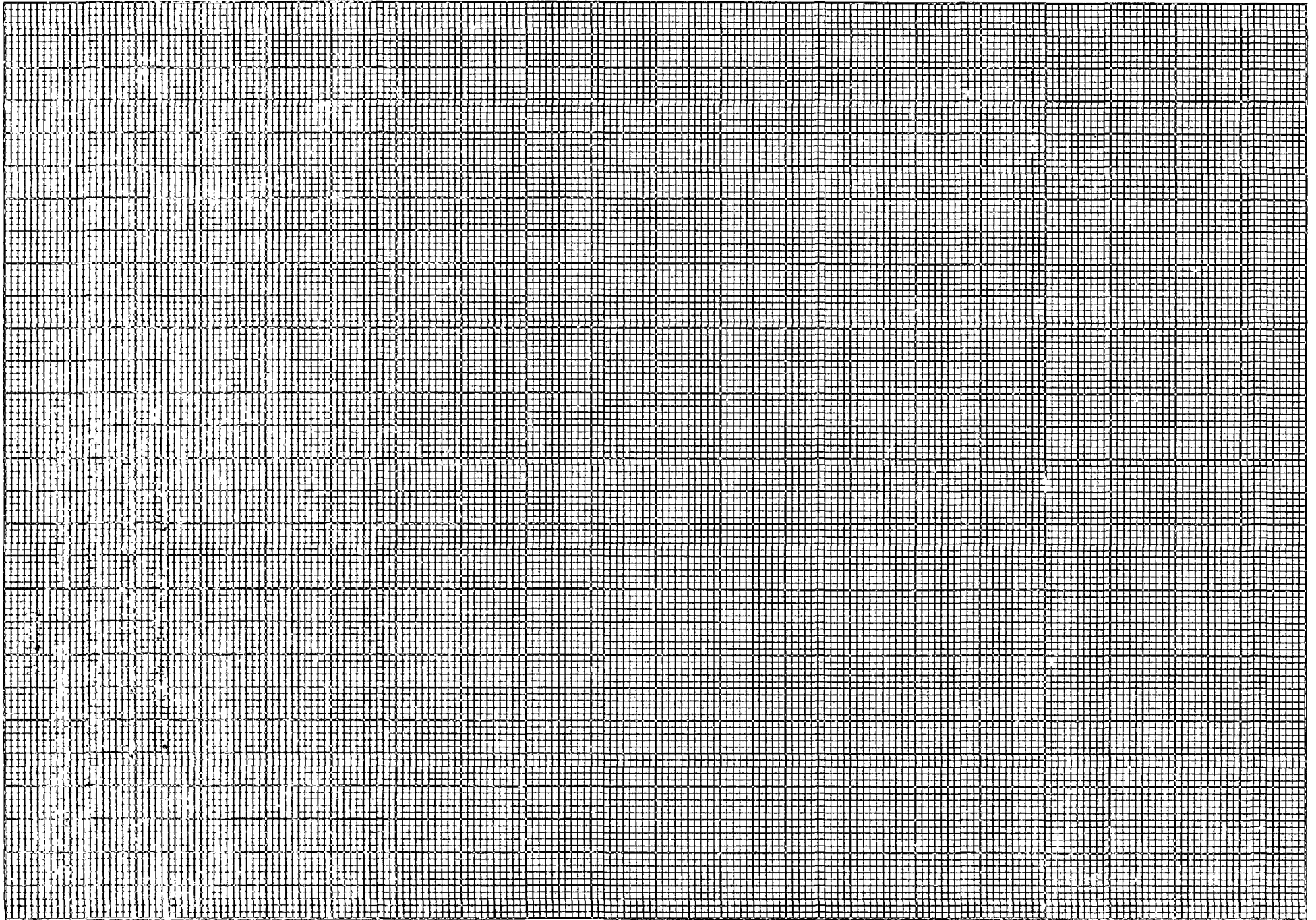
Figure 14

RELATIVE FREQUENCY OF SHADOW ENTRIES PER PASS
VERSUS TANGENT RAY LATITUDE (N. OR S.)
ORBITAL HEIGHT: 450 KM.
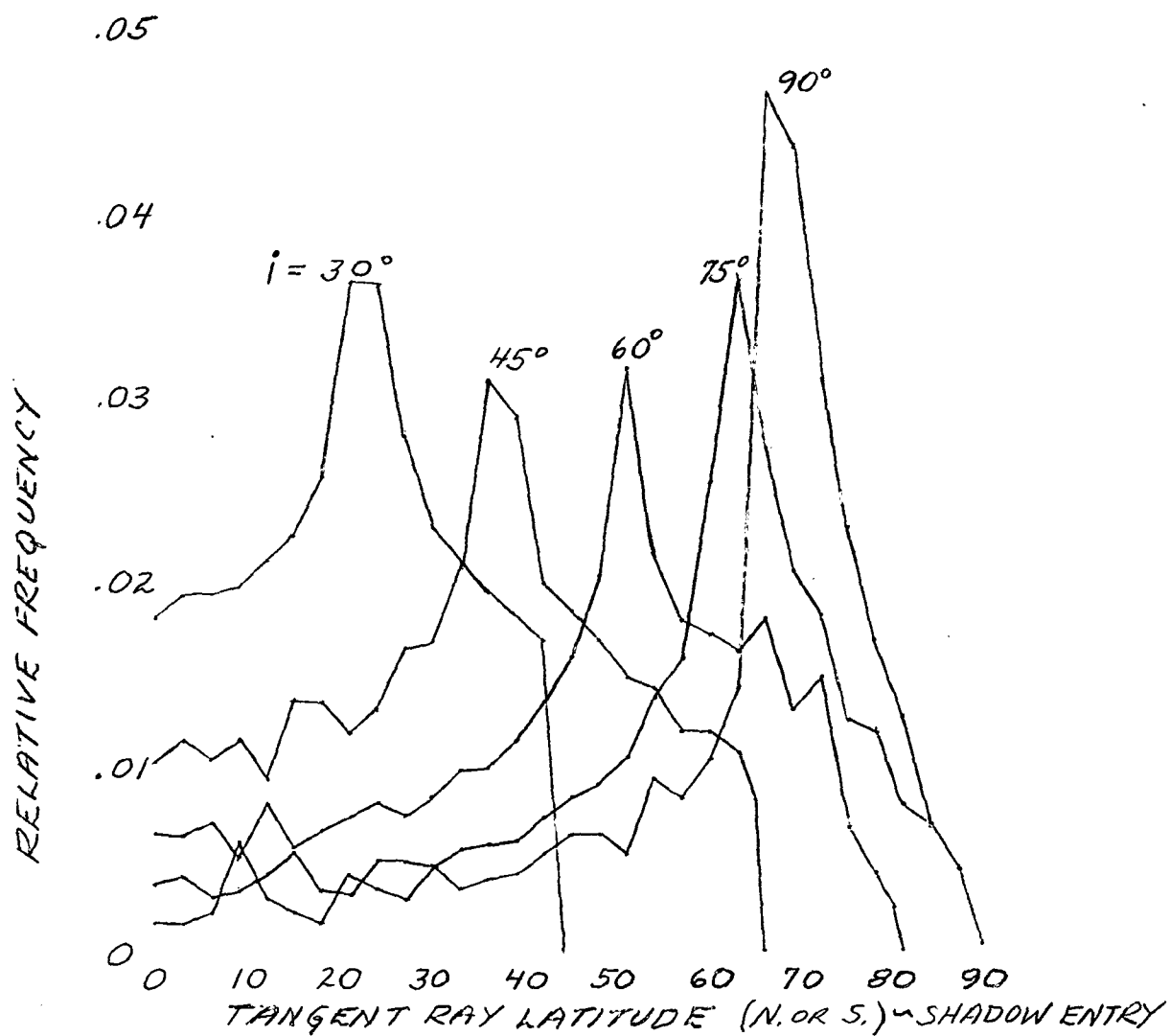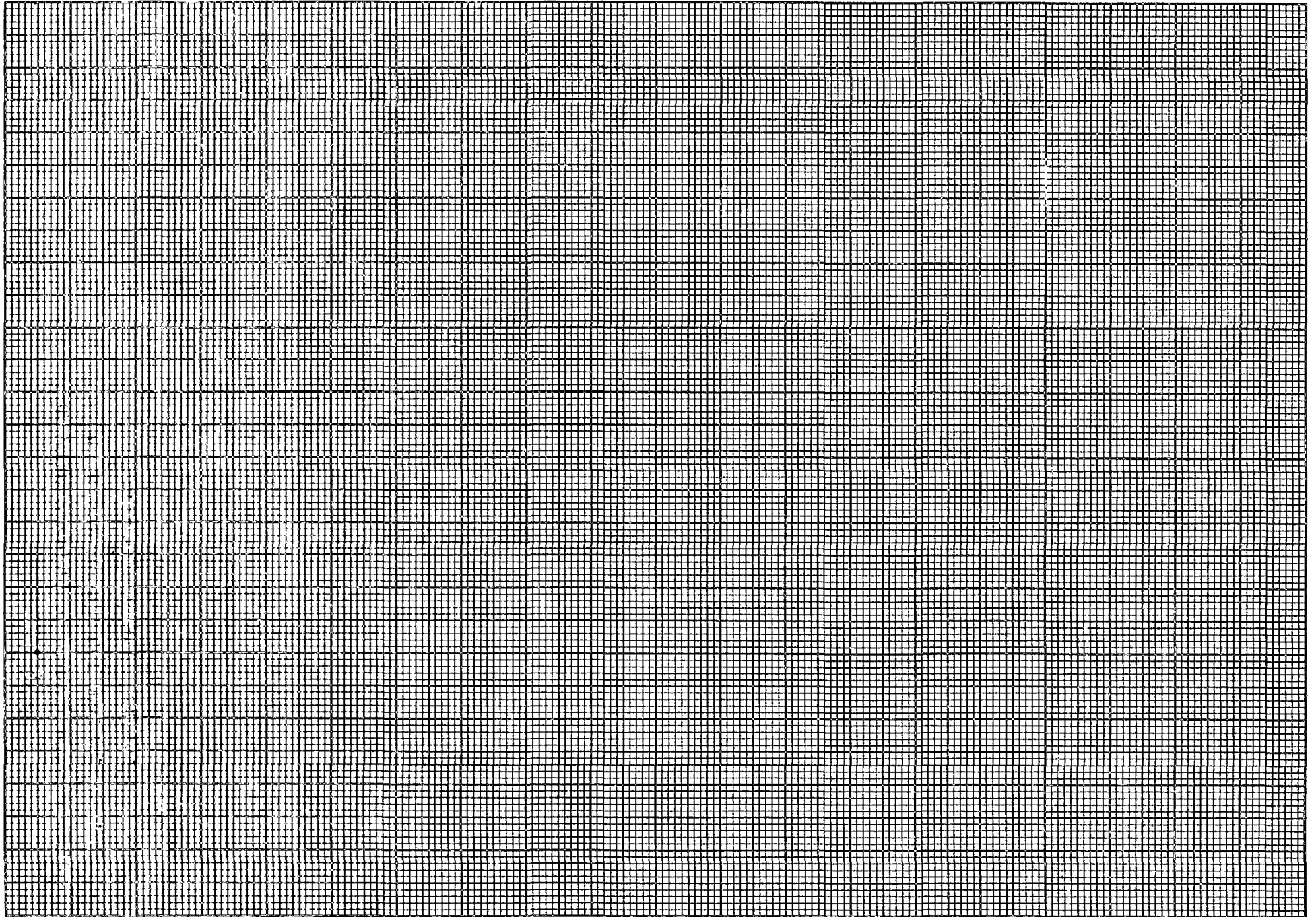
1000 KM

Figure 15

RELATIVE FREQUENCY OF SHADOW
ENTRIES PER PASS VERSUS
TANGENT RAY LATITUDE (N. OR S.)
ORBITAL HEIGHT: 1000 KM.

34
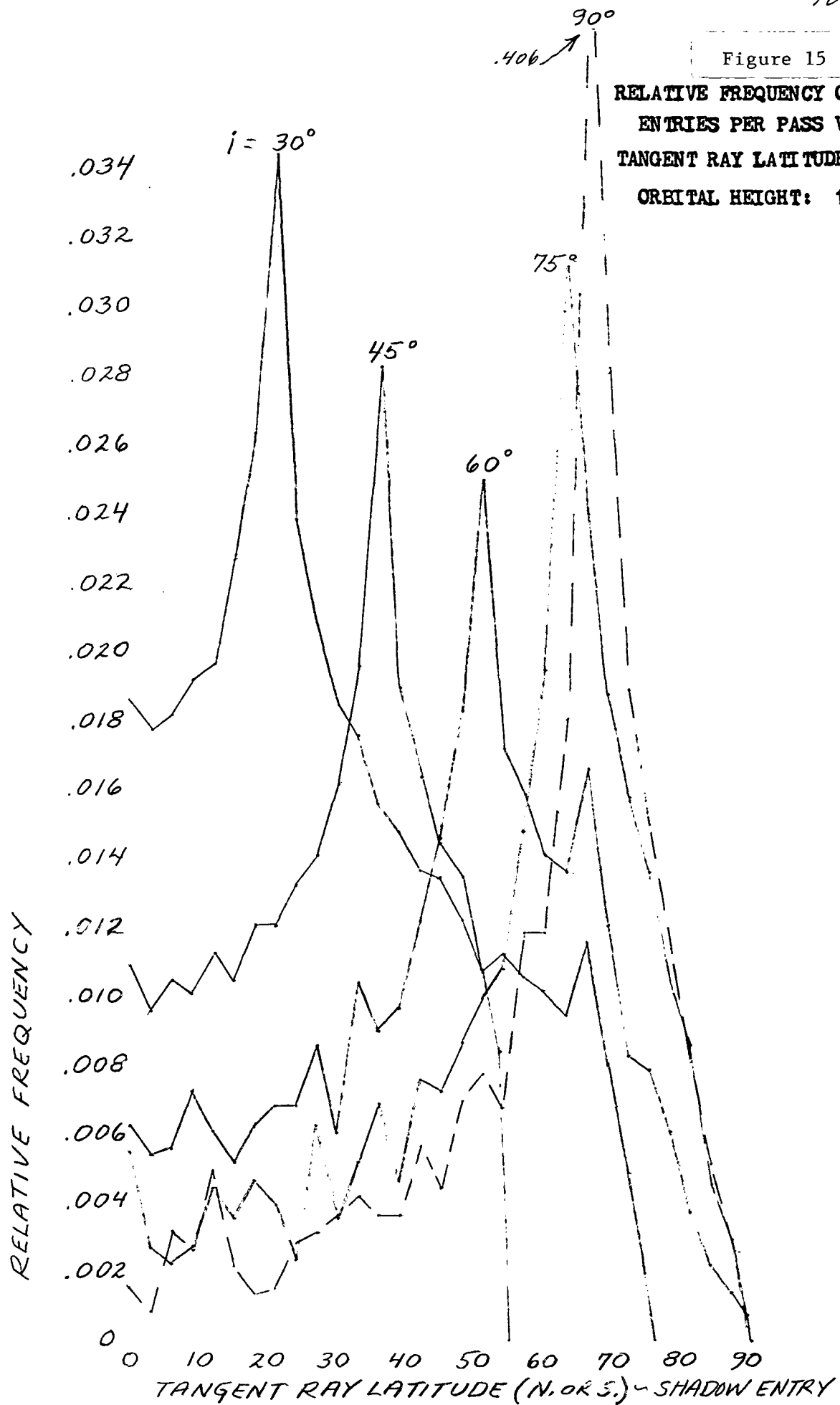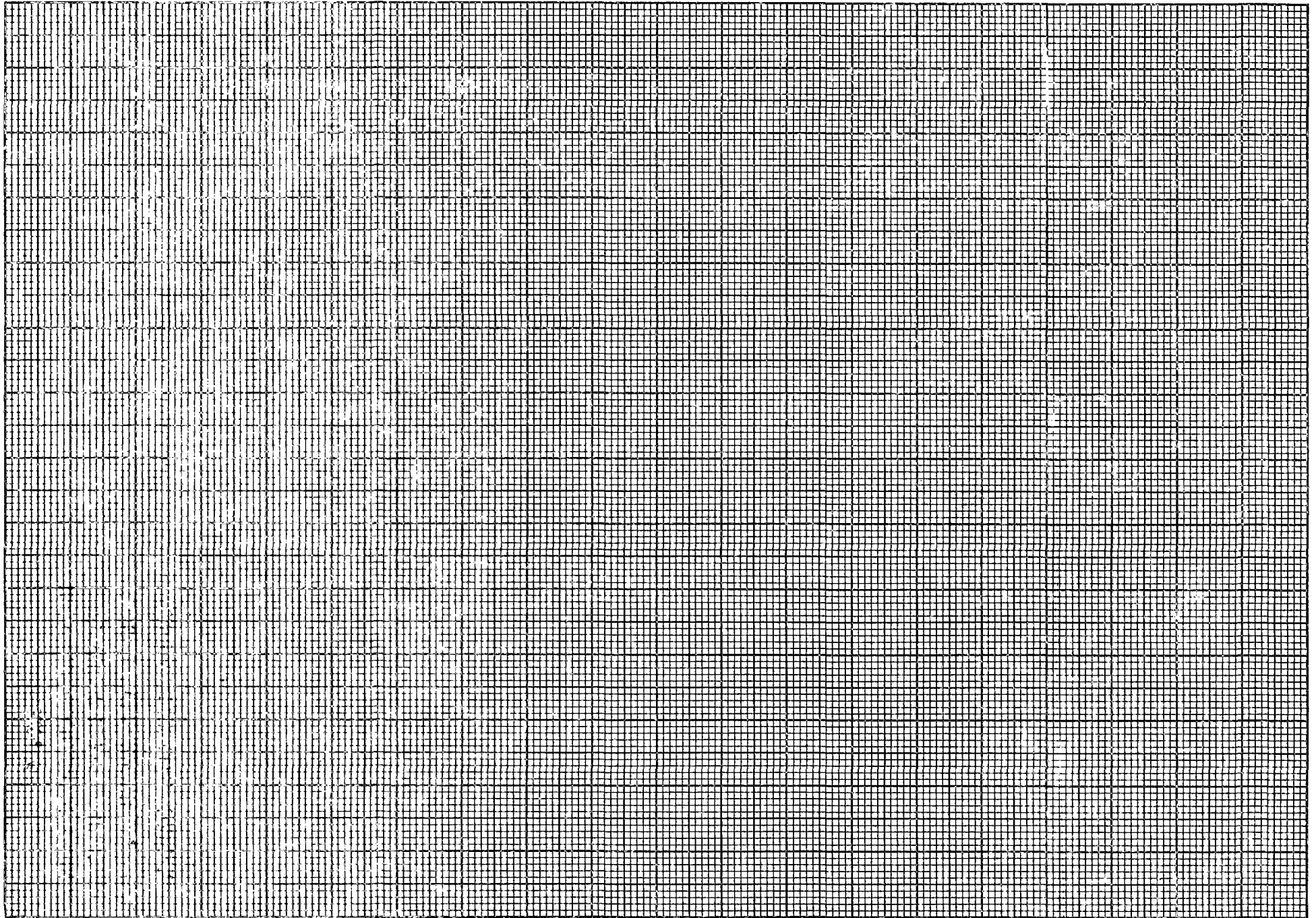
KEUFFEL & ESSER CO.

Figure 16

RELATIVE FREQUENCY OF SHADOW ENTRIES PER PASS
VERSUS TANGENT RAY LATITUDE (N. OR S.)
ORBITAL HEIGHT: 1600 KM.

35
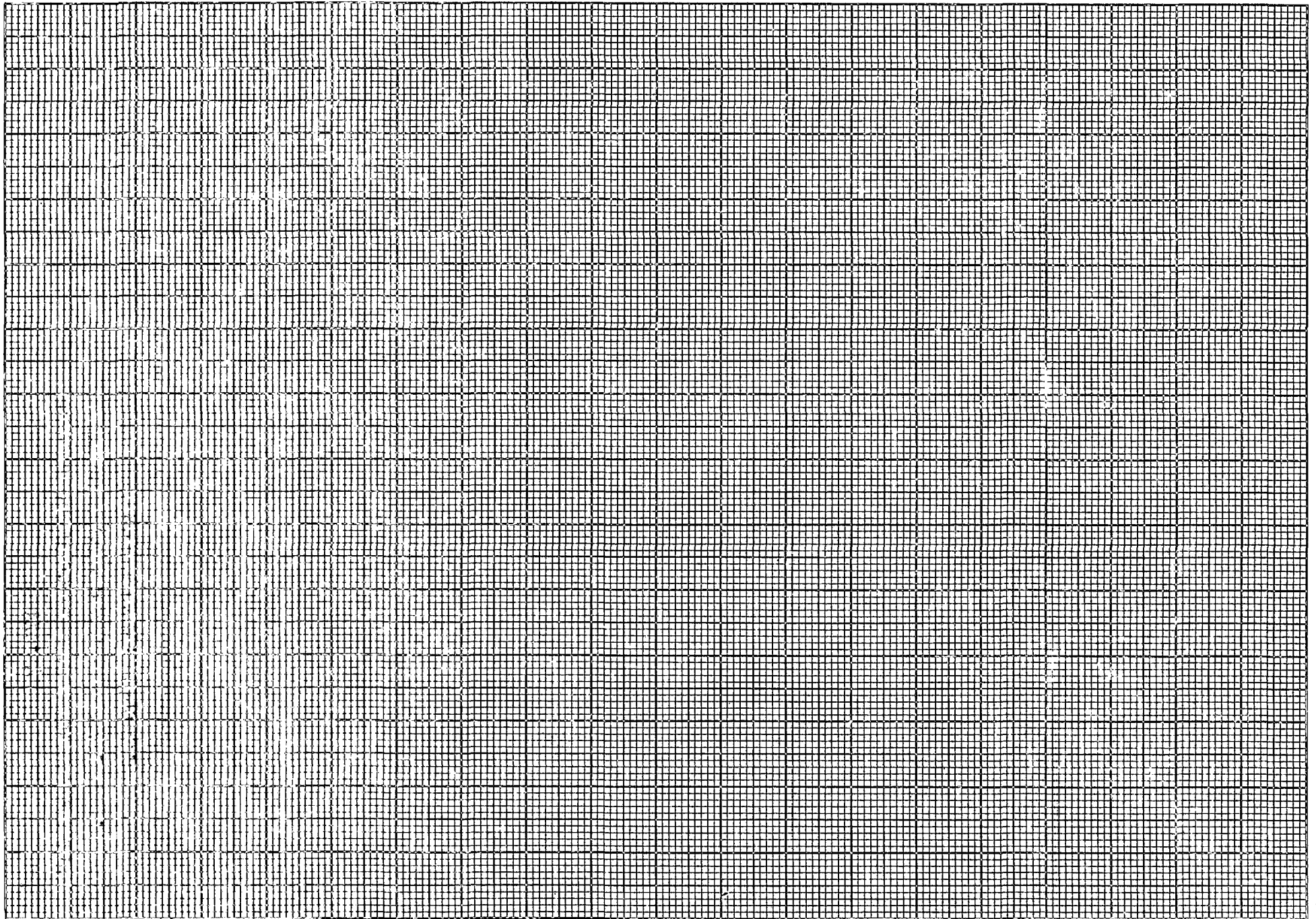
Figure 17

RELATIVE FREQUENCY OF SHADOW ENTRIES PER PASS
VERSUS TANGENT RAY LATITUDE (N. OR S.)
ORBITAL HEIGHT: 4200 KM.
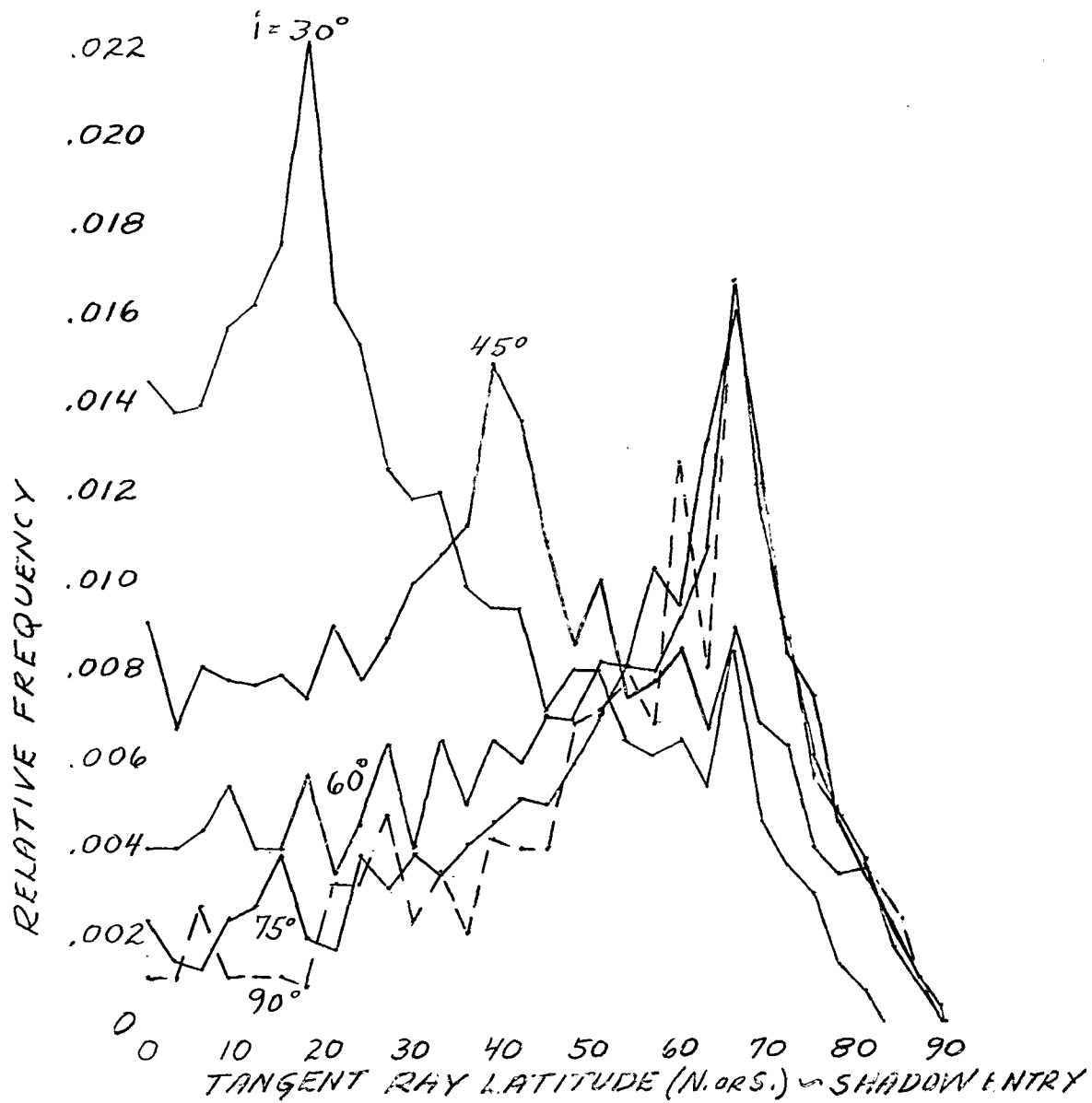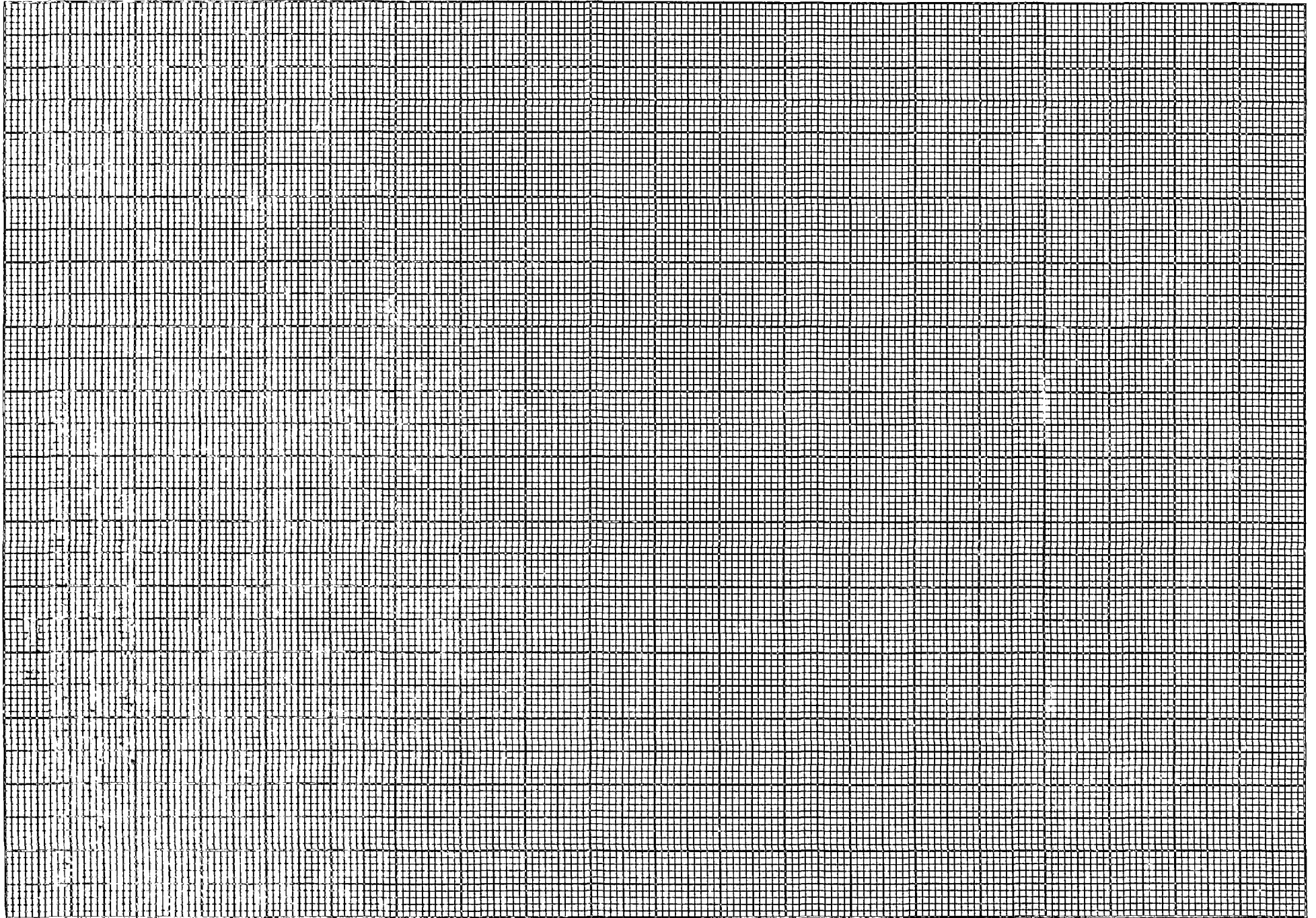
For low to moderate orbital heights and inclinations, a sharp maximum frequency occurs when the observer's latitude reaches the parallel at which the orbit's vertex rises above the poleward horizon to the specified minimum observational elevation (30 degrees). For these cases the remarkable sharpness and separation of the frequency maxima shows that observer mobility can be a positive asset in exploiting the shadow entry opportunities among a variety of target satellites.

Figures 14 through 17 are useful where there is interest in probing the ozone concentration at a particular latitude showing for selected orbits the relative frequency of shadow entries having a given latitude of sunset. Note that the frequency maxima for sunset latitudes tend to follow orbital inclination, although not closely. Frequency drops to zero at the geographic poles. For the middle latitudes moderately inclined orbits yield somewhat lower maximum frequencies. For a given sunset latitude the frequencies decrease as orbital altitudes increase.

While the results of these statistical studies provide guidance in preliminary program planning and target selection, specific mission planning will continue to depend upon the analyses of ephemerides for real satellites at postulated observing sites.

For an example of how these charts might be used, note that for ozone determination at a latitude of 35 degrees, a target satellite of low orbit (see Figure 14). Figure 10 shows that the maximum number of shadow entries for this orbit occurs at a site latitude of about 39 degrees, but whether this site is actually the optimum for the particular tangent ray latitude would require further investigation, as appropriate to specific mission planning.

Observing Site Considerations – Since the observatory is mobile there would seem to be complete freedom in choosing a site, on land, from which to perform the observations. In reality this far from being true. To be practical the site must offer a high probability of clear night skies. This, as always, remains a first consideration. High altitude is advantageous to reduce atmospheric extinction and sky brightness, but crew efficiency may be degraded above 3000 meters MSL. Site accessibility is certainly a practical consideration. These are all factors inherent in any astronomical observing mission, and are familiar to those who have planned the numerous missions of the mobile photometric observatory.

An important consideration that is new is the shadow entry observing mission is the desired latitude. The frequency of observable shadow entries is generally quite sensitive to latitude, as pointed out previously. For a specific target satellite the most desirable latitude is approximately equal to the satellite's inclination reduced by the great circle distance at which the satellite appears to the observer to be at an elevation of 30 degrees above the horizon. $(i - \Delta\phi)$.

For establishing the desired latitude for multiple target satellites in specific mission planning the following procedure is recommended.

Based on actual orbital elements of the selected target satellites, shadow entry latitudes are determined versus calendar date. (A geocentric ephemeris program such as Smithsonian's "Ephemeris VI" will suffice.) A graph is drawn of these results, similar to the example in Figure 18. Inspection of the graph, together with the assessed value of $\Delta\phi$ for each satellite (see Equation 21), will reveal desirable latitudes and preliminary calendar dates for the observing mission. The graph makes evident the latitudes and dates of maximum observational opportunities. When the desired latitude has been adjusted for other considerations and the site's actual latitude has been determined, actual topocentric ephemerides must be made to confirm the indicated observing window.

For example, Figure 18 shows shadow entry latitudes versus date for three satellites for which the information was readily available. The curves for Pageos and Explorer 19 terminate in all-sunlight orbits. The $\Delta\phi$ value for SKYLAB is 6 degress, for Pageos, 29 degress, and for Explorer 19, 11 degrees. Attention is drawn to the region of intersection of the SKYLAB and Explorer 19 curves. It is seen that for site latitude + 44 degrees shadow entries for both satellites should be observable in the same calendar period. SKYLAB's window appears to extend from August 22 through September 9, or 18 days. Explorer 19's window appears to extend from August 20 through October 1, or 42 days. By this approach we may find the latitude windows which appear promising, and then these may be fully investigated by topocentric ephemerides. It is to be expected that the full investigation will reduce the indicated window's calendar span.

Longitude is a less important consideration in site selection and generally may be chosen to satisfy other factors such as weather, economy, etc. There may be a longitude preference where simultaneous positional data is to be taken at an established tracking site, for improved geometric accuracy. Also, it is possible that due to phasing in the times of the satellite passes an adjustment of site longitude would be beneficial.

For shadow entry observations, more than for any other satellite photometry mission, it is clear that the mobility of the observatory is a positive asset. No one site can continuously provide the maximum density of shadow entry opportunities.

Available Satellites

Criteria for Target Satellites - In the selection of target satellites the essential requirement is that the satellite be sufficiently bright that it may undergo several (at least two) stellar magnitudes of attenuation during shadow entry and still provide measurable photometric signals in the narrow band channels. Engineering study of the capability of the up-graded photometric system shows that narrow band signals from a source that is attenuated down to a broad band visual magnitude of + 7 will be measurable (see the following section). It follows that a target satellite, before shadow entry, should be no fainter than magnitude 5. Since most satellites vary in brightness, it is their minimum illuminance to which this criterion must be applied. Target variability itself may be tolerated since the methodology of ozone determination depends upon the ratio of narrow band intensities rather than their absolute values.

Figure 18. *EXAMPLE SHADOW ENTRY LATITUDES (ACTUAL)*
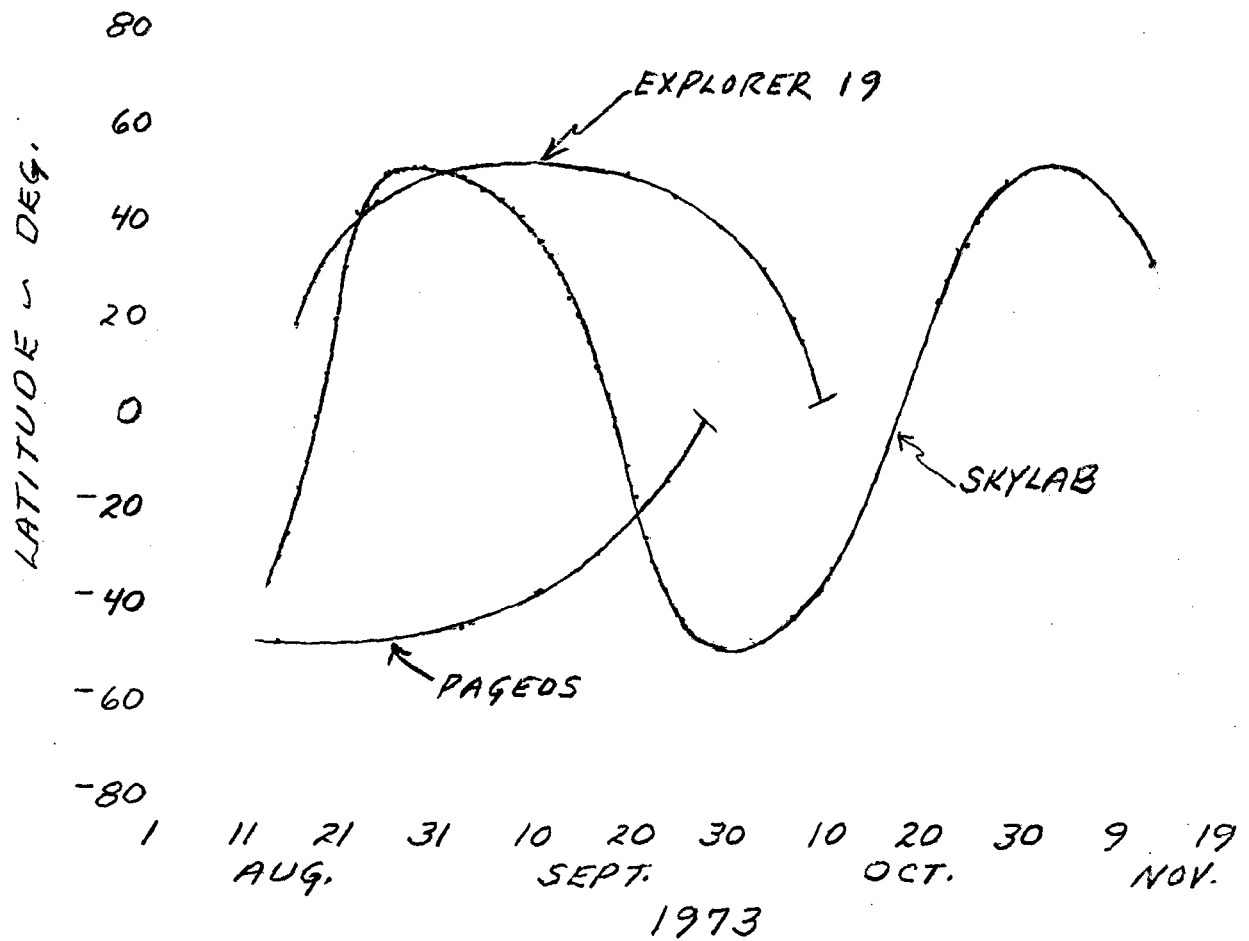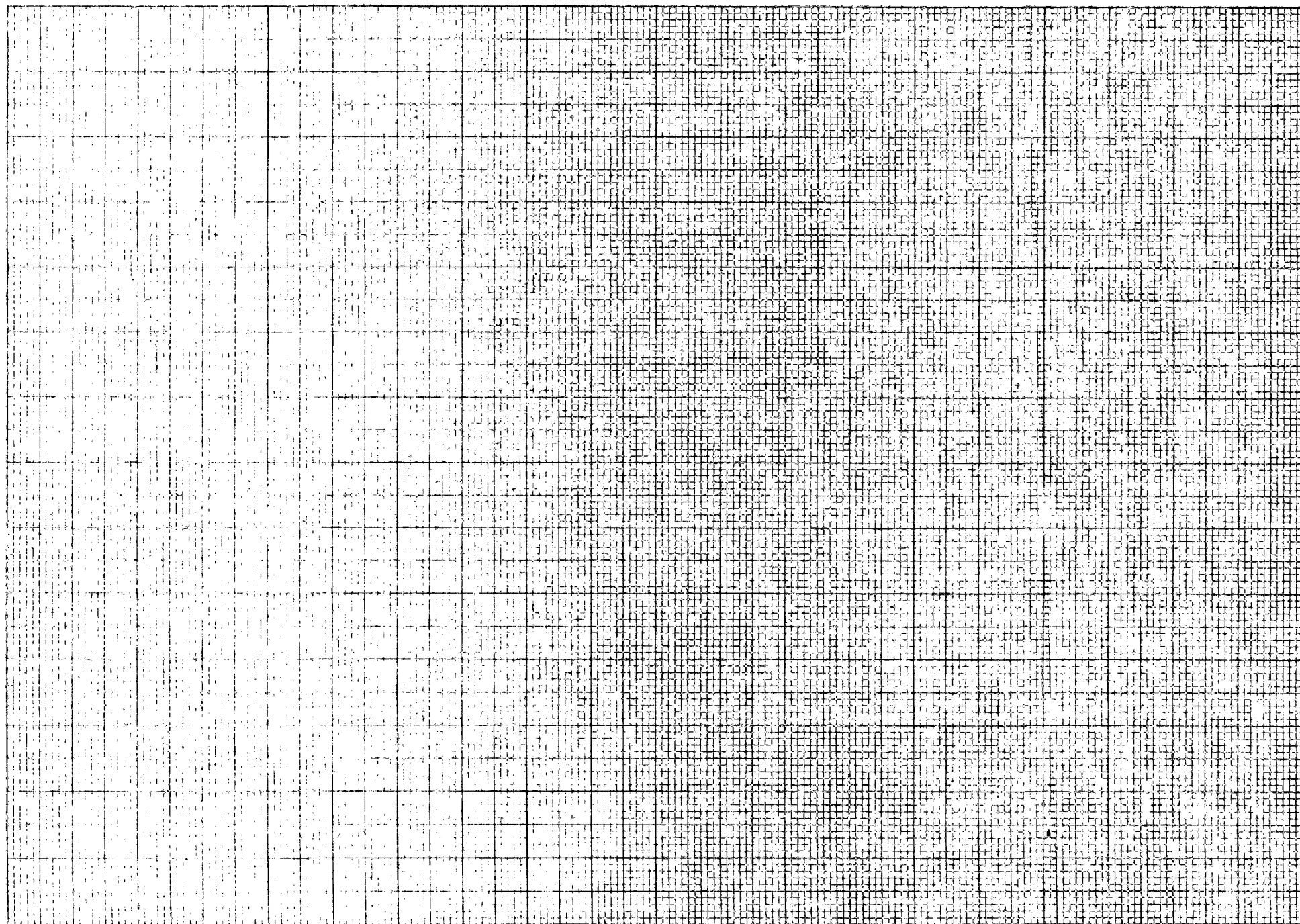
The second consideration in target selection is the accuracy with which the geometry associated with the observation can subsequently be defined. Preference should be given to those satellites whose orbits can be well defined, i.e., satellites having a high mass-to-area ratio and with orbital heights in the more stable 500 to 1000 km range. Thus payload satellites generally would be perferred to spent rocket bodies.

Since grazing shadow entries permit longer signal integration times and/or enable the taking of a greater number of data points, and also may relax final orbit accuracy requirements, consideration should be given to the target satellite's (A - i) orbital parameter, as explained in the following paragraphs. (See Equation 22.)

To maximize opportunities for grazing shadow entries the (A - i) parameter should be about -23 degrees. When the value of this parameter exceeds + 23 degrees no grazing shadow entries are possible.

If the latitude of the observing site can be assumed, the relative frequency of shadow entries can be approximated for candidate target satellites using graphs presented in this section. A satellite having a higher relative frequency of shadow entries obviously is to be preferred.

Finally, there could be compelling reason to select a particular satellite simply for the specific tangent ray (sunset) latitude it would probe during a given window of shadow entries, but this selection could result only from a thorough special investigation of the specific case.

Although these various considerations need be kept in mind during the target selection, compromise with all except the essential brightness requirement appears inevitable if any significant population of candidate targets is to be established.

List of Brightest Satellites - To assist in the selection of candidate target satellites an "Approximate List" of the 129 brightest satellites currently in orbit has been compiled (Table I). The table is self-explanatory, with several footnotes.

The list generally proceeds from the brightest to the fainter satellites but since reference magnitudes may differ, or one reference magnitude may be missing, in places the order is somewhat arbitrary.

It is estimated that the list is more than 90 percent complete for satellites brighter than visual magnitude 5 that are of special interest here. The list extends to some fainter satellites to include the brightest of the laser-tracked satellites, ERTS-1, whose orbit is being routinely determined to 100 meter accuracy.

The magnitude ranges have been furnished through the courtesies of Mr. Michael McCants, an experienced volunteer satellite observer at Austin, Texas, and Mr. Albert Werner, Chief of the Moonwatch Division of the Smithsonian Astrophysical Observatory, Cambridge, Massachusetts. Mr. McCants' magnitudes are from his own observations; Mr. Werner's magnitudes were compiled from sources available to him. Where these authorities appear to differ, the extreme magnitude should be used.

Table I. "APPROXIMATE LIST" OF BRIGHTEST SATELLITES (1973)

INT'L DESIG.	CATALOG NO.	NAME	RANGE OF APPARENT M_v				MEAN H (Km)	ΔH ± Km	i	A	A - i
			Ref. M		Ref. W						
73-027 B	6634	SKYLAB R	-2	2	0	1	398	38	50.0°	70.3°	20.3°
73-027 A	6633	SKYLAB	-1	3	0	0	432	8	50.0	69.5	19.5
65-009 A	1085	PEGASUS 1	-1	5	2	4	496	54	31.7	68.1	36.4
65-039 A	1381	PEGASUS 2	-1	6	4	5	535	66	31.7	67.3	35.6
68-110 B	3598	OAO-A2 R	0	6	1	5	764	47	34.9	63.3	28.4
65-009 B	1088	PEGASUS 1 CM	1	4			580	96	31.7	66.4	34.7
65-039 B	1385	PEGASUS 2 CM	1	5			593	96	31.7	66.2	34.5
65-060 B	1468	PEGASUS 3 CM	1	6			404	4	28.8	70.1	41.3
63-047 A	694	CENTAUR 2	1	7			1089	617	30.3	58.7	28.4
66-056 A	2253	PAGEOS	2	5	2	5	4190	811	86.3	37.1	-49.2
70-111 B	4807	COSMOS 387 R	2	5	4	6	506	10	74.0	67.9	-6.1
71-013 B	4956	COSMOS 395 R	3	7	2	5	519	14	74.0	67.6	-6.4
67-073 B	2896	OGO-4 R	4	8	2	4	408	62	85.9	70.0	-15.9
67-027 B	2721	COSMOS 151 R	3	5	3	4	600	26	56.0	66.1	10.1
71-103 B	5629	COSMOS 460 R	3	3+			515	18	74.0	67.7	-6.3
69-070 B	4071	COSMOS 292 R	5	8+	3	4	747	14	74.0	63.5	-10.5
68-095 B	3527	COSMOS 250 R	3	5	3	4	462	5	74.0	68.8	-5.2
68-070 B	3349	COSMOS 236 R	4	6+	3	4	582	26	56.0	66.4	10.4
69-021 B	3776	COSMOS 269 R			3	5	474	3	74.1	68.6	-5.5
67-104 B	3019	COSMOS 185 R	3	6+	3	5	676	152	64.0	64.7	0.7
71-075 B	5467	COSMOS 437 R	3	7+	3	5	516	13	74.0	67.7	-6.3
67-108 B	3023	COSMOS 189 R	3	5+	4	4	506	18	73.9	67.9	-6.0
67-102 B	3011	COSMOS 184 R	3	6	4	5	610	79	81.1	65.9	-15.2
70-024 B	4361	COSMOS 330 R	3	5	5	5	494	15	74.0	68.1	-5.9
66-038 B	2169	COSMOS 118 R	3	5	6	6	592	38	64.9	66.2	1.3
64-053 A	876	COSMOS 44	3	6+	6	6	728	132	65.0	63.8	-1.2
71-052 B	5282	COSMOS 426 R	4	6+	3	5	1170	784	74.0	57.7	-16.3

Table I. Continued

INT'L DESIG.	CAT. NO.	NAME	RANGE OF APPARENT M_v				MEAN H (Km)	ΔH ± Km	i	A	A -1
			Ref.M^c		Ref.W						
72-017 B	5895	COSMOS 479 R	3	5+	5	5	514	24	74.0°	67.7°	-6.3°
68-019 A	3150	COSMOS 206	3	5+			598	16	81.2	66.1	-15.1
70-113 A	4813	COSMOS 389	3	6			662	24	81.1	65.0	-16.1
69-068 B	4066	PAC-A	3	6			436	19	32.9	69.4	36.5
71-060 A	5329		5	5+	3	6	473	7	74.9	68.6	-6.3
65-081 B	1625	OGO 2 R	5+	7	3	6	848	439	87.3	62.0	-25.3
68-110 A	3597	OAO-A2	3	6+			769	5	35.0	63.2	28.2
71-105 B	5644	COSMOS 461 R	3	7+			476	18	69.2	68.5	-0.7
69-107 B	4274	COSMOS 315 R	3	7+			480	9	74.0	68.4	-5.6
65-053 F	1448	COSMOS 71-75 R	3	7+			556	37	56.0	66.9	10.9
64-031 C	815		3	8			830	10	99.8	62.2	-18.0
66-031 A	2142	OAO-A1	3	8+			796	6	35.0	62.8	27.8
69-051 B	3987	OGO 6 R	3	8+			655	257	81.9	65.1	-16.8
61-Alpha 1	70	SAMOS 2	3	?			307	6	97.2	72.6	-10.2
66-057 B	2257	COSMOS 122 R	3+	6			586	88	64.9	66.3	1.4
64-052 B	878	NIMBUS 1 R	3+	?			424	64	98.6	69.7	-11.7
71-028 B	5118	COSMOS 405 R	3+	6+			680	66	81.2	64.6	-16.6
67-053 B	2825	SURCAL	3+	7			919	4	69.9	60.9	-9.0
65-106 B	1844	COSMOS 100 R	3+	7+			629	14	65.0	65.5	0.5
65-027 A	1314	SNAPSHOT	3+	7+	6	6	1296	22	90.3	56.2	-33.5
69-018 C	3771	APOLLO 9 LMA	3+	7+			2748	2524	28.9	44.3	15.4
72-106 A	6328	COSMOS 542			4	4	582	58	81.2	66.4	-14.8
70-066 A	4503		4	4+	4	4	421	5	74.9	69.7	-5.2
70-064 B	4498	COSMOS 358 R	4+	7+	4	4	490	18	74.0	68.2	-5.8
69-029 B	3836	METEOR 1 R	4+	4+	4	4	(651)	(23)	81.1	65.1	-16.0
60-ZETA 1	0043	MIDAS 2	4	5			320	2	33.0	72.2	29.2
72-088 B	6273	COSMOS 536 R			4	5	522	28	74.0	67.6	-6.4
72-053 B	6098	COSMOS 500 R			4	5	516	24	74.0	67.7	-6.3

42

Table I. Continued

INT'N'L DESIG.	CAT. NO.	NAME	RANGE OF APPARENT M_v				MEAN H (Km)	ΔH ± Km	i	A	A - i
			Ref.M^c		Ref.W						
70-019 B	4350	METEOR 3 R	4	5+	4	5	574	112	81.1	66.6	-14.5
69-021 A	3775	COSMOS 269	4	5+			468	5	74.0	68.7	-5.3
67-039 B	2763	COSMOS 156 R	4+	4+	4	5	605	74	81.1	66.0	-15.1
71-050 B	5254	COSMOS 425 R			4	5	512	28	74.0	67.8	-6.2
65-053 B	1442	COSMOS 72			4	5	493	20	56.0	68.2	12.2
70-113 B	4814	COSMOS 389 R	4+	9	4	5	663	62	81.1	64.9	-16.2
63-053 A	714	EXPLORER 19	4	5+	4	6	1295	539	78.7	56.2	-22.5
73-003 B	6344	COSMOS 544 R			4	6	520	23	74.0	67.6	-6.4
68-090 A	3503	COSMOS 248	4+	7	4	7	466	62	62.2	68.7	6.5
66-057 A	2254	COSMOS 122	4+	6+	5	5	594	32	64.9	66.2	1.3
71-028 A	5117	COSMOS 405	4	7	5	5	676	2	81.2	64.7	-16.5
71-010 B	4923	COSMOS 394 R	4	7+	5	5	582	33	65.8	66.4	0.6
71-031 B	5143	METEOR 8 R	4	8	5	6	627	77	81.2	65.6	-15.6
70-111 A	4806	COSMOS 387	4+	7	5	6	514	4	73.9	67.7	-6.2
68-049 B	3283	COSMOS 226 R	4	5	6	6	604	84	81.2	66.0	-15.2
68-040 B	3230	COSMOS 220 R	4	6+	6	7	712	40	74.0	64.1	-9.9
68-019 B	3151	COSMOS 206 R	4	6			614	80	81.2	65.8	-15.4
69-107 A	4273	COSMOS 315	4	6			484	9	74.0	68.4	-5.6
67-018 B	2696	COSMOS 144 R	4	6+			589	80	81.2	66.3	-14.9
67-116 A	3047	COSMOS 192	4	6+			746	5	74.0	63.5	-10.5
71-111 B	5685	COSMOS 465 R	4	6+			986	16	74.0	60.0	-14.0
70-085 B	4584	METEOR 6 R	4	6+			638	89	81.2	65.4	-15.8
70-087 A	4590	COSMOS 373	4	7			486	127	62.9	68.3	5.4
71-031 A	5142	METEOR 8	4	7			617	12	81.2	65.8	-15.4
70-028 B	4370	COSMOS 332 R	4	7+			751	13	74.0	63.5	-10.5
69-084 B	4120	METEOR 2 R	4	7+			640	24	81.2	65.3	-15.9
66-031 B	2144	OAO 1 R	4	8+			790	9	35.0	62.8	27.8

Table I. Continued

INT'N'L DESIG.	CAT. NO.	NAME	RANGE OF APPARENT M_v		MEAN H (Km)	$\triangle$ H ± Km	i	A	A - i
			Ref.M^c	Ref.W					
70-108 B	4800	COSMOS 385 R	4 8+		976	6	74.0	60.1	-13.9
68-106 B	3577	COSMOS 256 R	4 9+		1194	25	74.0	57.4	-16.6
64-076 C	933	EXPLORER 24 R	4 ?		1491	959	81.3	54.1	-27.2
65-014 B	1098	COSMOS 58 R	4 ?		580	74	65.0	66.4	1.4
69-091 B	4139	COSMOS 304 R	4 ?		742	12	74.0	63.6	-10.4
67-116 B	3048	COSMOS 192 R	4+ 5+		748	7	74.0	63.5	-10.5
71-013 A	4955	COSMOS 395	4+ 5+		522	12	74.0	67.6	-6.4
71-103 A	5628	COSMOS 460	4+ 6		518	6	74.0	67.7	-6.3
72-005 B	5815	HEOS A2 R	4+ 6+	6 ?	652	341	89.7	65.1	-24.6
65-106 A	1843	COSMOS 100	4+ 6+		635	88	65.0	65.4	0.4
70-019 A	4349	METEOR 3	4+ 6+		568	42	81.1	66.7	-14.4
71-003 A	4849	METEOR 7	4+ 6+		640	14	81.2	65.3	-15.9
67-045 B	2802	COSMOS 158 R	4+ 7		786	58	74.0	62.9	-11.1
69-051 A	3986	OGO 6	4+ 7+		646	260	81.9	65.2	-16.7
71-003 B	4850	METEOR 7 R	4+ 7+		647	83	81.2	65.2	-16.0
70-086 B	4589	COSMOS 372 R	4+ 8		790	16	74.0	62.8	-11.2
70-047 B	4420	METEOR 5 R	4+ 8	5 7	867	55	81.2	61.7	-19.5
66-025 B	2122	OV1 5	4+ 9+		1021	35	144.6	59.5	24.1
68-066 A	3337	EXPLORER 39	5 6+	5 5	1468	744	80.7	54.4	-26.3
70-083 B	4579	COSMOS 371 R	5 8+	5 5	748	10	74.0	63.5	-10.5
71-054 A	5285	OPS 3850		5 5	554	15	90.2	66.9	-22.9
72-058 B	6127	ERTS 1 R		5 5	772	137	98.4	63.1	-18.5
71-114 B	5707	COSMOS 468 R		5 5	794	20	74.0	62.8	-11.2
72-106 B	6329	COSMOS 542 R		5 5	584	75	81.2	66.4	-14.8
71-059 B	5328	METEOR 9 R		5 5	636	81	81.2	65.4	-15.8
71-114 A	5705	COSMOS 468	5+ 6	5 5	796	12	74.0	62.8	-11.2
70-034 B	4392	CHINA 1 R	5+ 8	5 5	1362	930	68.4	55.5	-12.9
64-053 B	877	COSMOS 44 R	5 6+	5 6	734	69	65.0	63.7	-1.3

44

Table I. Continued

INT'N'L DESIG.	CAT. NO.	NAME	RANGE OF APPARENT M_v				MEAN H (Km)	ΔH ± Km	i	A	A - i
			Ref.M^c		Ref.W						
69-029 A	3835	METEOR 1	5	?	5	6	651	23	81.1°	65.1°	-16.0°
72-053 A	6097	COSMOS 500			5	6	520	17	74.0	67.6	-6.4
72-082 A	6235	NOAA-2			5	7	1454	3	101.7	54.5	-23.8
72-074 B	6207	COSMOS 521 R			5	7	988	2	65.8	60.0	-5.8
72-088 A	6272	COSMOS 536			5	7	528	20	74.0	67.4	-6.6
73-015 B	6393	METEOR 14 R			5	7	888	43	81.2	61.4	-19.8
72-065 A	6153	OAO 3	5	6+			740	5	35.0	63.6	28.6
71-038 B	5181	COSMOS 409 R	5	6+			1190	20	73.9	57.4	-16.5
64-001 A	727		5	6+	6	6	921	11	69.9	60.9	-9.0
68-070 A	3347	COSMOS 236	5	6+	6	6	594	17	56.0	66.2	10.2
71-035 B	5175	COSMOS 407 R	5	8+			800	23	74.0	62.7	-11.3
71-120 B	5732	METEOR 10 R	5	8+			886	44	81.2	61.4	-19.8
71-041 J	5218	COSMOS 411+ R	5	11+			1539	52	74.0	53.7	-20.3
64-063 A	893		5	?			1056	20	89.8	59.1	-21.1
67-108 A	3021	COSMOS 189	5+	6+	6	6	462	13	73.9	68.8	-5.1
68-023 A	3158	COSMOS 209	5+	9+	6	6	908	33	65.3	61.1	-4.2
72-009 B	5847	COSMOS 475 R	5+	?			974	21	74.0	60.2	-13.8
71-075 A	5466	COSMOS 437	5+	7+	6	7	520	15	74.0	67.6	-6.4
72-058 A	6126	ERTS 1 laser tracked	8	8	6	6	911	8	99.0	61.0	-20.0

Reference M^c — extremes of observed magnitudes at altitudes above 30 degrees, courtesy of Mr. Michael McCants, Austin, Texas, volunteer satellite observer (except magnitudes for satellites 6633 and 6634 were observed by R. H. Emmons, North Canton, Ohio)

Reference W — approximate magnitude ranges from available sources, courtesy of Mr. Albert Werner, Chief, Moonwatch Division, Smithsonian Astrophysical Observatory, Cambridge, Massachusetts

H — Orbital Height

+ — Fainter Than

i — Orbital Inclination

$$A = \sin^{-1} [R/(R + H)]$$

where R = earth's radius

Usable Target Satellites - Inspection of the list of 129 brightest satellites (Table I) reveals that 25 of these meet the essential brightness requirement, i.e., there are 25 for which neither reference shows a minimum brightness fainter than stellar magnitude 5. These are collected in the following table, together with qualifying remarks. It should be noted this list of usable targets could be readily extended to include additional variable satellites if a tolerable risk were accepted that the satellite will not be at its minimal brightness at the time of shadow entry.

<p style="text-align:center">Table II.   Usable Target Satellites</p>

Satellite	Maximum Brightness	Δ M	Remarks
Skylab Rocket	-2	4	Low Orbit
Skylab	-1	4	Payload; Low Orbit
Pegasus 1	-1	6	(A - i) > + 23°
Pegasus 1 CM	1	3	(A - i) > + 23°
Pegasus 2 CM	1	4	(A - i) > + 23°
Pageos	2	3	Very Low Density, High Orbit
Cosmos 151 Rocket	3	2	
Cosmos 460 Rocket	3	1	
Cosmos 250 Rocket	3	2	
Cosmos 269 Rocket	3	2	
Cosmos 330 Rocket	3	2	
Cosmos 542	4	0	Payload
70-066 A	4	1	Payload, Low Orbit
Meteor 1 Rocket	4	1	
Midas 2	4	1	(A - i) > + 23°, Low Orbit
Cosmos 536 Rocket	4	1	
Cosmos 500 Rocket	4	1	
Cosmos 156 Rocket	4	1	
Cosmos 425 Rocket	4	1	
Cosmos 72	4	1	Payload
71-054 A	5	0	Payload
ERTS 1 Rocket	5	0	
Cosmos 468 Rocket	5	0	
Cosmos 542 Rocket	5	0	
Meteor 9 Rocket	5	0	

When other than minimum brightness factors are considered, such as avoiding low density satellites and spent rocket bodies, stable orbital heights, and potential for grazing shadow entries, among the 25 usable targets listed in Table II, some preference emerges for the following five (which may themselves provide a sufficient density of observational opportunities for a given mission):

Skylab
Cosmos 542
70-066 A
Cosmos 72
71-054 A

Special attention is called to the characteristics of the Cosmos 542 payload, which appears to qualify as the single most suitable target.

Grazing Shadow Entry - If the satellite enters the shadow of the earth at a grazing angle, the satellite positional accuracy requirements are relaxed, and the signal integration time may be increased without decreasing the resolution of height at the tangent point (see the paragraphs on Error Sensitivity below). Therefore, an investigation was made of the conditions under which grazing entries occur.

There are three parameters which are important in determining if grazing will occur. They are δ , the declination of the sun; i , the inclination of the satellite; and A , the angle between the sun-earth line and the radius vector at shadow entry, given by

$$A = \sin^{-1} R/r \qquad (22)$$

where R is the radius of the earth and r is the radius vector. It may be seen that the last two of these parameters are constants of the satellite orbit which change only very slowly with time. Table III gives values of a A as a function of satellite height $(r - R)$.

Figure 19 shows the earth, its shadow, and a satellite orbit so oriented that a grazing eclipse occurs at the northern vertex of the orbit. It may be seen that

$$A = \delta + i \qquad (23)$$

or

$$A - i = \delta \qquad (24)$$

If i is increased while keeping the orbit orientation the same, there will be no shadow entry. However, a slight rotation of the node of the orbit with respect to the sun-earth line will again produce a grazing eclipse, but a lower latitude.

If i is decreased, however, grazing eclipse is no longer possible. Thus, we have a necessary condition for grazing shadow entry in the northern hemisphere:

$$A - i \leq \delta \qquad (25)$$

Table III. Error Sensitivity Parameters Relative to Orbital Height

H	V	A	SIN A	COS A	V COS A
KM	M/SEC	DEG			M/SEC
100.	7844.	79.92	0.9846	0.1750	1373.
200.	7784.	75.84	0.9696	0.2447	1905.
300.	7726.	72.76	0.9551	0.2964	2290.
400.	7669.	70.22	0.9410	0.3384	2595.
500.	7613.	68.02	0.9273	0.3743	2849.
600.	7558.	66.07	0.9140	0.4057	3066.
700.	7504.	64.30	0.9011	0.4336	3254.
800.	7452.	62.69	0.8886	0.4588	3419.
900.	7400.	61.20	0.8763	0.4817	3565.
1000.	7350.	59.82	0.8645	0.5027	3695.
1100.	7301.	58.53	0.8529	0.5221	3812.
1200.	7253.	57.31	0.8416	0.5400	3917.
1300.	7205.	56.17	0.8307	0.5567	4011.
1400.	7159.	55.09	0.8200	0.5724	4097.
1500.	7113.	54.06	0.8096	0.5870	4175.
1600.	7068.	53.08	0.7995	0.6007	4246.
1700.	7024.	52.14	0.7896	0.6137	4311.
1800.	6981.	51.25	0.7799	0.6259	4370.
1900.	6939.	50.40	0.7705	0.6375	4423.
2000.	6898.	49.58	0.7613	0.6484	4473.
2100.	6857.	48.79	0.7523	0.6588	4517.
2200.	6817.	48.03	0.7435	0.6687	4558.
2300.	6777.	47.30	0.7350	0.6781	4596.
2400.	6739.	46.60	0.7266	0.6871	4630.
2500.	6701.	45.92	0.7184	0.6956	4661.
2600.	6663.	45.27	0.7104	0.7038	4689.
2700.	6626.	44.63	0.7026	0.7116	4715.
2800.	6590.	44.02	0.6949	0.7191	4739.
2900.	6554.	43.43	0.6874	0.7262	4760.
3000.	6519.	42.85	0.6801	0.7331	4779.
3100.	6485.	42.29	0.6729	0.7397	4797.
3200.	6451.	41.75	0.6659	0.7460	4813.
3300.	6418.	41.23	0.6590	0.7521	4827.
3400.	6385.	40.71	0.6523	0.7580	4839.
3500.	6352.	40.22	0.6457	0.7636	4851.
3600.	6320.	39.73	0.6392	0.7690	4861.
3700.	6289.	39.26	0.6329	0.7743	4869.
3800.	6258.	38.80	0.6267	0.7793	4877.
3900.	6227.	38.36	0.6206	0.7842	4883.
4000.	6197.	37.92	0.6146	0.7889	4889.
4100.	6168.	37.50	0.6087	0.7934	4893.
4200.	6139.	37.08	0.6030	0.7978	4897.
4300.	6110.	36.68	0.5973	0.8020	4900.
4400.	6081.	36.28	0.5918	0.8061	4902.
4500.	6053.	35.90	0.5863	0.8101	4904.
4600.	6026.	35.52	0.5810	0.8139	4904.
4700.	5998.	35.15	0.5757	0.8176	4904.
4800.	5972.	34.79	0.5705	0.8212	4904.
4900.	5945.	34.44	0.5655	0.8247	4903.
5000.	5919.	34.09	0.5606	0.8281	4901.

Table III. Error Sensitivity Parameters Relative to Orbital Height

Similarly, consideration of Figure 20 leads to the necessary condition for grazing entry in the southern hemisphere:

$$A - i \leq -\delta \qquad (26)$$

The information conveyed by Equations (25) and (26) is succinctly displayed in Figure 21. Since A - i is relatively constant for any given satellite, a vertical line through the figure will represent the conditions throughout the year for that satellite.

It should be borne in mind that grazing entries are obtained at the expense of fewer total shadow entries. The satellites that exhibits graxing entry also spend considerable time in continuous sunlight, while those that never have a grazing entry pass into shadow on every revolution.

NOTE: The term "hemisphere" is used somewhat loosely in the above discussion and in Figure 21. To be strictly accurate, "northern hemisphere" should be replaced by "latitudes greater than $-\delta$".

Expected Number of Observational Opportunities - For the 25 usable target satellites listed in Table II, Figures 10 through 13 yield, at a moderate 35 degrees latitude, a mean daily frequency of observable shadow entries of 0.07. This figure projects a long-term average of 639 observational opportunities per year at a moderate site latitude. Pageos' observable shadow entry frequency is several times greater than the average for the others, and if it be excluded, the remaining 24 satellites would provide more than 500 observational opportunities at this latitude, on a continuing mission basis.

By taking advantage of "bunching" of shadow entry opportunities at various site latitudes, as suggested above, data gathering efficiency can be markedly increased. It is expected that multisatellite shadow entry windows will be found in each season of the year which would yield at least four observational opportunities per day, and which could be exploited by the mobility of the photometric observatory.

As can be seen from the curves presented previously (Figures 10 through 13) there may be a considerable potential for increasing observational opportunities by judiciously matching site latitudes to the satellites being observed at different periods in the specific mission planning. As an example, there are substantially more opportunities with Skylab (50°) at 40° latitude than 30 to 35°.
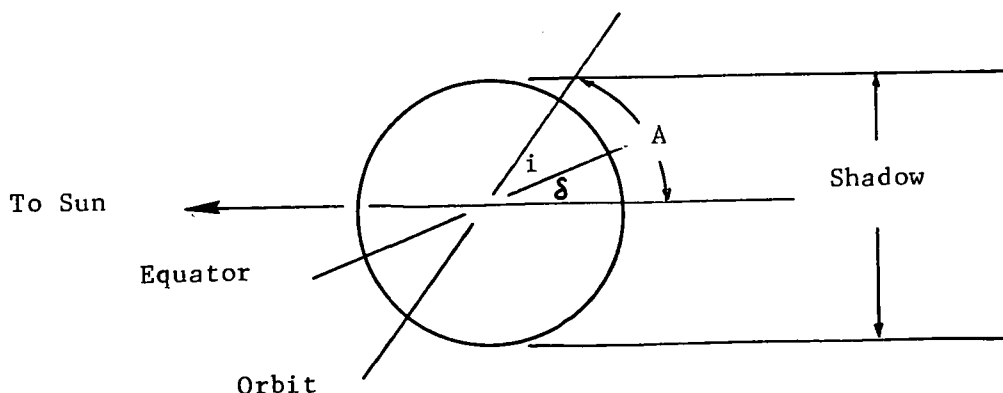

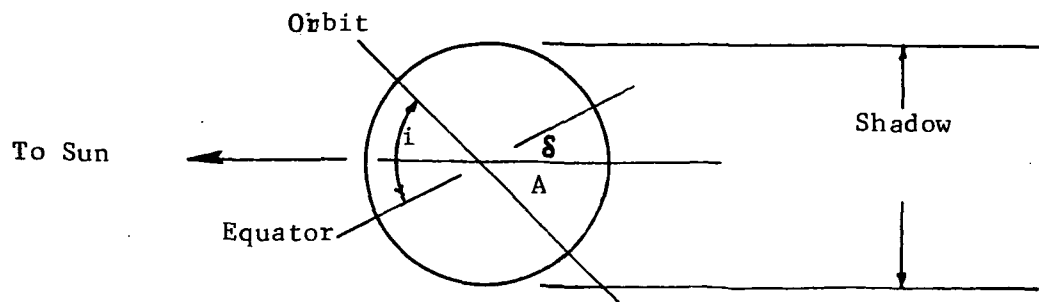FIGURE 19 Grazing Eclipse at Northern Vertex

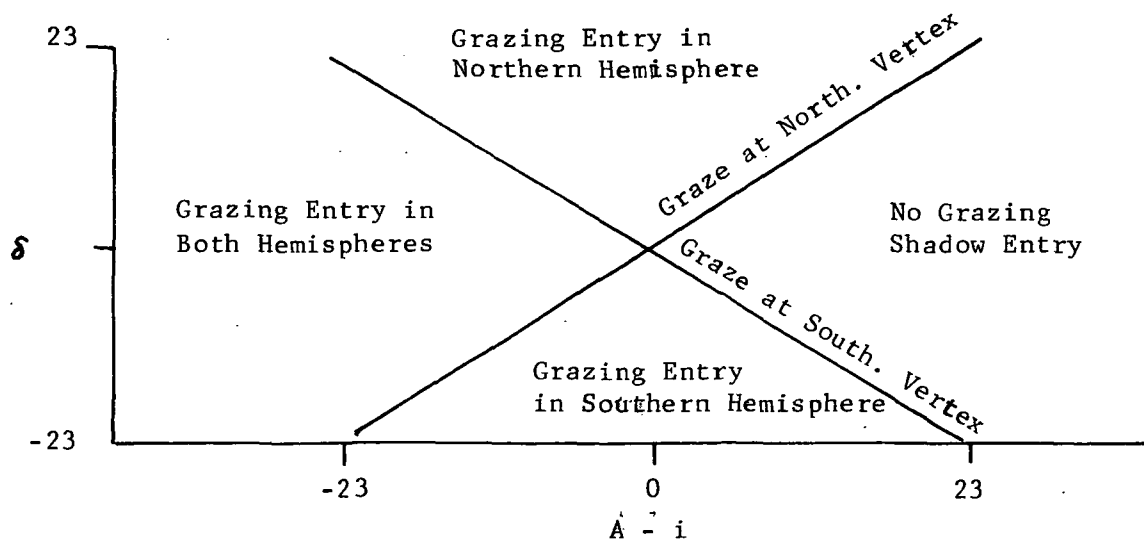FIGURE 20   Grazing Eclipse at Southern Vertex

FIGURE 21   Chart of Grazing Eclipse Situations

Southern Hemisphere Observing Aspects - Due to the principle of geometric symmetry, there are equal counterpart opportunities for observation in the southern hemisphere to those in the northern hemisphere. Therefore, everything stated above applies equally to the northern and southern hemispheres. So considering both hemispheres theoretically doubles the total number of opportunities over those for one hemisphere alone. However, from a single site at a given time (one site at a time - one MOSPO) the number would still be the same statistical average and would not increase - - except that as the site scheduling and moves might manage to take advantage of "bunchings" at each or any of the sites as it occurs, the opportunities could be pushed above the straight average number. Including both hemispheres in this game could increase the flexibility and therefore the effectiveness, of such judicious selection and planning.

For observing sites in the 30 to 40° south latitude belt, Chile offers excellent prospects - - relatively dry, clear seeing conditions; and with a number of good sites (at Cerro Tololo - near Santiago 35° from the Inter-American Observatory; and further to the north the site of the Cal Tech Group observatory. Further north along the coast, Peru offers some promising sites. Likewise in the northern hemisphere, there is no reason sites in Mexico, Canada or Alaska should not be considered whenever they offer significant advantages.)

A strong consideration in the degree of desirability of measurements using southern hemisphere sites would be the added value of the expanded coverage thus involved, and the opportunity it would afford for comparing measurements for the relatively unpolluted southern hemisphere with those being obtained for the northern hemisphere. This would provide further insight into both global ozone conditions, and the model of ozone activity in the atmosphere.

Satellite Position Geometry Determination

An apparently realizeable goal for ozone measurement was set at 300 meter vertical accuracy. To accomplish this by the direct method, corresponding satellite position data would have to be obtained through appropriate outside agencies (such as NORAD/SPADATS). Methods by which this could be done were investigated, with favorable results. This aspect is treated below.

Accuracy Considerations and Criteria - Definitive Orbit - Atmospheric ozone concentrations from narrow band photometric observations of a satellite during shadow entry are themselves of sufficient accuracy to warrant the requirement for better than 500 meter accuracy in the determination of their heights. Indeed, there appears no reason why the accuracy criterion for these heights should not be set at about 300 meters, which is within the state of art for definitive orbits established by radar. The accuracy advantage gained in projecting the satellite's position to the plane of the earth's sunset limb is variable (the factors generally range from 1.1 to 2.9 for usable target satellites during normal shadow entry) and is unually not significant.

The 300 meter criterion for satellite positional accuracy need not apply throughout the orbit, but only in that orbit segment containing the observed shadow entry. Thus precise positional observations should be made during this segment of the orbit in order that the criterion may be confirmed by the observational residuals.

Sources Considered and Contacted - Three possible sources for accurate satellite position information were considered and contacted: NASA-Goddard SFC, Smithsonian Astrophysical Observatory, and the Fourteenth Air Force Aerospace Defense Command's Cheyenne Mountain Facility at Ent AFB, Colorado.

Both Goddard and SAO are currently laser-tracking several satellites which are equipped with retro-reflectors, 72-058 A, 65-089 A and 68-002 A, which yield definitive orbits of 100 meter accuracy. But for noncooperative satellites such as our 25 bright usable targets such high accuracy is now unattainable. For these, Baker-Nunn observations processed by SAO's photoreduction system could provide positional accuracies better than 200 meters whthin the observed orbit segment. However, SAO has deactivated its precision photoreduction system and to re-establish it for a single satellite, e.g. Pageos, for a two-month observing period would require an effort characterized as "somewhat less than $45,000."

It appears that the positional accuracy requirement for our target satellites can be more efficiently met by the Aerospace Defense Command at Ent AFB. Their 1000 meter accuracy radar skin-tracking data can be further processed by their special perturbation program to yield positions of 300 meter accuracy at the 95 percent confidence level. For example, they can furnish a satellite's X, Y and Z coordinates, referred to the earth's center, and their time rates of change, at tenth second intervals during a specified time period. For this they need a high density of their radar observations, totaling about 1000 in a two-week period bracketing the desired time segment. Thirty to forty minutes of computer time are required to process these observations by the special perturbation program. In order to assure that the needed 1000 radar observations will be accumulated, a formal request for coverage of the target satellite should be submitted to the Aerospace Defense Command (on ADC Form 360) at least 30 days in advance.

Error Sensitivities - The errors, Δh, in the height at which the ozone concentration is measured due to errors in the position of the satellite are given by

$$\frac{\Delta h}{\Delta r} = \sin A \qquad (27)$$

$$\frac{\Delta h}{r\Delta v} = -\cos A \cos \beta \qquad (28)$$

$$\frac{\Delta h}{r\Delta \gamma} = \cos A \sin \beta \qquad (29)$$

where Δr is the error in radius vector, $r\Delta v$ is the positional error in the direction of satellite motion, $r\Delta \gamma$ is the error perpendicular to the plane of the orbit, A is the angle between the radius vector and the sun-earth at shadow entry, and θ is the angle between the orbital plane and the plane containing the sun-earth line and the radius vector.

Since the error along the orbit may be stated as a time error rather than as a positional error, Equation (28) may be restated as

$$\frac{\Delta h}{\Delta t} = -V \cos A \cos \theta \qquad (30)$$

where V is the satellite velocity.

For a circular orbit, V and A are functions only of the satellite height. θ, however, is dependent upon the orientation of the orbit; for grazing shadow entry, it is equal to 90°.

Table III gives values of V, A, sin A, cos A, and V cos A as a function of satellite height. It will be seen that V cos A is relatively constant over a wide range of height, the increase of cos A with height being almost compensated by the decrease in V.

Equation (30) will also give the rate of decrease in height with time, which may be used to determine the height resolution as a function of the integration time of the data collection system.

Results and Recommended Method - After discussing the satellite position geometry requirements with personnel at NASA-Goddard, SAO, and Ent AFB, the most feasible and preferred procedure is to request and obtain, in advance, the cooperation of Ent's Aerospace Defense Command in making the necessary positional radar observations and subsequently providing the precise satellite positions. As described above, a formal request should be submitted at least 30 days in advance on ADC Form 360, to Aerospace Devense Command, Ent AFB, Fourteenth Air Force. The precise time segments, each of the 20 seconds duration, for which the accurate positional information is needed, can be specified only after the photometric observations have been taken. This will require close coordination with personnel at Ent AFB, but should present no problem once their cooperation on the project has been approved.

Following this procedure it is expected that the needed satellite position geometry will be defined within 300 meters at the 95 percent confidence level, and thus determine the height of the ozone concentration measurements to at least this same accuracy.

Finally, it should be noted that simultaneous field-crew "Moonwatch" positional observations, while not at all competitive in accuracy, should continue to be taken as a precaution against conceivable system foul-ups and wild positional errors.

For the specific mission planning, the ephemeris data for the useful satellites from the list given above is obtained, and then the observing opportunities and windows determined with the proper computer programming and graphical representations. This will permit the juggling of sites and schedule for mission optimization with maximum yield and fulfillment of objectives. Then the specific mission preparation data is obtained as needed, and throughout the mission, using the appropriate computer programs. The methods for doing these things are discussed below.

Satellite Ephemeris Data Sources - The Aerospace Defense Command at Ent AFB is also a prime source for routine orbital elements of sufficient accuracy for mission planning and, when of recent epoch, for the mission's acquisition and tracking ephemerides. These elements, distributed by SPADATS Bulletins, are generated by a general perturbation program for each satellite when the along-orbit error of the previous elements reaches 12 kilometers. One observer has cautioned that the acceleration terms for these bulletin orbital elements are not always dependable. However, these elements can still be safely used to project orbit orientations many months ahead with sufficient accuracy for preliminary mission planning. Clearly, the final window confirmation and acquisition-tracking ephemerides should be based upon the latest available SPADATS Bulletins.

Alternative sources for routine orbital elements for some of the bright usable target satellites are NASA-Goddard and the Smithsonian Astrophysical Observatory. For completeness, however, dependence should be placed upon ADC at Ent AFB.

Shadow Entry Window Determination and Site Selection - It is recommended that the procedure described previously be used for determining multiple satellite shadow entry windows and optimum site latitude. The essential conditions for specific missions are revealed by study of graphs similar to Figure 18 above, in which shadow entry latitude is plotted versus calendar date for all candidate target satellites. The analyst who undertakes to interpret such graphs should understand the significance, assessment and use of the $\Delta\phi$ parameter defined by Equation (21) above. The $\Delta\phi$ parameter is a function of orbital height and will generally be different for each satellite. It may be useful to plot zones of suitable shadow entries versus calendar date, based on the computed shadow entry latitude and $\pm$ $\Delta\phi$. The areas of interest will be where these zones overlap.

A shadow entry latitude program which inputs actual orbital elements should be written to furnish the information for the above graph. The Smithsonian's geocentric "Ephemeris VI" program would suffice, but a more appropriate and efficient version is recommended, which would include instantaneous sunset latitude and $\Delta\phi$ as outputs.

The specific mission dates and site must finally be confirmed and defined by analysis of conventional topocentric ephemerides. Determination of the four-axis acquisition settings and ephemerides should await such mission confirmation, and should be based on the latest

available orbital elements. It is suggested that the present four-axis prediction program should be modified to further improve the fit of the tracking small circle to the actual satellite path in the vicinity of shadow entry.

As in previous photometric missions, up-dated four-axis and conventional predictions must be communicated to the field crew on a continuing basis throughout the mission.

EQUIPMENT MODIFICATION AND IMPROVEMENT

Introduction

In order to meet the requirements and objectives developed in the preceding sections, and particularly to acquire and process the large number of measurements needed and indicated to be practical if satellites to fifth magnitude can be used, it is essential that the equipment be modified so that

(1) Simultaneous photometry in four narrow bands is possible

(2) Sensitivity and signal to noise capability is adequate for measurement with fifth magnitude satellite

(3) Recorded data is compatible with computer data reducing and processing to permit obtaining fast, accurate, low-cost results from these measurements

Such modification requirements and recommendations are treated in this section.

The modifications required to provide these capabilities, and recommended so that maximum effectiveness can be obtained, include the following:

(1) Added beam splitter to allow four channel operation

(2) Upgraded photomultiplier sensor installation

(3) Pulse counting circuitry and equipment

(4) Autotrack system with smaller field stop

(5) Digital recording equipment (IBM compatible)

Of course, while full implementation of this to obtain full capability is recommended, a partial implementation with any of the above steps alone would yield a corresponding return, and could be separately considered. In each area there were a number of alternatives

55

and tradeoffs available for consideration, and the one selected and recommended represents that which seemed clearly superior or optimum in terms of capability versus cost. Perhaps the outstanding examples are the automatic tracker and digital recording. With the tracker selected, a substantially greater capability was obtained for a relatively modest cost difference (see trade-off curves presented), and with the digital recording substantially improved and less costly data processing is obtained for a relatively modest investment. However, the factors to enable NASA to decide for themselves are presented.

Adding Four Channel Capability

To bring the light from the satellite into all four channels simultaneously, a simple beamsplitter assembly like that shown between the Fabry lens and the existing beamsplitter in Figure 23B would be needed. The two mirrors would be half reflecting and hinge mounted, so that they can be swung out of the way manually as shown from outside the unit for dual channel sky differencing operations as at present. The control console would have to be modified to add the two channels of data and galvanometers would have to be added to the oscillograph.

Improving Signal to Noise Ratio

The major limitation to accuracy and magnitude reach of the narrow band light measurements encountered in satellite eclipse photometry with the NASA MObile Satellite Photometric Observatory (MOSPO) in the past has been due to the excessive noise content in the signal. The five noise sources considered in this study are as follows:

(1) Photomultiplier (PM) shot noise, or noise in signal

(2) Photomultiplier dark noise, or noise in the absence of signal

(3) Leakage current noise

(4) Preamplifier input current noise

(5) Sky background noise

The calculated standard deviation in the number of photoelectron events caused by some of these noise sources are presented in Figure 22. The calculations assume the present MOSPO configuration with a narrow band filter at 7000 Å with a one-half point bandwidth of 18 Å and are documented in Appendix B.

Shot Noise - As can be seen from Figure 22 in the region of usable signal-to-noise ratio, the dominant noise contribution is from the photomultiplier shot noise. This noise arises from the random nature of the photoelectron emission process and causes a standard deviation on the number of events, n, per integration time of $\sqrt{n}$. For example, for n equal 100 the standard deviation equals 10 or 10 percent of the signal. Therefore, at source magnitude of 5.9 the shot noise limits the accuracy of the system to 10 percent.

Integration Time Considerations - One way to reduce the shot noise limitation is to increase the integration time of the system. However, it has been determined that to obtain adequate resolution of ozone altitude (+250 to 300 m), it will be required to take data points at 1/20th of a second intervals during eclipse (see preceding section) thus fixing the maximum integration time. The equivalent integration time of the existing system is shorter than 1/20th of a second; so there is theoretical potential for improvement in signal-to-noise ratio by increasing the integration time to 1/20th second. However, since during the data reduction process the data is smoothed, averaged or integrated, the theoretical improvement available is reduced depending on the "integration time" of the person taking the readings.

Photomultiplier Survey - The second most obvious method to reduce the accuracy limitation due to shot noise is to increase the rate of photoelectron emission from the photomultiplier cathode. This may be done by choosing a photomultiplier with higher quantum efficiency in the wavelengths of interest assuming the relative contribution of dark noise stays constant. The photomultipliers considered in this study are listed in Table IV. The RCA C31034A-02 is recommended in view of the fact that its photoelectron yield is a factor of 5.2 greater than the existing EMI 9558QA at 7000 Å. A 10 percent accuracy limitation would then be extended down to a 7.7 magnitude source as compared to a 5.9 magnitude source for the EMI 9558QA.

Changing to the C31034A-02 requires a change in the instrument head optics since the active photocathode area is 4 mm x 10 mm as opposed to the existing photomultipliers which have an active area of approximately 5 cm diameter. The photomultiplier housing socket assembly must also be changed to accept the RCA tube. The UBVRI band filter responses will have to be recalculated in view of the new photomultiplier response in order to match the standard Johnson UBVRI system. Some of the filters will probably then require replacement.

Optics Modification - In order to obtain these improvements, it is necessary to make the corresponding changes to the optics within the photometer instrument head. The changes to accommodate the small photocathode area of the RCA C31034A-02 tube are shown in Figure 23, involving changing the focal length of the Fabry lenses (to a 40 mm F 1.9 lens) and adding a new collector lens (45 mm F 1.4) as shown for each photomultiplier. The optical path, by which a small 2 mm image of the primary mirror is focused on the photocathode, is shown in Figure 23A, and the corresponding lens installation is shown in Figure 23B. The new lenses are supported in a bracket mounted to the frame.

The ITT FW 130 photomultiplier (see Figure 24) was closely analyzed as a possible candidate to improve system sensitivity in view of the many recommendations from people at Palomar. It has a much superior dark count rate which accordingly produces much less dark noise than the C31034A-02 (see Figure 25). For long integration times (many hours at Palomar) dark noise sets the limiting accuracy of their system, thus their choice of the FW130 allows them to work to fainter light levels in reasonable integration times. However, for the short integration times, which are mandatory in the measurement of satellite eclipse (approximately 0.05 seconds), photomultiplier shot noise is the major limitation to system accuracy at low light levels. Thus the much higher quantum efficiency of the RCA C31034A-02 (26 percent at 7000 Å) produces a clearly defined advantage for the C31034A-02. For a standard deviation of 10 percent of the number of signal events, the FW130 allows measurement down to 5th magnitude, whereas the C31034A-02 allows measurement down to 7.7 magnitude.

Cost Effectiveness – Changing to the RCA C31034A-02 photomultiplier should theoretically allow measurement of sources 1.8 magnitudes fainter than the present system, thus doubling the number of available satellites, whereas the estimated cost level for this change is approximately 15K.

Dark Noise – As can be seen from Figures 22, 24 and 25, photomultiplier dark noise or noise in the absence of signal is not a major limiting factor since it is much less than PM shot noise. This is true for the existing system and with the recommended C31034A if the -02 version is specified which guarantees a dark count rate of 10 counts per second at -20°C.

Leakage Current Noise – Leakage current noise cannot be calculated because of its unpredictable nature. Contaminants and moisture around the PM base socket, and preamp input are the causes of leakage current noise. It is possible that this may be a significant contributor to the system noise. (Reference 29, page 148). Using the present analog photometer system, the only way to minimize leakage currents is to keep the PM tube base, socket, preamp and its socket immaculately clean. A better way to remove the effects of leakage current noise is to change the photometer circuitry from analog to a pulse counting system.

Pulse Counting Techniques – The anode current of the photomultiplier at very low light levels is not a continuous function but rather is composed of discrete, relatively large amplitude, short duration ($<$ 50 nanosecond) pulses as compared to the average current level. Leakage current noise, on the other hand, is a relatively low level, slowly varying phenomena. Therefore, a pulse counting circuit adjusted to count pulses whose amplitude is greater than a threshold value which is above the majority of the leakage noise peaks will effectively discriminate against leakage current noise. A block diagram of an amplifier/discriminator used to condition the photomultiplier output for pulse counting is shown in Figure 26.
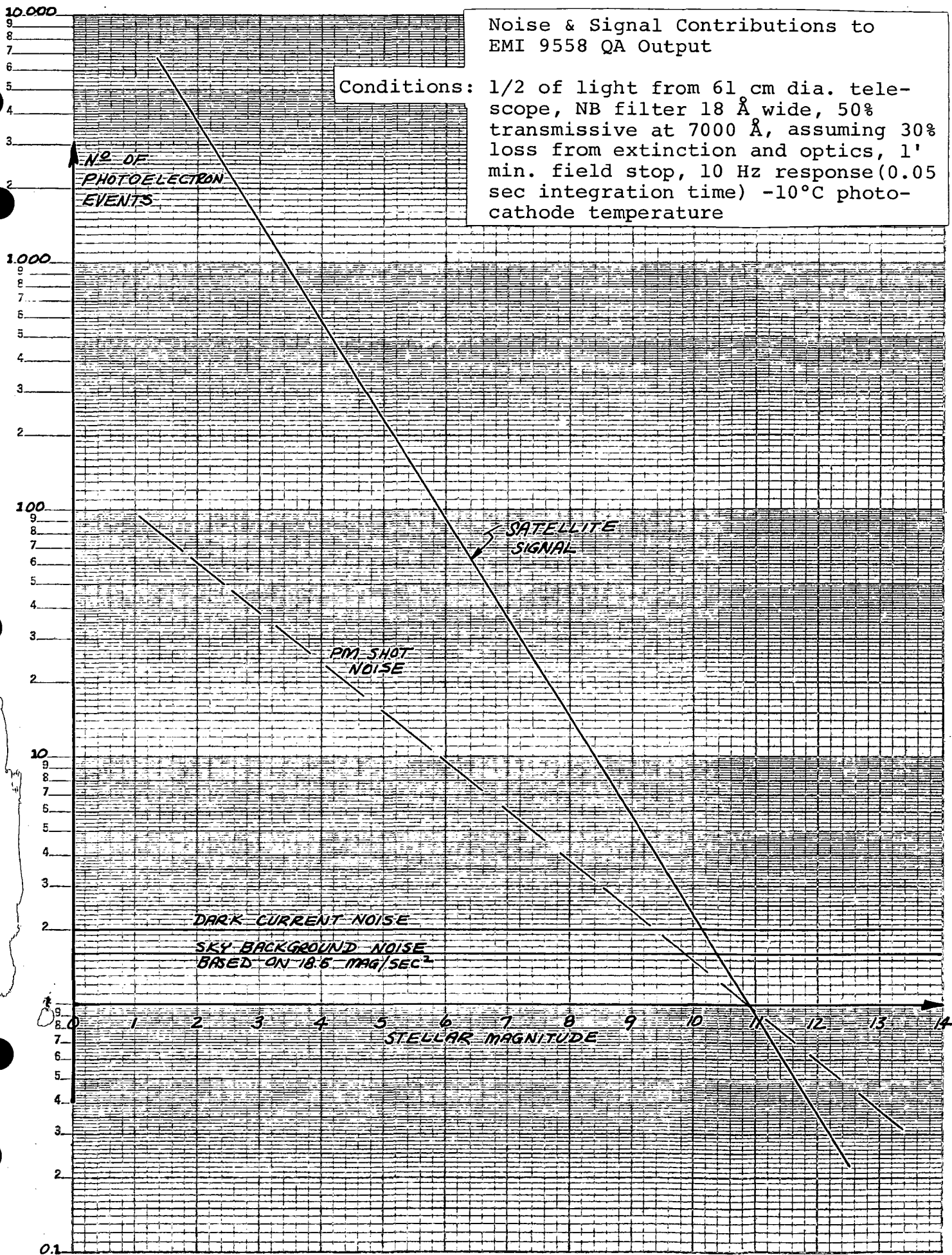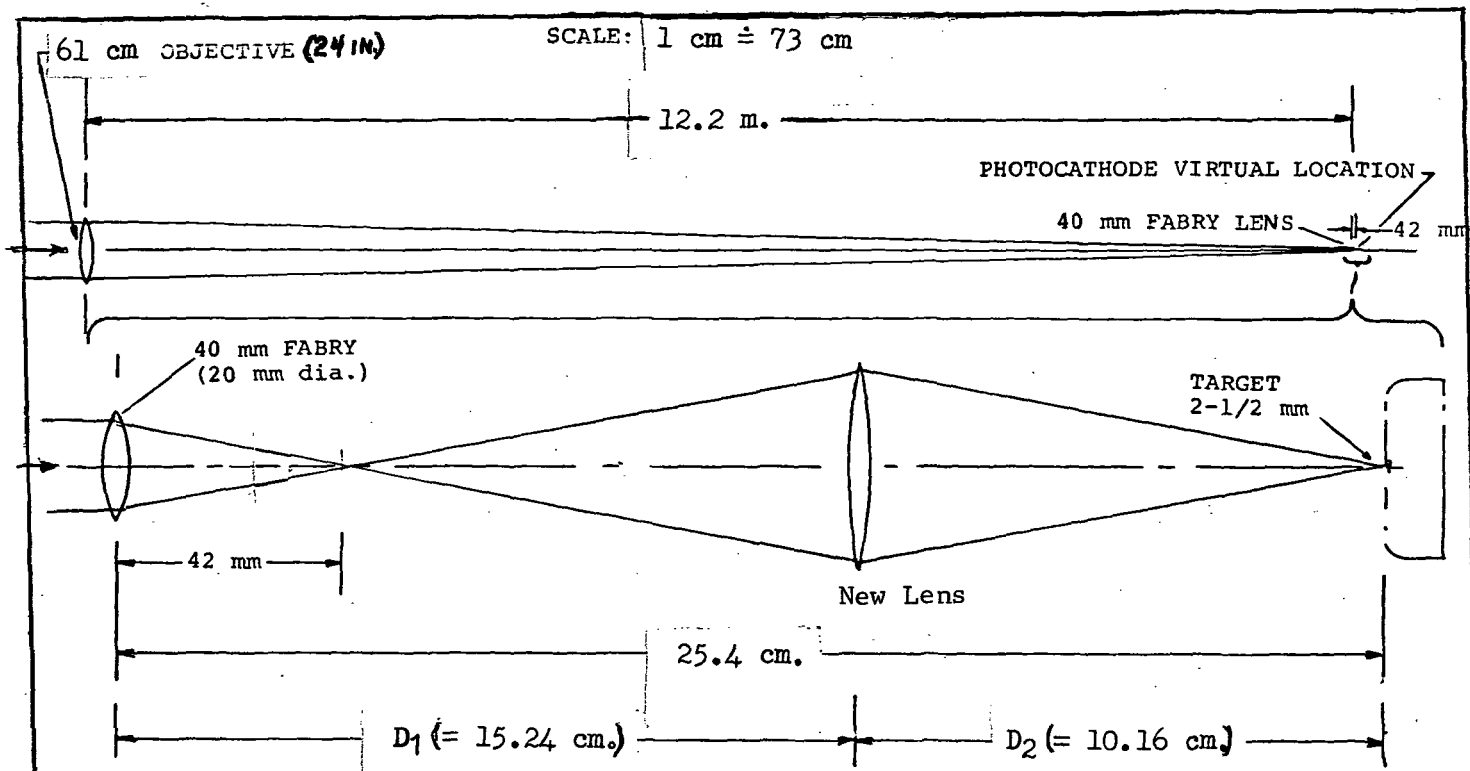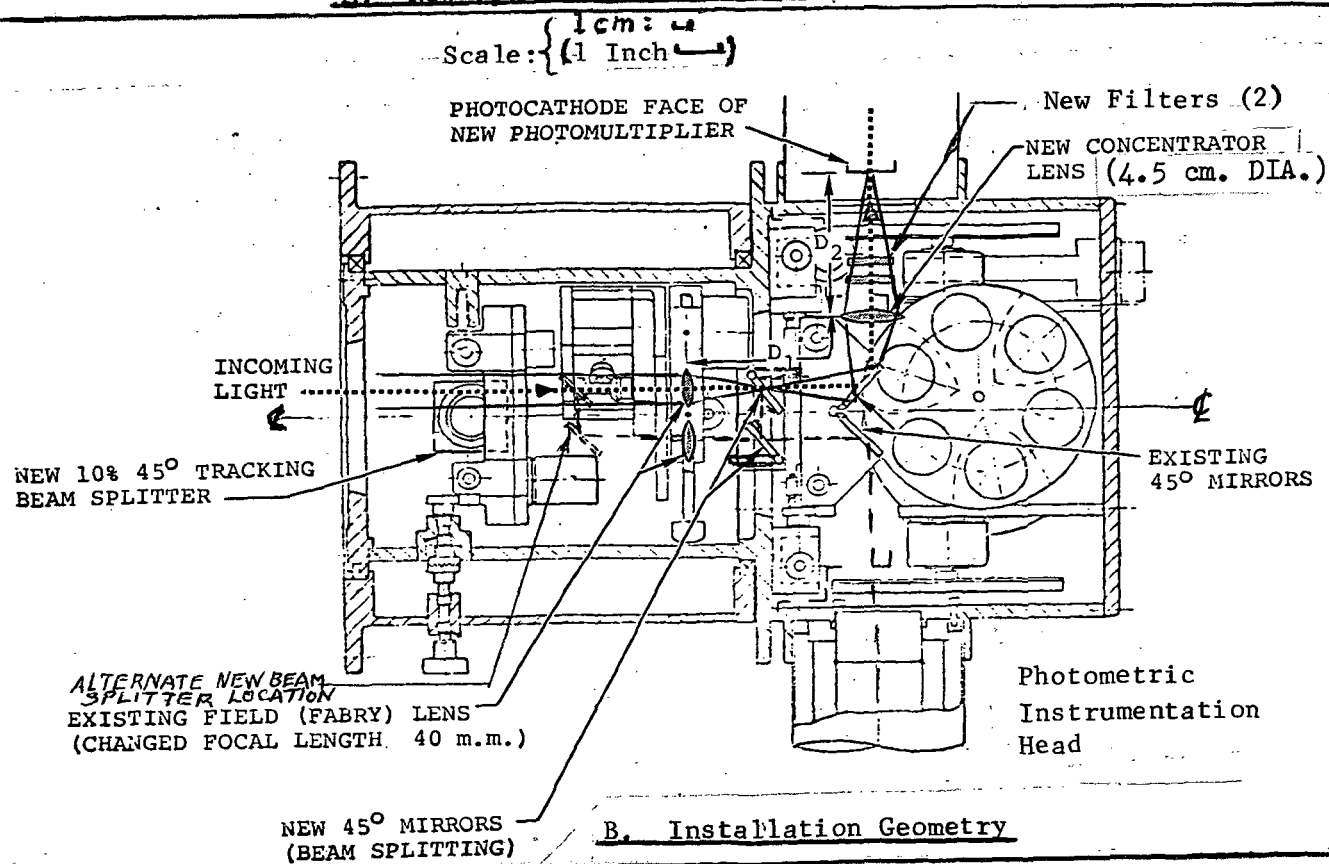
FIGURE 22.   MOSPO With EMI 9558QA

59

TABLE IV. PHOTOMULTIPLIER SURVEY

MANUFACTURER	TYPE	@ 7000Å	@ 6000Å	QE MAX	DARK COUNT RATE @ -10°C	SENSITIVITY	COST	COMMENTS
EMI	9558QA	5%	9%	22%	80 cts/sec	200A/lm	-	presently installed
RCA	C31034A	26%	30%	48%	45 cts/sec	400A/lm	$1100	4mm x 10mm cathode
	-01	26%	30%	48%	300 cts/sec	400A/lm	$1200	dark ct. guaranteed
	-02	26%	30%	48%	30 cts/sec	400A/lm	$1300	dark ct. guaranteed
RCA	C31034	12%	13%	21%	45 cts/sec	300A/lm	$ 395	4mm x 10mm cathode
	-01	12%	13%	21%	300 cts/sec	300A/lm	$ 495	dark ct. guaranteed
	-02	12%	13%	21%	30 cts/sec	300A/lm	$ 595	dark ct. guaranteed
ITT	FW130	2.5%	7.5%	20%	3 cts/sec	800A/lm		2.5mm dia. cathode
ITT	F4075	3%	7.5%	11%	(ENI 1×10^{-13}/lm)	200A/lm		2cm dia. cathode
Centronic	Q4283R	3%	8%	22%	(ENI 8×10^{-14}/lm)	200A/lm	$ 590	3.6cm cath dia-plug-in equiv to 9558QA
ENI	9817B	3%	7%	23%	(ENI 3.1×10^{-13}/lm)	200A/lm		fast linear focused
Schlumberger	541R-01-14	4%	10%		(ENI 3.8×10^{-14}/lm)	225A/lm		25mm dia cath-potted & ruggedized
Schlumberger	543E-01-14	2.8%	8.5%		(ENI 1.1×10^{-13}/lm)	150A/lm		43mm cathode dia-ruggedized
RCA	PF 1011	4.5%	7.5%	9%	35 cts/sec	2200A/lm		high gain first dynode

SCALE: 1 cm ≐ 73 cm

61 cm OBJECTIVE (24 IN.)

12.2 m.

PHOTOCATHODE VIRTUAL LOCATION

40 mm FABRY LENS — 42 mm

40 mm FABRY
(20 mm dia.)

TARGET
2-1/2 mm

42 mm

New Lens

25.4 cm.

D_1 (= 15.24 cm.)

D_2 (= 10.16 cm.)

A. New Optical Path Geometry

Scale: { 1 cm: ⊔
       (1 Inch ⊢──⊣)

PHOTOCATHODE FACE OF
NEW PHOTOMULTIPLIER

New Filters (2)

NEW CONCENTRATOR
LENS (4.5 cm. DIA.)

INCOMING
LIGHT

NEW 10% 45° TRACKING
BEAM SPLITTER

EXISTING
45° MIRRORS

ALTERNATE NEW BEAM
SPLITTER LOCATION
EXISTING FIELD (FABRY) LENS
(CHANGED FOCAL LENGTH 40 m.m.)

Photometric
Instrumentation
Head

NEW 45° MIRRORS
(BEAM SPLITTING)

B. Installation Geometry

Figure 23. Optics Modification for RCA C31034A Photomultiplier

61

Noise & Signal Contributions to
ITT FW 130 Output

Conditions: 1/2 of light from 61cm dia.telescope,
NB filter 18 Å wide 50% transmissive
at 700 Å, assuming 30% loss from ex-
tinction and optics, 1' min. field
stop, 10Hz response (0.05 sec inte-
gration time), -10°C photocathode
temperature

NO. OF
PHOTOELECTRON
EVENTS

SATELLITE
SIGNAL

PM
SHOT
NOISE

SKY BACKGROUND NOISE
BASED ON 18.5 MAG/SEC²

STELLAR MAGNITUDE

DARK CURRENT NOISE

FIGURE 24.   MOSPO With ITT FW 130

62

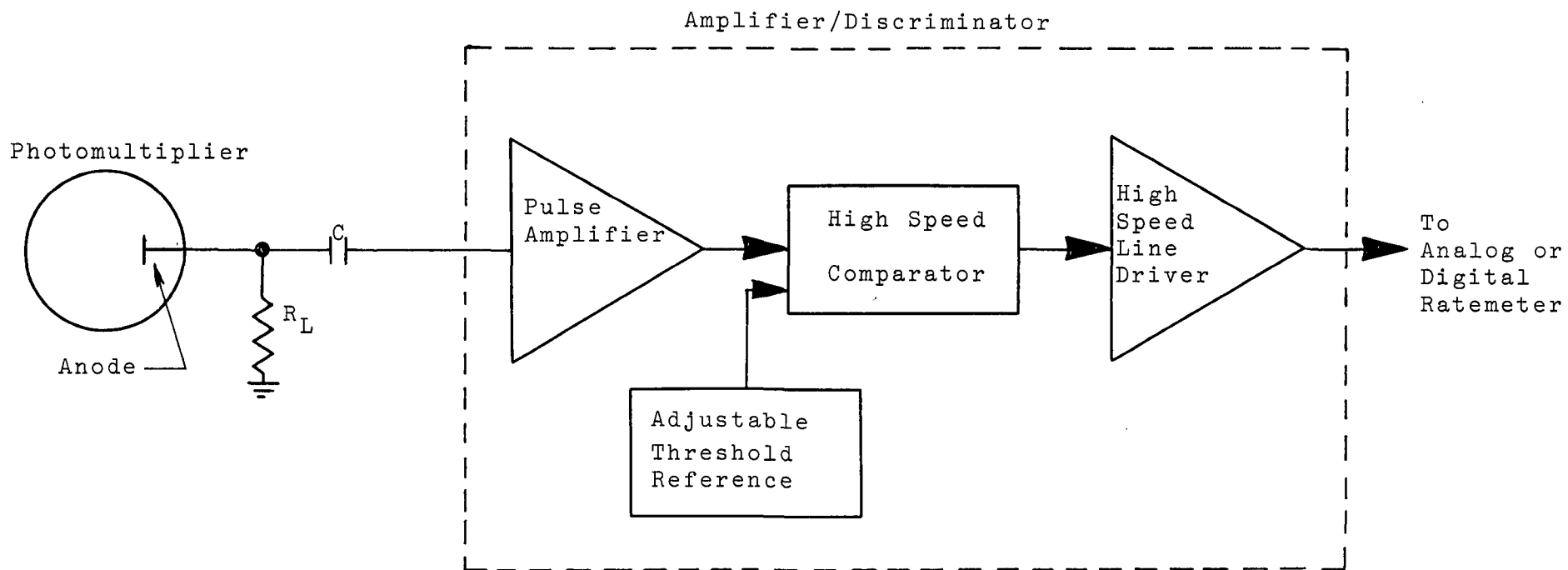FIGURE 25   MOSPO With C31034A

FIGURE 26   Pulse Counting Block Diagram

The photomultiplier anode is terminated in a low resistance R_L, usually 50 Ω , and capacitively coupled to a high speed pulse amplifier. The capacitance, C, is chosen to effectively block the lower frequency components which comprise much of the leakage current noise energy. The relatively high amplitude, short duration pulses are amplified by the pulse amplifier. Those pulses which are greater than the threshold value produce a uniform amplitude pulse at the high speed comparator output. The threshold is adjusted to discriminate against the majority of the noise peaks. By feeding the uniform amplitude and width pulses into gated counters, a precise digital representation of the pulse rate, i.e., intensity, is available for direct digital recording. The resolution of pulse rate is down to the level of one photoelectric event at the photocathode. By this method, the human errors resulting from measurements on the oscillograph records during data reduction are completely eliminated and amplifier gain steps to improve resolution are no longer required. Pulse counting removes the amplitude variation of the photomultiplier output pulses which, in the analog system, would be contributing to system noise.

The amplifier/discriminators required for pulse counting are commercially available from several companies. The largest unit, physically, of those surveyed was 31.75 cm x 3.18 cm x 6.4 cm and weighed 793 grams. Therefore, it is anticipated that the four required units could be mounted in the same area as was the Electronic Assembly 369N100-101 (yoke) on the telescope.

Dynamic Range Considerations - The one significant limitation to this technique is pulse pile-up at high light levels. For narrow band photometry, this is not a problem. When the pulse rate exceeds $\approx 10^6$ pulses/second, the output of the pulse amplifier, discriminator will start to show nonlinear effects because of the finite width of the pulses. This corresponds to a -0.3 magnitude source with the existing narrow band system. However, an upper limit of anode current of 10×10^{-6} amps is recommended for the 9558QA photomultiplier on the basis of stability and long life considerations. This corresponds to a source magnitude of -4.1 magnitude in the existing narrow band system. The calculations are as follows:

Pulse Pile-up 9558QA at 6000 Å

$$I_{cath} = \frac{pulse\ rate}{0.625 \times 10^{19}} = \frac{10^6}{0.625 \times 10^{19}} = 1.6 \times 10^{-13}\ amp$$

$$S_c = \frac{0.6 \times 10^{-6} \times 0.09 \times 10^6}{1.2395} = 0.436\ amp/watt$$

$$W = \frac{1.6 \times 10^{-13}}{0.044} = 3.64 \times 10^{-12}\ watts$$

$$M = \frac{-11.57 - \log W}{0.4} = \frac{-11.57 + 11.44}{0.4} = \frac{-0.13}{0.4} = -0.3\ mag$$

Maximum Exposure 9558QA at 6000 $\overset{\circ}{A}$

$$I_{\substack{cath \\ max}} = \frac{10 \times 10^{-6}}{2 \times 10^6} = 0.5 \times 10^{-11} \text{ amp}$$

$$W = \frac{0.5 \times 10^{-11}}{0.044} = 1.14 \times 10^{-10} \text{ watts}$$

$$M = \frac{11.57 + 9.94}{0.4} = \frac{-1.63}{0.4} = -4.1 \text{ mag}$$

$$I_{anode} = I_{cath} \times G$$

$$(G = PM \text{ gain})$$

Ave Pulse Rate = $I_{cath} \times 0.625 \times 10^{19}$ (pulses per second)

$$I_{cath} = S_C \times W$$

S_C = absolute sensitivity of cathode in amps/watt at the wavelength of the radiation

W = radiant power received by the photocathode in watts

$$\log W = -11.57 - 0.4M$$

$$M = \frac{-11.57 - \log W}{0.4} \quad \text{(in magnitudes)}$$

Pulse Pile-up for C31034A occurs when the average pulse rate equals 10^6 pps. Therefore

$$10^6 \text{pps} = I_{cath} \times 0.625 \times 10^{19}$$

and

$$I_{cath} = 1.6 \times 10^{-13} \text{ amp and:} W = \frac{1.6 \times 10^{-13}}{0.146} = 1.1 \times 10^{-12} \text{ watts}$$

and

$$M = \frac{-11.57 + 11.96}{0.4} = +0.98 \text{ mag}$$

Maximum Exposure for C31034A based on 1×10^{-6} amps max anode current:

$$I_{cath} = \frac{1 \times 10^{-6} \text{ amps}}{4 \times 10^5 \text{ gain}} = 25 \times 10^{-13} \text{ amp}$$

$$W = \frac{25 \times 10^{-13}}{0.146} = 1.71 \times 10^{-11} \text{ watts}$$

$$M = \frac{-11.57 + 10.77}{0.4} = \frac{-0.8}{0.4} = -2 \text{ mag.}$$

Thus pulse counting for the existing system would reduce the maximum allowable source intensity by about 3.8 magnitudes. In the recommended system, using the C31034A-02 photomultiplier, pulse pile-up begins to show effect at about first magnitude in narrow band. Considering a 10 percent loss for auto track, and a conservative upper pulse rate limit, attenuation of the signal in narrow band will probably not be required for sources up to zero magnitude. However, when using UBVRI photometry, sources brighter than fifth magnitude will require attenuation or means for switching to analog signal conditioning would be required in order to circumvent pulse pile-up. A dual system which would be switchable from pulse counting to analog seems to require an excessive amount of instrumentation in view of the limited space on board and in view of the large amount of complex electronic equipment which already causes maintenance and calibration problems. Also, the dual system requires switching at the photomultiplier output which is the most critical area in the system. Therefore, for standard UBVRI measurements, it is recommended that neutral density optical filters be made available for insertion into the light paths whenever the pulse rate exceeds 10^6 pps. The estimated source magnitudes producing this pulse rate are listed in Table V. The attenuation step size is recommended to be 2.5 magnitudes based on maintaining a maximum probable measurement error of 1 percent due to shot noise. The additional advantage to optical attenuation is the simultaneous capability of protecting the photomultiplier from over exposure.

For a count interval of 0.1 seconds, this would be a pulse rate of 100,000 pps. Thus the attenuation step size is $\frac{10^5}{10^6}$ or $\frac{1}{10}$ or 2.5 magnitudes.

Optical Attenuators - There are many methods of implementing the neutral density optical attenuators. For maximum system flexibility, accuracy and operator convenience, it is recommended that two independent, solenoid actuated, neutral density filters per photomultiplier be designed and installed behind the filter wheel assembly of the photometer head. This concept is shown in Figure 27. One of the

optical attenuators (neutral density filters) should correspond to about 2.5 magnitude attenuation and the other should correspond to about five magnitudes of attenuation. Thus, four values of attenuation can be selected 0, 2.5, 5, and 7.5 magnitudes by varying the combinations of the optical attenuators inserted in the light path. This will allow pulse counting measurements up to a source magnitude of -2 in standard V band.

Controls for the optical attenuators must be added to the system. A block diagram of the optical attenuator control circuit for one of the four photomultipliers is shown in Figure 28.

Table V. Attenuation Requirements to Avoid Pulse Pile-Up
(See Appendix C for Calculations)

Mode	Maximum Exposure	10^6 PPS Pulse Pile-up	Total Attenuation Required for -2 Mag Source	Steps Required (2.5 mag)
Continuous NB (4) (nondiff)	-2.75	0.25	2.25	1
Continuous NB (2) (diff)	-2.0	1.0	3.25	2
Std U Band (diff)	0.8	3.8	5.8	3
Std. B Band (diff)	2.17	5.17	7.17	3
Std. V Band (diff)	2.45	5.45	7.45	3
Std. R Band (diff)	3.0	6.0	8.0	4
Std. I Band (diff)	-0.2	2.8	4.8	2

NOTE: Attenuation step size was determined based on error contribution due to shot noise not exceeding 1%. Thus $\sqrt{n}$ = 100 where n = number of events per count interval = 10,000

It is desirable to design the attenuators such that under conditions of no power applied that both attenuators are in the light path. This will afford protection against accidental overexposure of the photo multipliers. It is recommended that provisions be made for monitoring any one of the four amplifier/discriminator outputs with the oscilloscope to ensure pulse pile-up is not occurring.
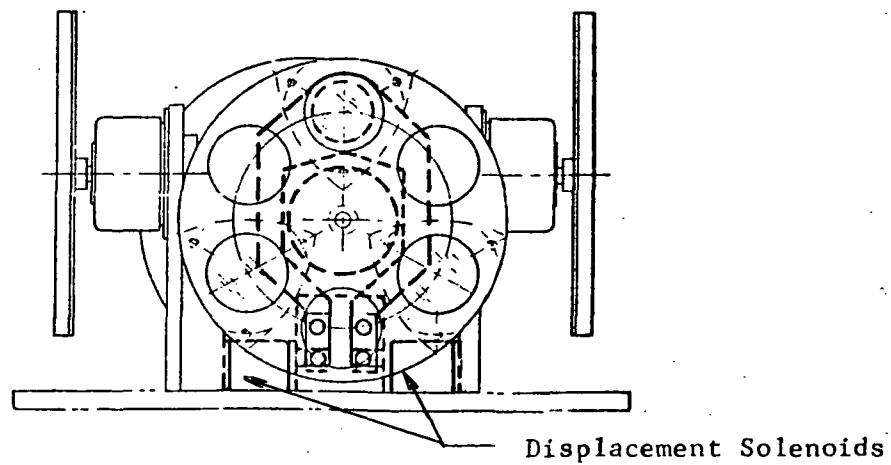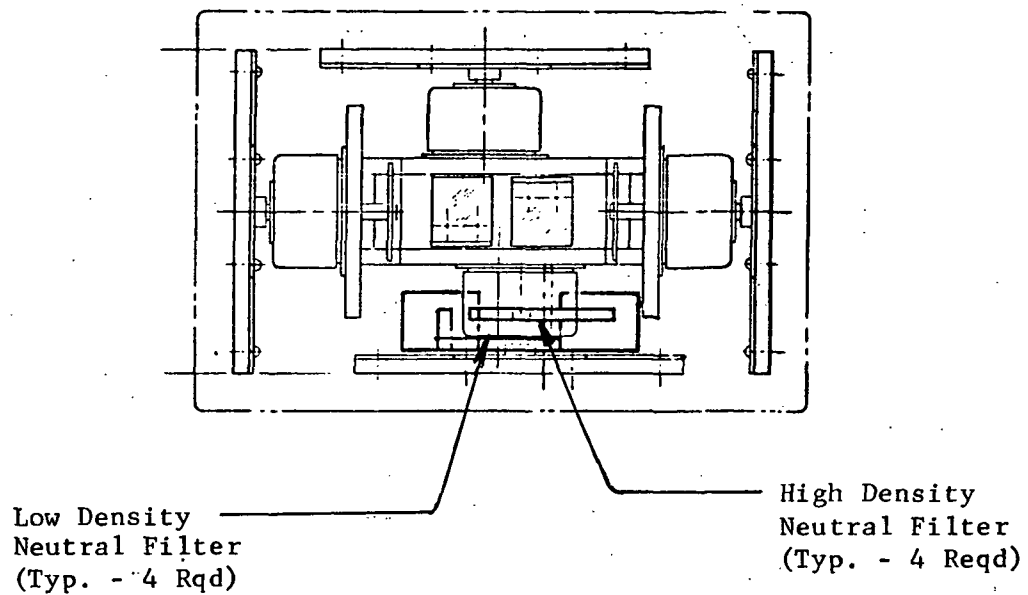
FIGURE 27. Filter Installation for RCAC31034A Photomultiplier Tube
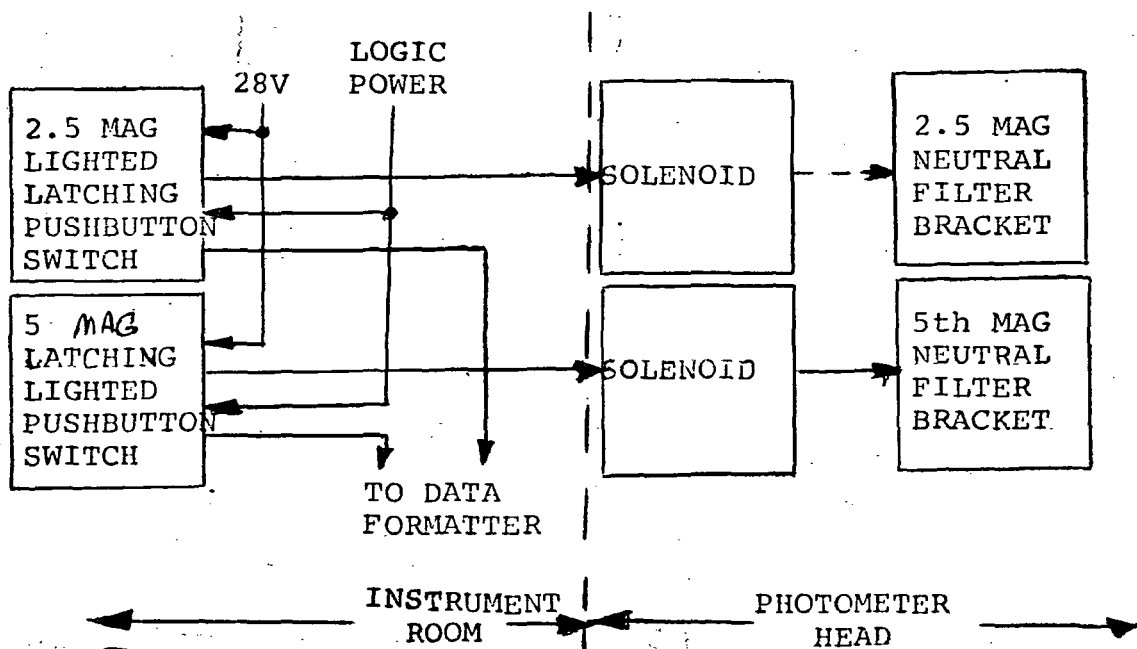With Pulse Counting (Typical for each Channel - 4 Rqd)

FIGURE 28. Optical Attenuator Control

The advantages and disadvantages of pulse counting may be summarized as follows:

Advantages

(1) Discriminates against leakage current noise and photo-multiplier non-photo-induced secondary emission.

(2) Allows maximum resolution of light level down to one photoelectron at the photocathode without gain steps being required.

(3) Allows precise control of integration time with low complexity digital circuitry.

(4) Eliminates the need for A to D converters when interfacing with a direct digital tape recording installation.

Disadvantage

(1) Maximum light level permitted to expose the photo-multiplier is reduced due to pulse pile up considerations.

It is very difficult to precisely predict the actual amount of signal-to-noise ratio improvement for pulse counting. However, the indication from Palomar is that the required integration time for the same statistical accuracy has been reduced by a factor of two since changing to pulse counting and Baum (Reference 29, Page 31) indicates an estimated improvement which correlates with an increase in quantum efficiency by a factor of 1.5.

Intuitively, since pulse counting normalizes the current pulse heights, it removes that component of noise arising from the amplitude modulation of the pulses. The only remaining noise producing mechanism is the random spacing of the pulses. If these two noise producing mechanisms were of equal importance then removal of one of the sources would reduce the noise by a factor of 1.4 since the total noise is the square root of the sum of the squares of the noises. Therefore, it is expected that pulse counting should allow for usable observations of sources which are about 0.4 magnitudes fainter than could be observed with the conventional analog system. The estimated cost level for changing to pulse counting is $15K.

Preamplifier Input Current Noise - Investigation of the effect of preamplifier input current noise for the present system has indicated an insignificant level as compared to photomultiplier shot noise. As calculated for the Analog Devices 301 Amplifier, the standard deviation in the measurements due to this noise source was 0.015 events per system integration time of 0.05 seconds. This level was not plotted on Figure 22 since it is much less than the other noise sources. The calculations are in Appendix B.

Sky Background Noise - Light from the sky background varies as the square of the field stop diameter. This light causes a noise-in-signal component in the same manner as the light from the source being measured. The noise produced therefore varies with the square root of the number of sky background events or, correspondingly, varies directly with the field stop diameter.

Sky brightness varies with nearness to the horizon, milky way, ecliptic, anti-sun, or any noctilucent clouds. It is very much increased in twilight, moonlight or near city lights depending on the scattering coefficient. One square second of dark night sky at zenith has been estimated to be equivalent to a source magnitude of +21.5. However, considering that most observations will not be made at zenith and that many of the other sky brightening effects will be present, a more conservative estimate of sky brightness equivalent to +18.5 magnitude per square second of arc has been used and plotted on Figures 22, 24, and 25. From Figure 22, it can be seen that sky background noise is not a major contributor to the noise problem at usable signal to noise ratios with a 1' (one minute) field stop. However, for a 2' (two minute) field stop the sky noise level would be four times as large and therefore is a major contributor to the noise problem. For the four-minute field stop, sky noise is contributing 50 percent of the total noise where the signal to noise ratio is 10. If an auto track system could be provided which would permit the use of a 30" field stop then sources whose brightness was 0.7 magnitude fainter could be observed with the same signal to noise ratio (evaluated for signal to noise ratio of 10). Eclipse photometry by virtue of the typically short duration (30 seconds) of usable data, makes it imperative that loss of track must not occur because of the relatively long reacquisition time. It is therefore recommended that an automatic tracking system be incorporated into the MOSPO.

Auto Track   -   The recommended auto track concept utilizes the
existing telescope servo drive system.   A 10 percent reflecting
45-degree mirror would be placed in the main light path to direct
10 percent of the light to the auto track system.   The auto track
would be required to provide a usable error signal to the existing
servo drive for sources down to eighth magnitude.   Thus, a nominal
fifth magnitude source could be tracked into eclipse over a three
magnitude range. If extensive use of the system in the polarimetric mode
is anticipated, the polarization effects of the proposed 45-degree
mirror for the auto track should be thoroughly investigated and
resolved since the limited scope of this study did not permit a
detailed analysis of the polarization effects of the additional optics.

The 10 percent reflecting mirror and a focusing lens would be mounted
on a counterpart assembly to the currently provided monitor eyepiece
assembly as indicated in Figure 23B.   The tracker sensor unit would
also be mounted on this new assembly at the same location as the
eyepiece on the current assembly.   Electrical signal leads from this
unit would be run to the control rack in the instrument room for tie-in
to the servo system.   Tracker sensor units have been proposed by
Schlumberger, Kollsman, and DBA, Inc. representing respectively
increasing price and performance, as shown in Figure 29.   This
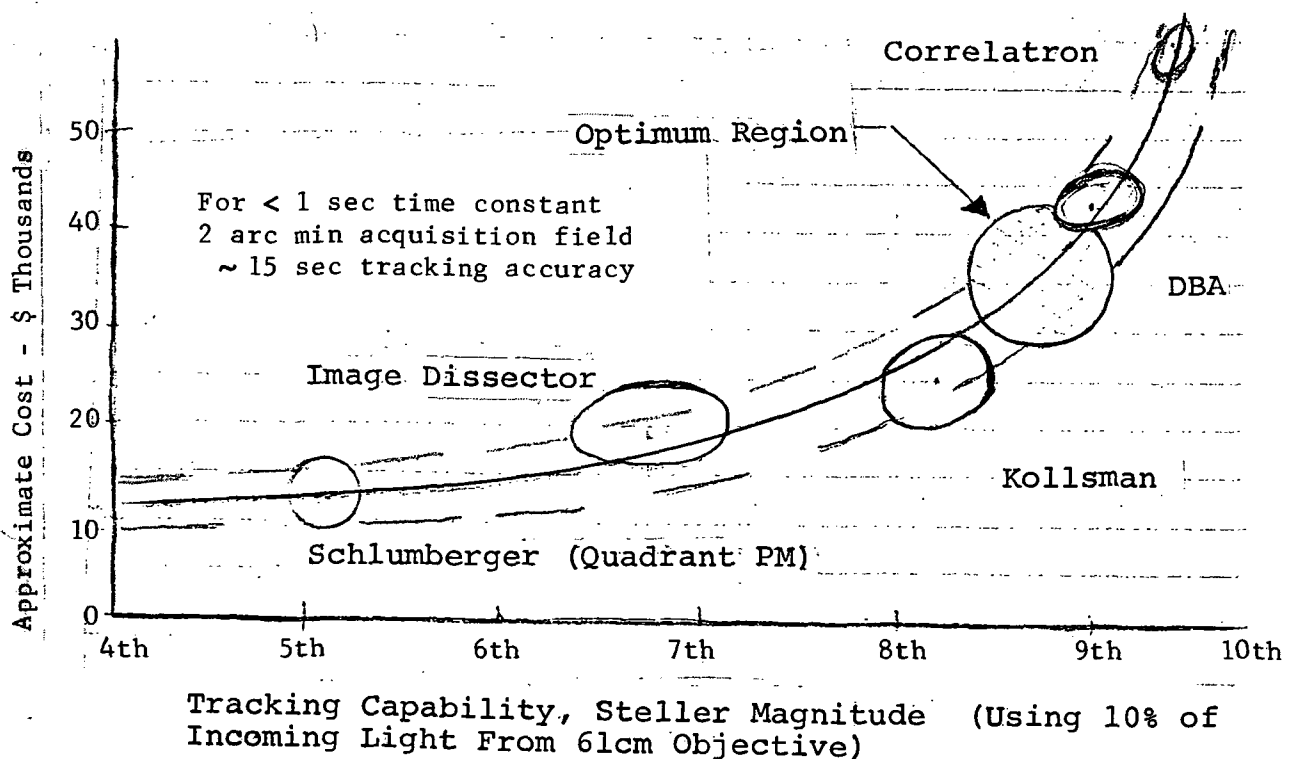represents the tradeoff that will have to be considered in deciding

FIGURE 29   Cost Effectiveness Curve - Autotrack System Tracker Unit

which meets the objective, though GAC tentatively recommends the DBA
Isocon TV centroid tracker approach.   An analysis of both the Isocon
and image dissector approaches, performed by DBA, is given in Appendix I
Using the DBA recommended auto track system, it whould be possible to
use a 15-arc second aperature for the detection system with a 2-arc
minute acquisition field on the auto track system.

Several companies which manufacture star trackers have been contacted as well as some individuals for inputs concerning possible auto track techniques.

Ed Tyson of the Cloudcroft Observatory was contacted and recommended DBA Systems of Melbourne, Florida. GAC preliminary evaluation indicates that a correlatron version would be feasible.

C. L. Rogers, consultant, has an approach to auto track (shown in Appendix E.).

Inputs received are given below along with an approximate cost range.

Nutation with Quadrature Oscillator ($5 to 10K). The cost is attractive. The frequency of nutation must be kept low, i.e., approximately 0.25 Hz to stay within the servo bandpass. This means that error information is only obtained once every 4 seconds. This would not be adequate for a low error tracking system.

A possible improvement would be to nutate only the light beam with a wobble mirror. A higher nutation frequency of 30 to 60 Hz could be obtained in this manner.

Maximum potential tracking accuracy for this system must still be determined. (See Appendix E.)

Schlumberger ($10 to 15K). This system utilizes a photomultiplier tube whose active surface is divided into four quadrants. Positional error is determined by algebraic summation of the light values received on each quadrant. This technique is analogous to a monopulse auto track radar.

Kollsman ($20 to 25K). The Kollsman system utilizes an image dissector and provides a tracking accuracy of 0.25 to 0.5 seconds of arc. A nine-month delivery time is anticipated.

DBA Systems ($35 to 40K). This system utilizes an image-isocon/TV display. Probable system parameters are 2 minute acquisition with 1 or 2 TV lines of tracking accuracy to yield 0.5 second of arc tracking accuracy. Advantages are ease of boresighting and acquisition because of the TV display of the main telescope video. (See Appendices D and F.)

Correlatron System ($50 to 75K). Goodyear Aerospace could develop a correlatron or similar type system to suit the requirements of the proposed system.

ITT work in this area was also investigated, but they did not have available hardware for this purpose.

Over-all performance and lower cost will probably be obtainable by purchasing an auto track system from a manufacturer rather than developing such an item from scratch, and is therefore recommended.

Among the manufacturers listed, accuracy seems inherent and is therefore not a tradeoff item versus cost. However, reliability, maintainability, ease of operation, compatibility with existing installation, and inherent magnitude sensitivities will have to be compared to determine the optimum approach. The DBA system is favored.

For reference purposes Figure 30 shows a block diagram of the present polar axis control system. Figure 31 shows the polar axis control system in an auto track mode. This change of configuration can be relay switched and presents no problems.

As shown by the inset diagram in Figure 31 the system will operate as a Type II position loop. This means that for targets moving with essentially constant velocity no positional error will occur from the mount drive. Any position errors will be a result of (1) tracker error, and (2) target acceleration.

Target acceleration errors will be on the order of 0.25 RAD per rad/sec^2 acceleration of target.

Control system stability and structural response characteristics should remain essentially as they are now.
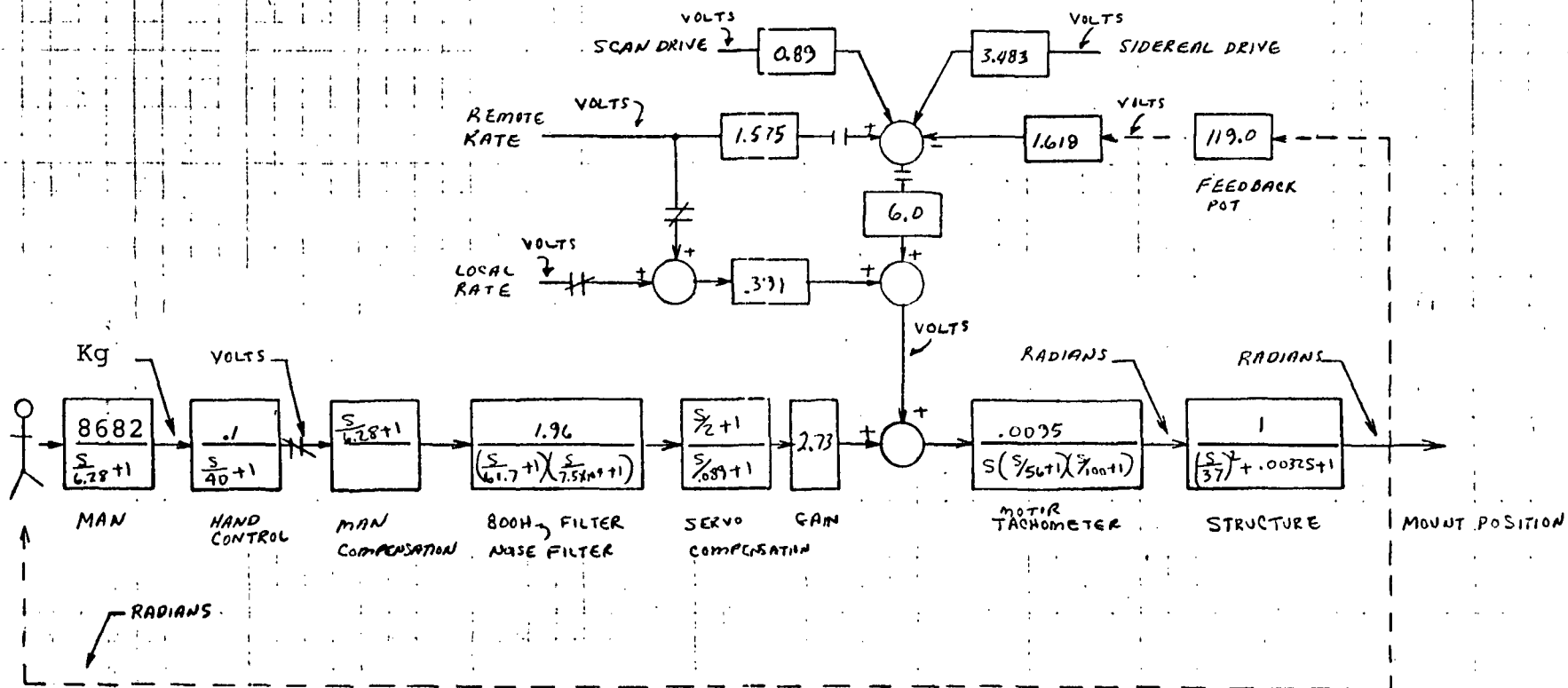
There are several operational features desirable in the auto track mode which are not shown in Figure 31 but will be a part of the modification.

> (1) Bias-Operator control to adjust tracking axes, if needed, to place target video in center of field of view.

> (2) Coast-Operator control to place servo drive system in a rate-hold mode if another light source temporarily coincides with the target.

No significant problem areas are evident at this time.

Data Recording and Reduction

Analog Versus Digital Recording - When using pulse counting techniques it is possible to convert the pulse rate into an analog voltage which could in turn be recorded by the existing oscillograph and backup FM recorder. However, in view of the magnitude of the data reduction effort required when recording on the oscillograph, it is recommended that the data pulse rates be appropriately formatted and digitally recorded. This will allow a much more direct route to the computer while eliminating the possibility for human error in the data reduction process. It has been estimated that on the average, two minutes per data point is required to reduce data from the oscillograph record. For 229 meter of altitude resolution at the sunset point, 160 points would be required for each eclipse excluding calibration points for 120,000 feet. Thus each eclipse would require 320 minutes or 5 1/3 hours of data reduction time before reaching the computer. With a properly formatted and controlled digital data recording system, it is estimated that this time could be effectively reduced to 1/10 of the manual reduction time. A block diagram of the digital data formatting system concept is shown in Figure 32. One possible data format is shown in Table VI.

FIGURE 30 Photometric Observatory Polar Axis Servo Drive Block Diagram

INTEGRAL + PROPORTIONAL

ERROR VOLTAGE

RADIANS
SATELLITE POSITION

TRACKER TRANSFER FUNCTION

$\frac{K}{S}$

F

ADDITIONAL COMPENSATION IF NEEDED

RADIANS

$\frac{.0095}{S\left(\frac{S}{56.1}+1\right)\left(\frac{S}{60}+1\right)}$

MOTOR/TACH

$\frac{1}{\left(\frac{S}{37}\right)^2 + .00725 + 1}$

STRUCTURE

MOUNT POSITION

OPEN LOOP GAIN (db)

-40 db

-20 db

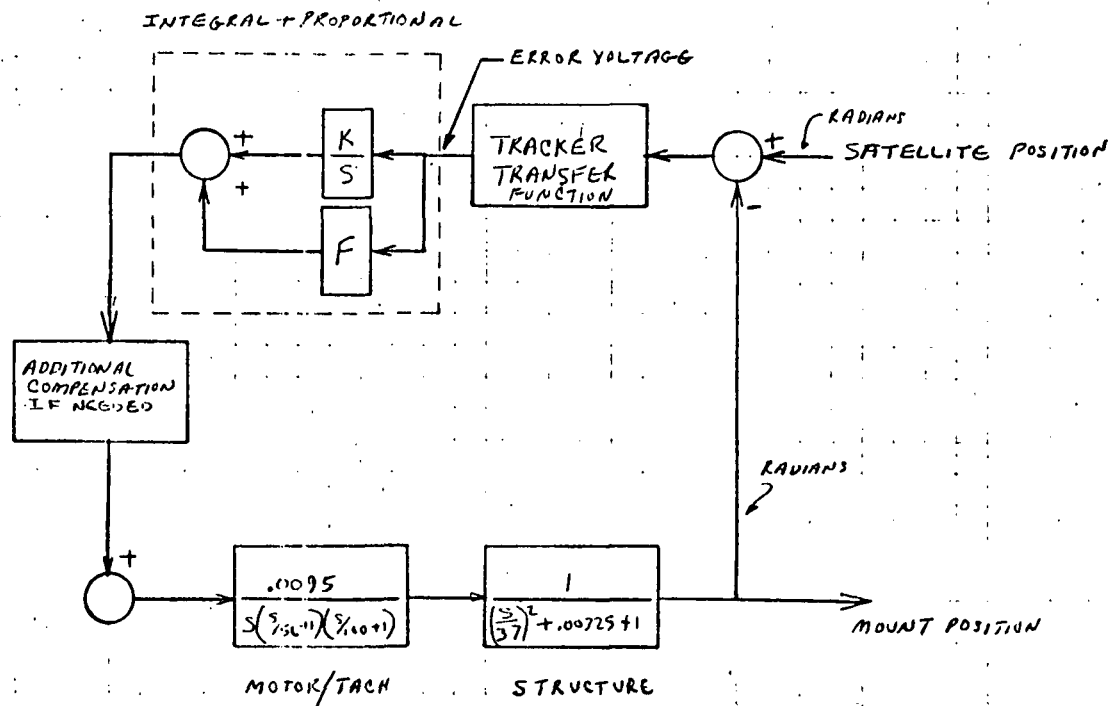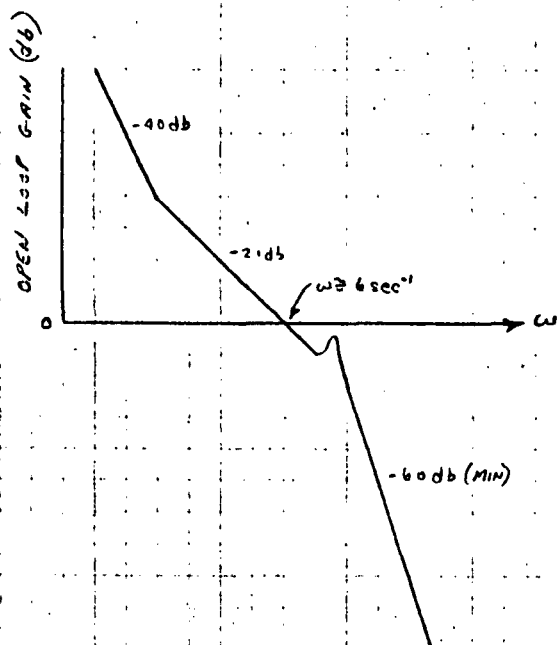$\omega \approx 6 \sec^{-1}$

0

ω

-60 db (MIN)

76

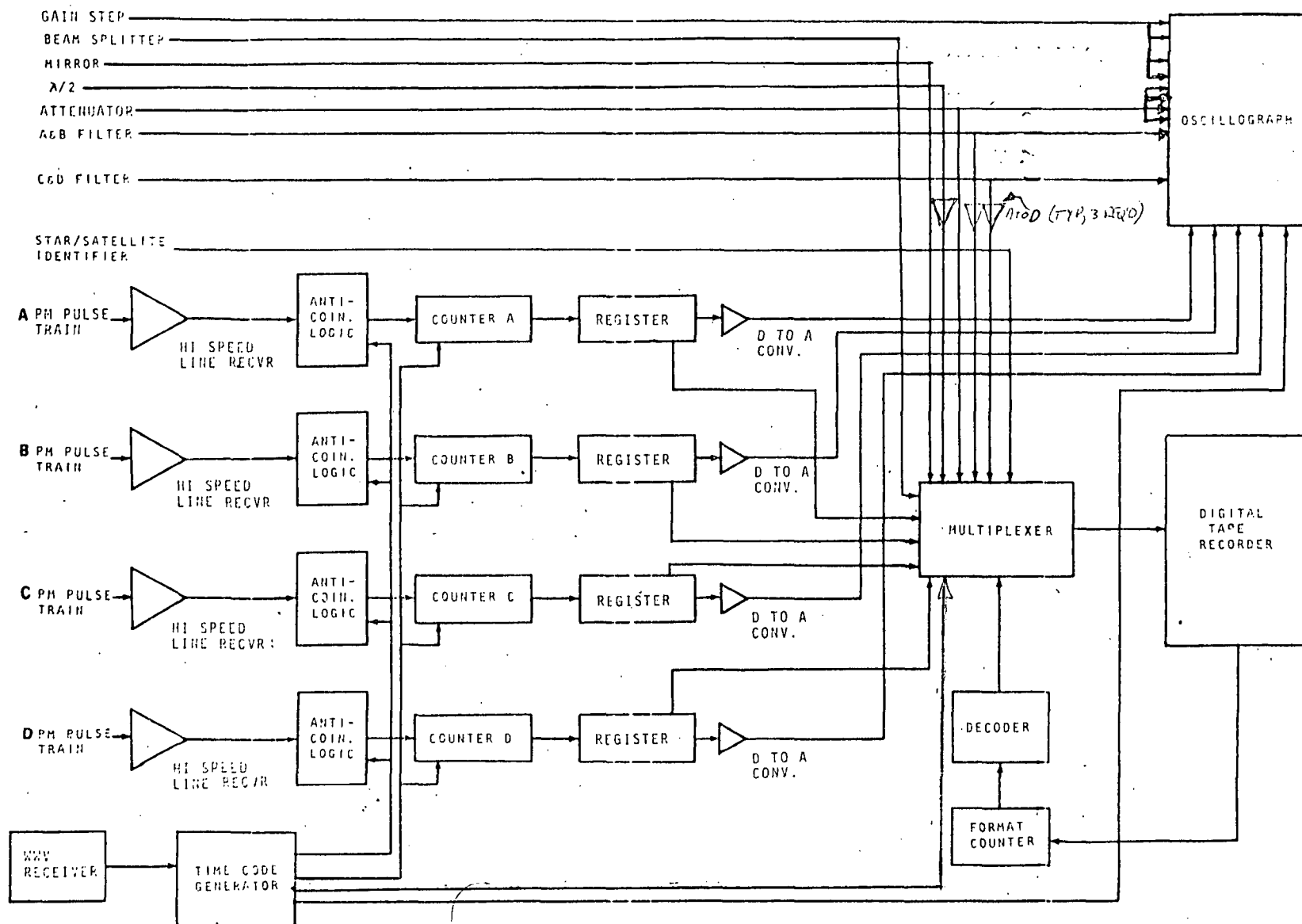FIGURE 31 Servo Drive Block Diagram Photometric Observatory Autotrack Mode

FIGURE 32 Digital Data Formatting Concept

Page intentionally left blank

Digital Recording Concept - The basic concept is to record the data in an IBM compatible format with a synchronous digital, 8-bit plus parity, tape recorder. The oscillograph would be used as a real time monitor for data and as a backup recording of the data. The existing FM tape recorder would not be used. The formatter would consist of a format counter, decorder, storage registers and pulse counters. The decoder sequencially directs the storage registers to feed data to the tape recorder input via the multiplexer. The format counter advances at each "red" strobe sent by the tape recorder thus addressing the next data byte. The pulse counters integrate the photoelectron pulses over an integration time interval controlled by one of the time code generator's outputs. Anticoincidence logic is required to prevent count ambiguities from arising from a pulse count occurring during transfer of data from the counters into the storage registers. The auxiliary data itmes of half-wave plate and filter wavelength require analog to digital conversion since they are presently coded into voltage levels.

Time Recording Requirements - It is recommended that a time code generator be installed which gives day of year, hour day, minutes, seconds, and milliseconds with parallel BCD outputs and which can be manually synchronized with WWV to within one millisecond. Accurate determination of the altitude of the light path through the upper atmosphere requires precise correlation of the universal time with signal level. The stability of the time code generator should be such that error buildup from initial sync with WWV would be less than one millisecond per hour. With this stability, synchronization with WWV would only be required once for each nightly observation period. The typical rate of change of altitude at the sunset point is 4.6 meters per millisecond so one millisecond of error is insignificant compared to the expected position accuracy of the satellite of about 305 meters. Propagation delays from WWV for 1.6 km range would be about five milliseconds which is also insignificant compared to the error in positional determination. Also, the propagation delay of the light received from the satellite tends to reduce this error. This time code generator would also provide the timing pulses to control the reset of the pulse counters and transfer of data to the storage registers thus controlling the integration time of the signal.

Data Monitoring - Monitoring of real time data acquisition should be accomplished using the oscillograph. This also provides a backup record of the data in case of loss of data on the digital recording system. To accomplish this, four medium accuracy digital-to-analog converters will be required along with associated grain adjusting features for the four photomultiplier signal channels. Four additional low accuracy digital-to-analog converters will be required for the new optical attenuators. A comparison between the existing and recommended oscillograph format is summarized in Table VII and shows that additional galvanometers are required to record data from the six extra channels.

In the past, WWV time ticks were recorded on the oscillograph with the instrumentation operator being required to write on the record to identify the hours and minutes. Since the WWV time code is compressed into a one-second time frame, it is not resolvable except at chart speeds of about 10 cm per second. Adequate resolution of eclipse photometry can be achieved with a paper speed of about 2.5 cm per

second. At this speed, 0.25 cm corresponds to a maximum altitude
change of about 457 meters at the sunset point. Since WWV time code
is not resolvable at the normal paper speed of 0.6 cm per second

TABLE VII   Oscillograph Recording Channel Requirements

Channels	Existing	Recommended
Signal Channels	2	4
Gain Step Channels	4	4 optical atten., 4 gain
Filter Wavelength Channel	2	2
Time	1	1
Total	9	15

used for noneclipse photometry and is not resolvable at the 2.5 cm
per second during eclipse photometry, it is recommended that the time
code generator is configured to produce the IRIG Format C serial time
code which has a time frame of one minute. This removes much of the
work load from the instrumentation operator and guarantees a readable
time record every minute regardless of WWV dropouts and regardless of
whether a paper speed of 0.6 cm per second or 2.5 cm per second is
used.

Sky Background

If a sky background image shifter to adjacent sky (for reference level
measurement) is decided upon rather than the other recommended options
(see paragraph on sky background in first main section on principles
and objectives), then probably the simplest of several alternatives
(solenoid, cam actuator, etc.) would be a rotating glass wedge
mounted in the light path above (or upstream) of the other optical
elements in the instrument head - - that is, ahead of the field stop -
that would shift the image slightly more than 1 field diameter. This
shifter wedge could be mounted on a small wheel covering the right
hand incoming light beam for an interval of 1/10 second out of each
second or more, driven at 60 rpm; or, if desired, it could be driven
more slowly (half speed, for example for longer eclipses). Its
installation would be quite simple, since its alignment is not
critical - - i.e., a slight tilt or displacement will not significantly
effect the optical path. (See Figure 33).

OPTICAL AXIS
LIGHT BEAM
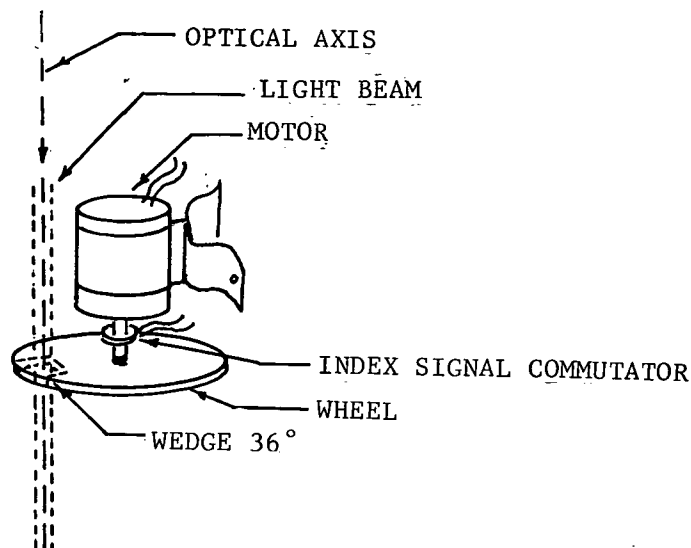MOTOR
INDEX SIGNAL COMMUTATOR
WHEEL
WEDGE 36°

FIGURE 33   Adjacent Sky Background Shifter Wheel

Concluding Observations on Equipment Improvement

In summary, the problem of fully exploiting the potential for narrow
band photometry of satellites going into eclipse is a very respectable
one because of the extemeely low light level source and the rapid rate
of change of this level. Accordingly, every possible improvement in
signal-to-noise ratio should be employed. If photomultipliers are
obtained with higher quantum efficiency thus reducing shot noise,
then the dominant noise contributor becomes sky background; and
therefore, to optimize the complete system, smaller field stops
should be used which in turn requires the auto track system. The
estimated improvement is system sensitivity for each of the areas
considered (i.e., photomultiplier upgrading, pulse counting, and auto
track) were determined assuming that the type of noise affected by
that system component was the dominant noise contributor. In reality,
the noises are intermixed and removal of one noise source unmasks the
presence of another. Therefore, the estimated improvement in system
sensitivity assumes all recommended modifications to improve signal-
to-noise ratio are incorporated and if only one of the changes are
made, its improvement to the system will be somewhat less than
indicated. In particular, pulse counting allows the system to reach
the theoretical sensitivity improvements as presented in this report.
For example, it is extimated that without pulse counting instead of
a 1.8 magnitude improvement arising from the new photomultiplier, an
improvement of only 1.4 magnitudes or less could be expected - - aside
from the other advantages it offers.

EXPECTED PERFORMANCE CAPABILITIES

While numerous alternatives were examined, and many found worthy of
consideration, most of those recommended were clearly superior and
offered substantial performance gain for the cost involved. They
represent quite well the inherent performance capbaility readily
attainable by modifications aimed at the stated objectives of ozone
measurement.

81

A relatively flexible choice remains as to which of the reasonable alternatives is finally selected; and, indeed, which are even included. Such choices will eventually be the result of NASA evaluation and direction, taking into account the results and recommendations of this study. However, the achievable performance capability indicated is as follows:

(1) Narrow band photometric measurements for ozone studies should be usable on satellites down to about the 5th magnitude corresponding to 9th magnitude in broadband, or 12th without eclipse (auto track can only be used to 9th magnitude - unless a 20% mirror is inserted.)

(2) Up to 4 filter channels can be selectively employed simultaneously, depending upon satellite brightness. This would permit various combinations, including measurement in both the Chappius band and near-UV (Hartley-Huggins bands) regions (e.g. 3300, 4500, 6000 and 7000Å).

(3) Measurement capabilities can be maintained through relatively adverse sky conditions (e.g., moonlight, twilight, ambient, etc.) with substantial magnitude reach through employemnt of 30 arc seconds (or even 15 arc seconds) field stop apertures, made practical by incorporation of the recommended quality auto track system.

(4) Data recorded on tapes at 0.05 second intervals can be rapidly and accurately processed by computer at low cost. The recommended quality signal processing circuitry techniques, and digital recording format (with real time analog monitoring and backup capability) plus appropriate software insures this capability.

(5) Required precision satellite position data to support measurements to a resolution and accuracy of ± 300 meters can be acquired by the recommended procedures.

(6) Between 500 and 1000 vertical ozone profile measurements per year over a wide geographical range (using 25 to 35 eclipses of 20 to 30 satellites, at 4 or 5 successive sites, depending on bunching, weather, etc.) would be obtainable by following the recommended mission planning and operational processes with the MOSPO modified as outlined. These could be successfully conducted with a 3-man field crew at nominal cost.

(7) The mobility and other characteristics of the MOSPO as modified for this purpose would permit global scope of measurement, dependent upon the need and pattern decided upon. Added real possibilities would be Chile, Alaska, Mexico, Australia, and Hawaii (Mauna Kea) - - all of which have good quality high altitude sites available. Ship, C5A, plus its own land mobility could be used, depending on schedule, etc.

(8) These capabilities would provide ozone measurement
     accumulation at a rate, scope, and quality plus low cost
     that would greatly exceed that obtainable by any other means.

OPERATIONAL TECHNIQUES

Operation of the new modified MOSPO system, with its refined and
improved capabilities, features and characteristics, will result in
a corresponding refinement in the operating procedures and techniques
for maximum effectiveness in the use of its capabilities for meeting
ozone measurement objectives. Additionally, the over-all mission
approach will likewise justify appropriate modifications oriented
toward maximum yield and attainment of measurement objectives.

Field Missions

As a first consideration, indicated by the second major section of
this report (under "Mission Considerations:), the observing windows
for ozone eclipse measurements are of a nature which brings in both
latitude and longitude in relation to orbit orientations of the
satellites to be used for the measurements, as well as other observing
parameters such as site altitude, climatic and sky characteristics, etc.
Examination of these factors have indicated that typical mission
planning would result in judicious selection of four or five sites for
sequential use during a full year's measurement operations, with time
at a given site ranging from perhaps 5 to 15 weeks.

Representative locations and sites for such an operation would be
expected to span a wide latitude belt between 30 and 45 degrees, and
sufficient longitude to accommodate both seasonal weather (affecting
both cloudiness and seeing conditions) and some added geographical
dispersion. Typical sites for consideration might well include:

Climax, Colorado	High Altitude Observatory Site
Mt. Hamilton, California	Lick Observatory
Mt. Hood or Mt. Ranier region	
Mt. Palomar, California or Table Mountain	
Mt. Lemmon or Mt. Hopkins, Arizona	
Yuma, or Kitt Peak, Arizona	
Cloudcroft, or Organ Mts., New Mexico	

While there are some other promising sites (e.g., the Southwestern
Texas mountains between Big Bend and El Paso, the Lowell Observatory/
Flagstaff area, and some sites up to 50° latitude in the Idaho and
Northern Washington and Montana regions), the ones listed have all
been surveyed at one time or another for MOSPO satellite photometric
work. They also offered attractive operational features for the
specific needs previously outlined for ozone eclipse work, particularly

in terms of sky conditions, altitude, etc. Some of the higher sites listed, running to over 14,000 feet, would be particularly favorable for simultaneous measurements in the near UV regions, as recommended earlier. Site access and support considerations are adequate at these locations, and well within the operational and mobility envelope of the MOSPO.

Field Operations

On-site field operations for the ozone measurement mission would not differ radically from those of previous photometric missions for measurement of satellite characteristics. However, calibration requirements would differ, being in general less stringent - - particularly in avoiding the need for second order extinction coefficient and scale factor measurements. Measurements of primary coefficients might also be reduced, the actual extent dependent on experience at the actual observing sites. Whenever given results significantly differ from computations made without them (which will result from extinction variation with color in addition to zenith angle, transparency and other effects) they should be made; but where such differences are not encountered, they can be reduced or eliminated.

In conducting the actual ozone eclipse pass measurement with the new equipment, the axes will be set up as before. However, acquisition and tracking range need only be sufficient to fully embrace the eclipse, including 30 to 60 seconds or more before and after. Acquisition will be made by manual control using the acquisition and guide scopes as before to bring the satellite tracking within a 2-minute acquisition field area. Then the operators auto track button is depressed and he observes the tracking system closure to within a field size of about 10 seconds or less. The operator should continue to monitor the tracking until it is extablished that satisfactory solid track is being held prior to eclipse, or even continue the monitoring through eclipse under a long (e.g. grazing) eclipse and/or windy night conditions. If track is lost, the acquisition process should be repeated. If necessary, wind shielding can be improved under extreme conditions by raising the windward side panel an appropriate amount to provide optimum shielding without interference with any part of the telescope through eclipse track. (If in doubt, a "swing through" check should be made.)

Prior to acquisition, instrumentation operationsshould be checked out on a star of comparable magnitude. Then prior to eclipse, and during it, the instrumentation operator should monitor the signal recording, observing the real time record on the oscillograph along with the other indicators provided (tracking signal level, photometric signal, time reference signal, attenuation and gain levels, etc.). A check should be made to endure that the main recorder is recording properly. During any calibration runs, proper identification should be set on the index coder. At the end of the eclipse the auto track should be allowed to run in "rate hold" mode with sky background photometric signals being recorded for another 30 seconds or so, completing the measurement.

Moonwatch points, if and when planned, will of course have to be taken ahead of the eclipse by the third crew member.

Data tapes can be mailed in, or if circumstances warrant, can be transmitted in for immediate processing. Satellite phone and data service makes this practical even from remote sites such as Alaska or Australia. The oscillograph recordings should also be labeled and mailed in to the project office for backup use if needed.

Maintenance

Maintenance of the new equipment will in general be somewhat improved, if anything over previous requirements. Optical alignment is more critical but will be bench aligned at the plant and should not change because of the rigidity on the housing and mountings. Main telescope alignment characteristics and requirements are not effected by the changes - - the requirement is still for proper alignment and columnation (see manual) with the main beam covering the field stop area. Auxiliary scope boresighting needs are the same as before for acquisition use, but probably somewhat less critical because of auto track.

The new signal processing circuitry will tend to be much more stable if anything than the previous d.c. analog circuitry. In general, if good maintenance practices as previously spelled out, including proper checking and adjustment, cleanliness and equipment protection, are followed in accordance with the manual and good practice, relatively little trouble should be encountered.

Operational Measurement Modes

Should it be desired to make regular satellite or other type photometric measurements during ozone missions, the recommended modifications all provide for maintaining the previous operating modes (with improved signal processing and recording). For UBVRI photometry in the various modes (beam splitting, time sharing, etc.), for polarimetric, or any of the previous capabilities, the corresponding external and control settings can be made (see manual), and then just as easily restored to the new narrow gand ozone photometry configuration.

Note that there are a number of modes for ozone measurement available with the equipment newly modified as recommended: - - either 4 or 2 channel oepration(doubling the light level), variation of pulse counting (integration time) interval, attenuation filter settings, narrow band filters used, etc. The optimum settings for each measurement will have to be established as a matter of judgement based on experience taking into account such factors as satellite brightness, eclipse duration, sky conditions, measurement objectives, etc., using the values given in the operations manual and guidelines established by the project office to fit the mission objectives.

SUGGESTED IMPLEMENTATION PLAN

The recommended changes to the equipment to bring about the full ozone measurement capability described are quite straightforward and relatively simple. All lie well within current state-of-the-art and use currently available materials and equipment. Therefore, the implementation time required for equipment modification is fairly short and largely effected by considerations of adequate procurement lead time after decisions and selections are made. The missions could be initiated as soon as schedules and site locations are established following analysis of the eclipse measurement windows for meeting the objectives established.
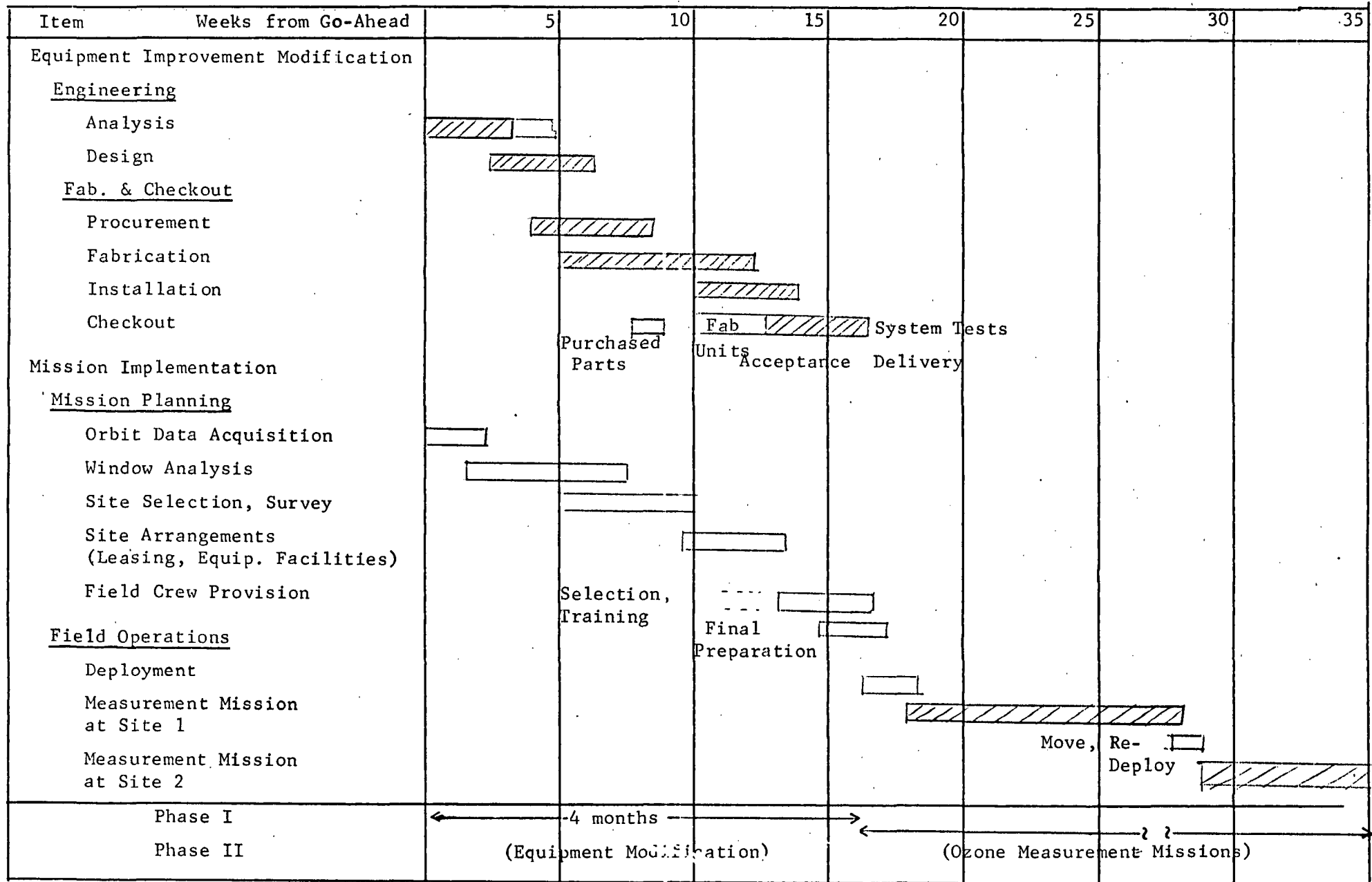
It would be possible to implement the program completely on a one-step basis, or to do a partial or step-wise incremental implementation program, and also to follow correspondingly any mission operations cycle desired form intermittent to continuous. Clearly, the direct one-step implementation of the full modification at one time would be most efficient and least costly over-all, and the continuous mission plan would be most effective in providing maximum yield at the lowest cost per measurement obtained. Therefore, since it is the most straightforward and simplest to show, this full implementation plan will be shown, and is recommended for the reasons stated. Any other approach plan can be derived from the elements included in the full plan presented.

The optical and mechanical modifications (including installation of new phototubes and all assocaited changes), the electronic signal processing equipment changes, the auto track installation, and recording equipment changes can all procede essentially in parallel without significant interference with each other, including individual checkout. Then as they are completed, system integration and final checks are carried out together on the system as a whole. The general plan and a typical (nominal) schedule is given in Figure 34.

As can be seen, this is approximately a four-months plan for the improvement modification of the equipment as recommended for optimum ozone measurement capability. All parts are going along in parallel through the engineering design, procurement, fabrication and checkout cycle. If considered urgent or worthwhile, procurement expediting could shorten this. The over-all plan is based on acceptance test and delivering in four months with immediate deployment and field mission capability at that time.

The field mission implementation plan allows ample time for the preliminary mission planning, window analysis, site survey and selection, arrangements, and crew parparation to be ready for operation at the time the equipment is ready for deployment; with the field crew participating fully in the final checkout. This conforms closely to the general plan followed in original and subsequent deployment of the MOSPO, which worked out very successfully. Since this is a relatively minor operation by comparison, there should be no difficulty in carrying it out according to this plan.

Figure 34. Recommended Implementation Plan and Schedule

Item — Weeks from Go-Ahead	5	10	15	20	25	30	35

Equipment Improvement Modification

<u>Engineering</u>

    Analysis

    Design

<u>Fab. & Checkout</u>

    Procurement

    Fabrication

    Installation

    Checkout   Fab   System Tests

Purchased Parts   Units   Acceptance Delivery

Mission Implementation

<u>Mission Planning</u>

    Orbit Data Acquisition

    Window Analysis

    Site Selection, Survey

    Site Arrangements (Leasing, Equip. Facilities)

    Field Crew Provision   Selection, Training   Final Preparation

<u>Field Operations</u>

    Deployment

    Measurement Mission at Site 1   Move, Re-Deploy

    Measurement Mission at Site 2

| Phase I | ←———— 4 months ————→ | | | | | |
| Phase II | (Equipment Modification) | | ← | (Ozone Measurement Missions) | | → |

87

"THIS PAGE LEFT BLANK ON PURPOSE"

APPENDIX A

COMPUTER PROGRAM FOR RELATING OBSERVABLE ECLIPSE FREQUENCY
WITH SITE LATITUDE AND SATELLITE ORBIT PARAMETERS

```
1           INTEGER LAT(180), LATS(180), PRINT
2           DATA EPS /23.4427/, RE /6378.16/
3           REAL I
4           ARSIND(X) = ARSIN(X)*57.29578
5           ARCOSD(X) = ARCOS(X)*57.29578
6           SINE = SIND(EPS)
7           COSE = COSD(EPS)
8         1 READ (1,5,END=99) H, I, DLONG, DNODE, DPHI, ALTMIN, PRINT
9         5 FORMAT(6F10.0, I5)
0           ISKIP = 0
1           IF (PRINT .GT. 0) ISKIP = 1
2           DO 7 J = 1, 180
3           LAT(J) = 0
4         7 LATS(J) = 0
5           SINI = SIND(I)
6           COSI = COSD(I)
7           SINA = RE/(RE+H)
8           A = 180. - ARSIND(SINA)
9           COSA =-SQRT(1. - SINA**2)
0           DELPHI = ARCOSD(SINA*COSD(ALTMIN)) - ALTMIN
1           PD = 17.043629*SQRT(SINA**3)
2           J1 = 180./DLONG
3           K1 = 360./DNODE
4           CON1 = 1./J1/K1
5           CON2 = CON1*PD*DELPHI/360.
6           WRITE (3,10) H, I, DLONG, DNODE, DPHI, ALTMIN, A, DELPHI, PD
7        10 FORMAT('1   H        I      DLONG   DNODE    DLAT   ALTMIN        A        D
           1ELPHI     REV/DAY'/F6.0,F8.1,2F7.0,F9.2,F7.0,F10.2,2F9.2/)
8           DO 25 J = 1, J1
9           XLONG = (J-1)*DLONG
0           SINL = SIND(XLONG)
1           X = COSD(XLONG)
2           Y = SINL*COSE
3           Z = SINL*SINE
4           ALPHA = ARGD(Y, X)
5           DELTA = ARSIND(Z)
6           IF (PRINT .EQ. 1 .OR. PRINT .EQ. 3) WRITE (3,15) XLONG, X, Y, Z,
           1    ALPHA, DELTA
7        15 FORMAT(F10.2, 10X, 3F10.5, 2F10.2)
8           DO 25  K = 1, K1
9           XNODE = (K-1)*DNODE
0           COSN = COSD(XNODE)
1           SINN = SIND(XNODE)
2           P = X*COSN + Y*SINN
3           S = -X*SINN + Y*COSN
4           Q = S*COSI + Z*SINI
5           R = -S*SINI + Z*COSI
6           ALPHAP = ARGD(Q, P)
7           DELTAP = ARSIND(R)
8           COSV = COSA/SQRT(P**2 + Q**2)
9           IF (COSV .LE. -1) GO TO 25
0           V = ARCOSD(COSV) + ALPHAP
```

```
      SINP = SIND(V)*SINI
      PHI = ARSIND(SINP)
      PHIS = (SINP - COSA*Z)/SINA
      IF (ABS(PHIS) .GT. 1) PHIS = SIGN(1., PHIS)
      PHIS = ARSIND(PHIS)
      IF (PRINT .GE. 2) WRITE (3,20) XNODE, P, Q, S, R, ALPHAP, DELTAP,
     1    V, PHI, PHIS
   20 FORMAT(10X, F10.2, 4F10.5, 5F10.2)
      M3 = ABS(PHIS/DPHI) + 1.5
      LATS(M3) = LATS(M3) + 1
      M1 = (PHI - DELPHI)/DPHI + 1000.5
      M2 = (PHI + DELPHI)/DPHI + 1000.5
      DO 25 M = M1, M2
      M4 = IABS(M - 1000) + 1
   25 LAT(M4) = LAT(M4) + 1
      WRITE (3,30) ISKIP
   30 FORMAT(I1,' LAT', T23, 'SHADOW', T48, 'SUNSET'/)
      J2 = 90./DPHI + 1
      XLAT = 0.
      LAT(1) = LAT(1)*2
      LATS(1) = LATS(1)*2
      DO 40 J = 1, J2
      PROB1 = LAT(J)*CON2/COSD(XLAT)
      PROB2 = LATS(J)*CON1
      WRITE (3,35) XLAT, LAT(J), PROB1, LATS(J), PROB2
   35 FORMAT(F6.2, 2(I15, F10.4))
   40 XLAT = XLAT + DPHI
      GO TO 1
   99 CALL EXIT
      END
```

91

INPUT DATA CARD

COL.	SYMBOL	FORMAT	DESCRIPTION
1-10	H	F10.0	HEIGHT OF SATELLITE
11-20	I	F10.0	INCLINATION
21-30	DLONG	F10.0	INCREMENT IN LONGITUDE OF SUN
31-40	DNODE	F10-0	INCREMENT IN RIGHT ASCENSION OF NODE
41-50	DPHI	F10.0	SIZE OF LATITUDE CELL FOR FREQUENCY DISTRIBUTION*
51-60	ALTMIN	F10.0	MINIMUM ALTITUDE ANGLE AT WHICH AN ECLIPSE ENTRY CAN BE OBSERVED
61-65	PRINT	I5	CONTROLS AUXILIARY PRINTOUTS:

PRINT - 1 or 3: PRINT SUN'S LONGITUDE AND RECTANGULAR EQUATORIAL COORDINATES

PRINT = 2 or 3: PRINT ORBITAL COORDINATES OF SUN AND SATELLITE, AND SHADOW AND SUNSET LATITUDES

NOTE: RUNS MAY BE STACKED BY INCLUDING MORE THAN ONE DATA CARD.

*IF DPHI IS LESS THAN .5, THE DIMENSIONS OF LAT AND LATS MUST BE CHANGED

APPENDIX B

NOISE CONTRIBUTIONS IN NARROW BAND PHOTOMETRY USING

THE MOBILE SATELLITE PHOTOMETRIC OBSERVATORY 1973

NOISE CONTRIBUTIONS IN NARROW BAND PHOTOMETRY USING

THE MOBILE SATELLITE PHOTOMETRIC OBSERVATORY   1973

The photomultiplier shot noise was calculated to be the square root of the number of photoelectron events per integration time of the signal.

The number of photoelectron events due to a particular stellar magnitude of signal were calculated as follows: [*]

Since the sun's magnitude is -26.73 and the energy produced by the sun on a normal surface above the atmosphere is 0.192 watts $cm^{-2}u^{-1}$ at 0.55u, the magnitude of. any G2 star can be related to the energy received by a telescope of diameter D (cm) by

$$\log W (0.55u) = 2 \log D - 0.4 m_v + \log \Delta \lambda \qquad -11.51$$

where $\Delta \lambda$ is measured in microns and W in watts. In order to determine the energy at some other wavelength or temperature, Wien's approximation to Planck radiation law for hemisphereical radiation per unit area per unit wavelength interval was combined withthe above equation. This was done by multiplying a correction factor of $\frac{J(\lambda, T)}{J(\lambda_0, T_0)}$ where $J(\lambda_0, T_0)$ is Wien's approximation evaluated at $\lambda_0 = 0.55u$ and To = 6000°K.

*Reference GER-12807 S/4, 6 December 1966, SP-5073, Filter Selection and Determination of the Limiting Accuracy of the new Photometric System for the Mobile Observatory, Goodyear Aerospace Corporation, Akron, Ohio

Wien's approximation is

$$J(\lambda, T) = c_1 \lambda^{-5} e^{-c_2/\lambda T}$$

where $C_1 = 2\pi \hbar c^2$ and $C_2 = \dfrac{hc}{K} = 14380$ micron degree

The resulting equation in logarithmic form is

$$\log W(\lambda, T) = 2 \log D - 0.4\, m_v + \log \Delta \lambda - 11.51 - 5 \log \frac{\lambda}{0.55}$$

$$- \frac{6240}{T} \left(\frac{1}{\lambda} - 1.82 \right)$$

where W is measured in watts, D in centimeters, λ in microns and T in degrees Kelvin (Reference 2).

Using the above equation, the number of signal events versus magnitude were plotted. This was done by multiplying energy in watts by the current yield per watt of the photomultiplier, which was converted from quantum efficiency q into the current yield Y by the equation

$$q = \frac{1.240}{\lambda \text{ (microns)}} \quad (\text{amperes watt}^{-1})$$

However, after calculating the energy in watts, a correction factor based on optical and atmospheric losses was determined. The current yield was then calculated and converted into electrons per second. This rate of photoelectron events was then multiplied times the integration time of the system (.05 seconds). The calculations follow.

- -

Reference 2 Whitford, A.E. "PHOTOMETRIC TECHNIQUES" Handbuch der physik
pages 240-255

Existing System (9558QA Photomultiplier)

$$\Delta \lambda = .0018\mu \quad \text{for NB filter at } 7000\text{A}^\circ$$

$$\log W = 2 \log 24 \times 2.54 - 0.4\, m_v + \log .0018\mu$$

$$-11.51 \quad -5 \log \frac{.7}{.55} - \frac{6240}{6000} \left(\frac{1}{.7} - 1.82\right)$$

$$= -10.81 \quad -0.4 m_v$$

Assuming 7000A° light path is one of 2, a 50% transmissive NB filter and a 30% loss due to atmospheric extinction and miscellaneous optical losses then:

W must be multiplied by $1/2 \times .5 \times .7 = .175$

let $W' = .175 \times W$

then $\log W' = -10.81 - 0.4\, m_v - .76 = -11.57 - 0.4 m_v$

$$Y \text{ (amp/watt for 9558QA @ } 7000\text{A}^\circ) = \frac{q}{1.240} \times \lambda = \frac{.05}{1.240} \times .7$$

$$= .0282 \text{ amp/watt}$$

$$Y \times .625 \times 10^{19} \text{ e/sec amp} = .0176 \times 10^{19} \text{ e/sec watt}$$

let n = number of events

then $n = W' \times .0176 \times 10^{19} \text{ sec.}^{-1} \times .05 \text{ sec}$ where .05 sec is the integration time of the system.

$$\therefore n = W' \times 8.8 \times 10^{15}$$

In logarithmic form:

$$\log n = \log W' + 15.94$$

$$= -0.4\, m_v + 4.37$$

Dark count $= 4$ e/cm^2 x $\pi (2.54)^2$ = 80 cts/sec = 4 cts/system integration time

Dark noise for 9558QA @ $-10°C$ = $\sqrt{4}$ = 2

<u>for C31034A</u>   q = .26 @ 7000A$^{\circ}$

$$Y = \frac{.26}{1.240} \times .7 = .146 \text{ amp/watt}$$

$$\frac{.146}{.0282} = 5.2 \text{ increase over } 9558QA$$

$\therefore$ log n = -0.4 m$_v$ + 5.09

Dark count C31034A @ $-10°C$ = 45 cts/sec = 2.3 cts/system integration time

Dark noise = $\sqrt{2.3}$ = 1.52

<u>For ITT   FW 130</u>

Y = .012 amp/watt

decrease $\frac{.028}{.012}$ = 2.34
compared
to 9558QA

$\therefore$ log n = -0.4 m$_v$ + 4.37 $-$ log 2.34

log n = -0.4 m$_v$ + 4

Dark count $= 2.5$ cts/sec x .05 sec = .125 cts/system integration time

Dark noise = $\sqrt{.125}$ = .35

log .35 = $-.455$

<u>Preamplifier Current Noise</u> = .01 pa per HZ(pp) for Analog Devices 301

for 10 hz b.w., noise current = .01 x $\sqrt{10}$

= .032 x 10^{-12} amp pp

referred to PM cathode, this noise current is $\dfrac{.032 \times 10^{-12} \times .625 \times 10^{19} e/sec.}{6 \times 10^5}$

= 0.3 e/sec

for integration time of .05 sec n = .015

<u>Sky background</u> based on 21.5 mag/sec^2 for 1' diameter field stop

= 21.5 = $\dfrac{\log \pi \, 30^2}{\log 2.51}$ = 21.5 - $\dfrac{\log 2820}{.4}$

= 21.5 - $\dfrac{3.45}{.4}$ = 12.9 magnitude

Sky background based on 21.5 mag/sec^2 for <u>30"</u> field stop =

= 21.5 - $\dfrac{\log \pi \, (15)^2}{\log 2.51}$ = 21.5 - $\dfrac{2.85}{.4}$ = 14.4 mag

log n for C31034 @ 14.4 mag = -1

log (corresponding noise) = -.5

Sky background based on 18.5 mag/sec^2 for 1' diameter field stop

= 12.9 mag -3 = 9.9 mag

for C31034A this corresponds to n = 14

sky backgorund noise then = $\sqrt{14}$ = 3.75

log 3.75 = .575

APPENDIX C

CALCULATIONS OF ATTENUATION REQUIREMENTS FOR AVOIDANCE

OF PULSE PILE UP

CALCULATIONS OF ATTENUATION REQUIREMENTS FOR AVOIDANCE
OF PULSE PILE UP

	U	B	V	R	I	
Effective Wavelength	.36	.44	.55	.70	.90	microns
① Approximate Relative Solar Energy	.61	1	.95	.73	.46	
② Relative Atmospheric Transmission	.42	.60	.72	.78	.82	(at sea level)
③ Bandwidth of Filter	.07	.10	.10	.19	.21	microns
④ C31034A Absolute Sensitivity	.11	.12	.13	.14	.01	amps/watt
① x ② x ③ x ④	.0020	.0070	.0089	.0150	.0008	
Relative System Response (Magnitudes)	2.2	.83	.55	0	3.2	

18Å Narrow Band response relative to "R" band $= \dfrac{\log \dfrac{.19}{.0018}}{.4}$

$\approx$ 5 magnitudes

Maximum exposure NB, 2 light paths = -2 magnitudes

Pulse pile-up NB = +1 magnitude

100

APPENDIX D

GOODYEAR STAR TRACKER

FEASIBILITY/PROPOSAL

Prepared by: DBA SYSTEMS, INC.
                        Electro Optics Division
                        P. O. Drawer 550
                        Melbourne, Florida 32937

Prepared for: Goodyear Aerospace
                        1210 Massillon Road
                        Akon, Ohio 44315

Dated: 27 September 1973

CONTENTS

FIGURES

i

LIST OF SYMBOLS

I   incident radiant energy on surface of the earth

Io   incident radiant energy at the top of the atmosphere

m   air mass number

a   transmission coefficient for air mass 1 at a given wavelength

T   transmission through the earth's atmosphere

f optical focal length

λ wavelength

N_s star flux generated electrons

θ instantaneous field of view in radians

H   height

R   theoretical angular diameter discernable by an optical system

d   lens diameter

r   radius

S   photocathode sensitivity

Q   quantum efficiency of photocathode

E_s star illuminance

α scan efficiency factor

σ attenuation coefficient

t   dwell time

E   illuminance of an image through the optical system

A_a area of electronic aperture

A   area of scan field

G   optical gain of the telescope

FEASIBILITY

1.0   STAR ANALYSIS

The irradiance for a zero magnitude star, assuming a Planckian

emitter, is:

$$I_o = 2.65 \times 10^{-10} \text{ lumens/cm}^2$$

$$\text{or } 0.25 \times 10^{-6} \text{ ft candles.}$$

Therefore, the irradiance for an M magnitude star becomes:

$$I_m = (0.25 \times 10^{-6})(2.512^m)^{-1} \text{ ft-candles}$$

$$\therefore I_9 = (0.25 \times 10^{-6})(2.512^9)^{-1}$$

$$= 6.25 \times 10^{-11} \text{ ft candles}$$

These figures are based on star irradiance as observed above the earth's atmosphere.
The next section describes the absorption and scattering of the earths atmosphere
and how this effects the detection of stars.

2.0   ATMOSPHERIC ABSORPTION

The absorption of radiation through the atmosphere can be expressed

by:

$$I = I_o a^m$$

I_o = incident radiant energy at the top of the atmosphere

a = transmission coefficient for an air mass of 1 at a given wavelength

m = the air mass number

I = incident radiant energy on the surface of the earth.

The transmission coefficient through the atmosphere varies as the wavelength
of the radiation under consideration. Figure 1 shows the atmospheric absorption
as a function of wavelength and without regard to strong absorption bands.

-1-

The principle contributors to atmospheric absorption, through a perfectly clear sky, are molecular absorption and molecular scattering. Molecular scattering varies inversely with the fourth power of the wavelength, and accounts for the blue color of the sky. Molecular absorption is due primarily to ozone and water vapor in the atmosphere.

Transmission through the earth's atmosphere may be expressed as:

$$T = e^{-\sigma n}$$

σ = attenuation coefficient

n = number of equivalent atmospheres

when A = 1 (Zenith) the transmission is

$$Tz = e^{-\sigma}$$

therefore $T = T_z^n$

Figure 2 is a plot of n versus elevation angle. Thus, Figures 1 and 2 may be used in conjunction to determine the amount of radient energy reaching the surface of the earth's atmosphere.

For example:

What is the irradiance of a + 9^m star on the surface of the earth, at an elevation angle of 90°, as viewed in the visible region.

From equation $Iq = 6.25 \times 10^{-11}$ ft candles

From Figure 1: % transmittance = 85%

From Figure 2: # of equivalent atmosphere at 90° elevation = 1.0

$\therefore$ $1 = 6.25 \times 10^{-11}$ (.85) (1.0) foot candles

$1 = 6.25 \times 10^{-11}$ (.85) foot candles

$1 = 5.3 \times 10^{-11}$ foot candles for a $+9^m$ /star at a 90° elevation angle and at a wavelength of .556 μ.

-2-

% TRANSMISSION OR ATTENUATION
-3-

WAVELENGTH λ IN MICRONS
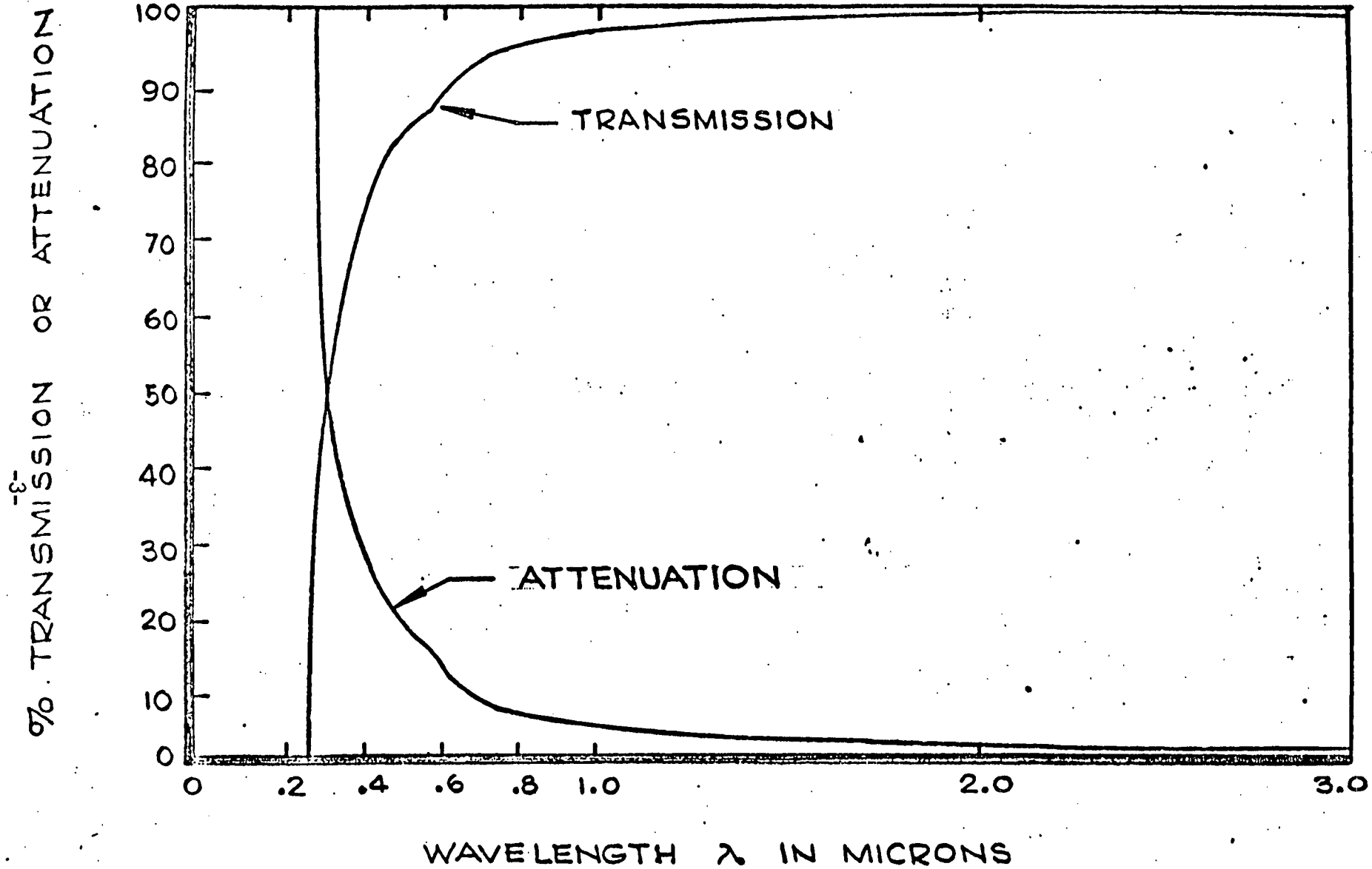
ATTENUATION AND TRANSMISSION OF CLEAR
ATMOSPHERE NEGLECTING ABSORPTION BANDS

FIGURE 1

105
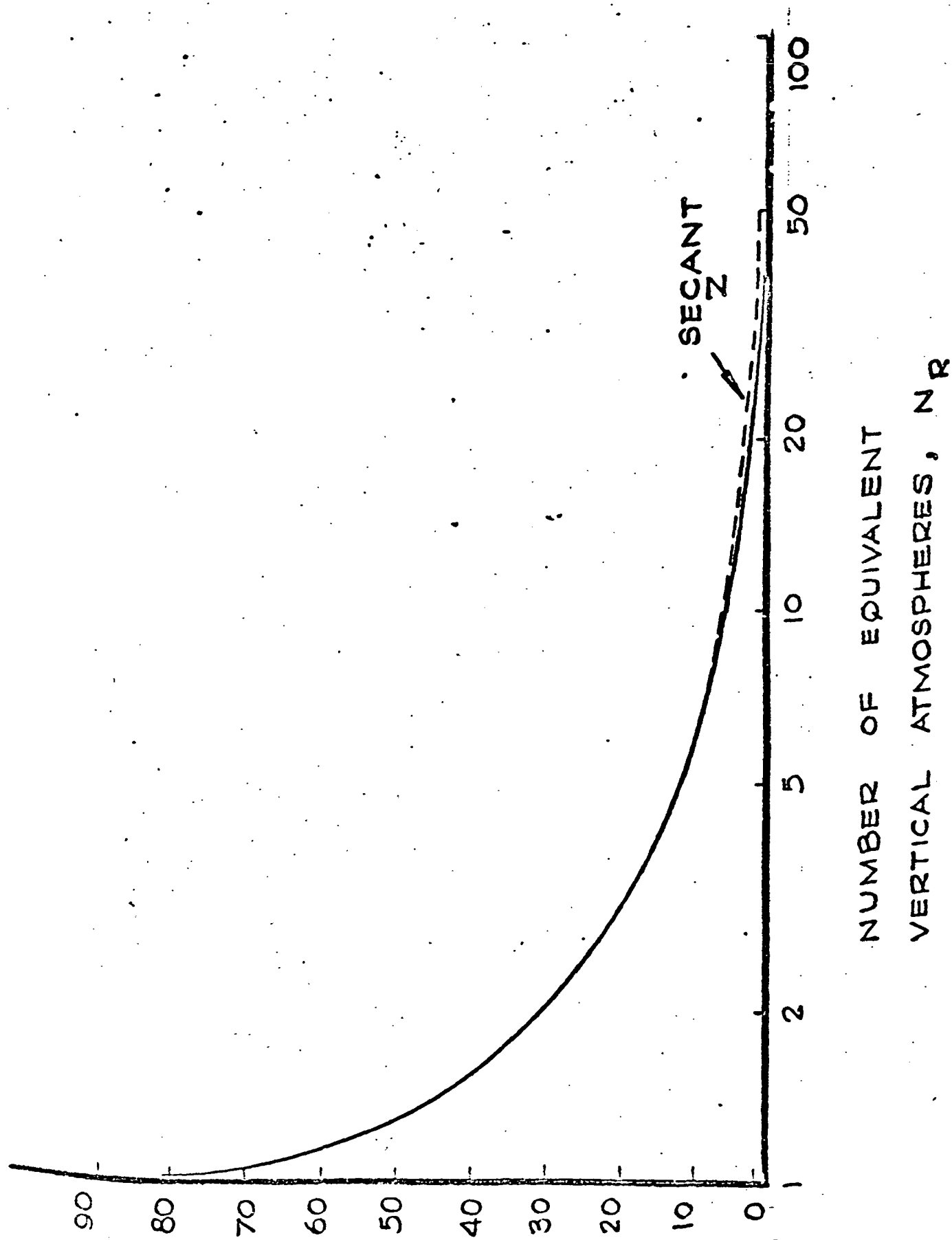
ELEVATION ANGLE IN DEGREES

Figure 2

NUMBER OF EQUIVALENT VERTICAL ATMOSPHERES, N_R

SECANT Z

106

-4-

3.0 OPTICAL SYSTEM FOR TELEVISION SENSOR.

The lens system to be utilized is a 61 cm dia, f/20 system with 36mm isocon system at the image plane. From this information the field of view may be determined.

Field of view:

$$FOV = Tan \frac{\theta}{2} = \frac{H}{2F}$$

where   H = width or height

F = focal length

$$\therefore \quad Tan\frac{\theta}{2} = \frac{1.0}{2(480)}$$

$$Tan \quad = 2.08 \times 10^{-3}$$

$$FOV \approx 7 \text{ arc minutes}$$
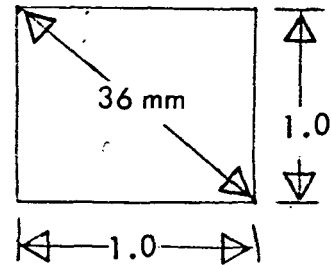
Figure 3

The 12m focal length lens is an f/20 system and has a clear aperture of 61 cm. The theoretical angular diameter discernable by an optical system is:

$$R = \frac{4.5 \text{ sec}}{d}$$

where   d = lens diameter

For the stated aperture the theoretical angular diameter is .16 sec.

Due to obscuration in the optics and atmospheric effects, the practical star image size ranges from 2 to 4 sec. Assuming a 3 sec stellar image, the size of the image at the focal plane would be.

$$3 \text{ sec } (\frac{25.4 \text{ mm}}{420 \text{ sec}}) \quad \text{or} \quad .18 \text{ mm}$$

A 36 mm Isocon sensor format is utilized with 1 sec equal to .06 mm on the face of the sensor. The horizontal or vertical field of view contains 420 sec, therefore

-5-

$$C = \frac{.00273 - .00267}{.00270}$$

$$= \frac{.00006}{.0027} = \frac{.6}{27} = 0.022$$

$$= 2.2\%$$

a TV system with 700 equivalent lines would have a resolution of 0.6 $\widehat{sec}$/TV
line. A 3 $\widehat{sec}$ star would then encompass 5 TV lines.

The illuminance of an image through the optical system is expressed
by:

$$E = \text{Gain} \times I$$

where Gain = gain of the optics is expressed as the area of the
optics divided by area of the image.

$$I = \text{illuminance from the star in question}$$

From the previous example, a 9^m star has an illuminance of 5.3×10^{-11} ft
candles, and the gain is equal to:

$$\text{Gain} = \frac{R^2 \text{ optics}}{R^2 \text{ image}}$$

where R optics = 304.8 mm

R image = .09 mm

$$\therefore \text{Gain} = \frac{9.3 \times 10^4 \text{ mm}^2}{8.1 \times 10^{-3} \text{ mm}^2}$$

$$= 1.15 \times 10^7$$

The illuminance of a 9^m star at the focal plane of the optics, with 10% available
light, is then:

$$E_{star} = \text{Gain} \times I \times 10\%$$

$$= 1.15 \times 10^7 \times 5.3 \times 10^{-11} \times .1$$

$$= 6.1 \times 10^{-5} \text{ ft candles}$$

From Figure 7 this signal level represents a S/N ratio of 5 at the sensor output.
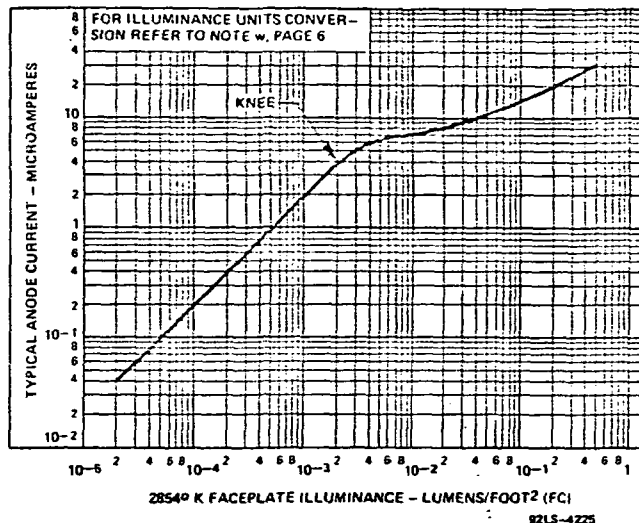
-6-
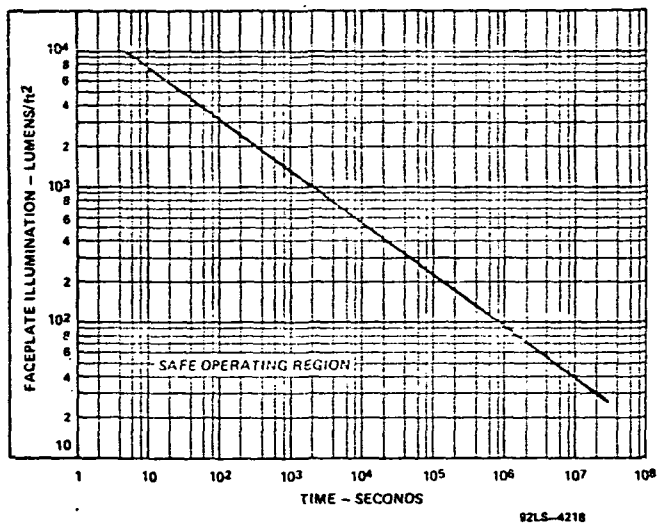
Figure 4 — Faceplate Exposure Limit

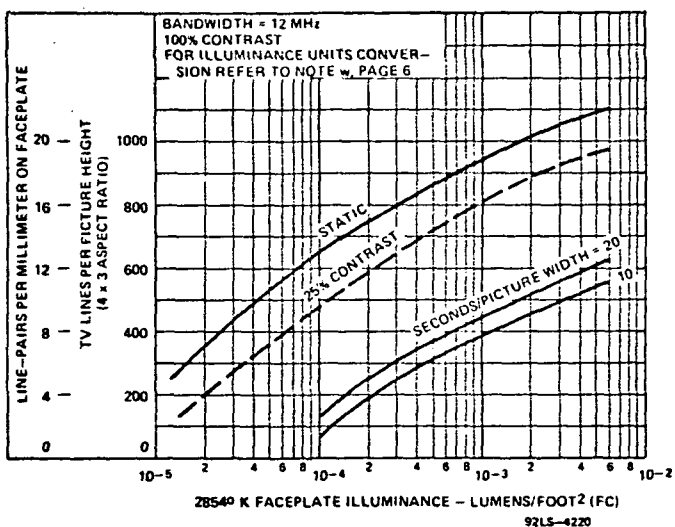Figure 6 — Typical Transfer Characteristic
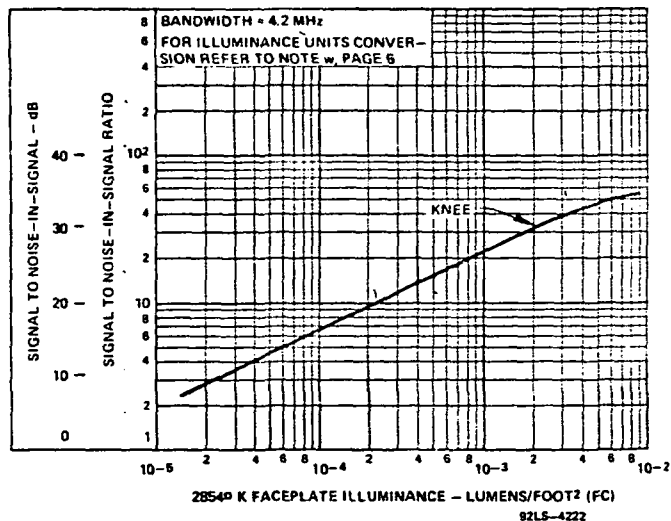

Figure 5 — Typical Dynamic Limiting Resolution

Figure 7 — Typical Signal to Noise-In-Signal Ratio As A Function of Faceplate Illuminance or Irradiance From Flux Levels Within A Given Scene. (Beam Adjustment Fixed At 2 x Knee Setting)

-7-

109

4.0   CENTROID TRACKER

From the optics analysis of the preceeding paragraphs, a signal to noise ratio of 5: 1 was derived.

The detection of an optical image in the presence of random fluctuations requires that the signal-to-noise ratio (S/N) be equal to or greater than a certain threshold value S/N. Studies of reconnaissance data shows that a signal-to-RMS noise ratio of two is needed to detect a target in the visible spectrum and that a signal to RMS noise ratio of three will produce a good television image. A signal to noise ratio of 4::1 represents a trackable target.

The centroid tracker error processing circuitry incorporates line to line digital correlation. This technique results in an effective S/N ratio increase of a factor of 2.5. Thus, the tracking S/N ratio will be greater than 10: 1.

The centroid tracker with the television sensor presents an excellent star tracking possibility. Section 5.0 will describe an image dissector approach to the problem and section 6.0 will discuss which technique would be the most suitable.

5.0 IMAGE DISSECTOR

5.1 Acquisition Mode

The feasibility of employing an image dissector as the primary target sensor is considered in the following section.

The acquisition arc is given as 2 minutes. The resultant FOV in terms of the maximum field diagonal is calculated as follows:

$$d = \theta f$$

where θ = instantaneous FOV in radians

f = optical focal length in centimeters

$$d_f = 5.82 \times 10^{-4} \text{ rad} \times 1.22 \times 10^{3} \text{ cm} = 7.1 \times 10^{-1} = .71 \text{ cm}$$

Dwell time, t, is given by

$$t = \alpha \left(\frac{A_a}{A_f} \right) T$$

where

A_a = Area of electronic aperture

A_f = Area of scan field

T = period of a single complete scan

α = Scan efficiency factor

$$A_f = \pi r_f^2 = \pi \left(\frac{d_f}{2} \right)^2 = 3.14 \times (3.55 \times 10^{-1})^2$$

$$= 3.14 (12.6 \times 10^{-2}) = 39.6 \times 10^{-2} \text{ cm}^2$$

$$d_a = 7.27 \times 10^{-5} \times 1.22 \times 10^{3} \text{ cm} = 8.87 \times 10^{-2} \text{ cm}$$

$$A_a = \pi r_a^2 = \pi \left(\frac{d_a}{2} \right)^2 = 3.14 (4.435 \times 10^{-2} \text{ cm})^2$$

-9-

$$A_a = 61.85 \times 10^{-4} cm^2$$

$$T = 1 \ sec$$

$\propto$ = .5 for a round aperature with appropriate overlap
and scan retrace time.

$$t = .5 \left(\frac{61.85 \times 10^{-4} cm^2}{39.6 \times 10^{-2} cm^2} \right) \ 1 \ sec$$

$$t = .5 \ (1.561 \times 10^{-2}) \ sec = 1.22 \times 10^{-4} \ sec$$

$$t = 7.8 \ ms$$

The number of electrons collected in the absence of a star target, N, is determined in the following way:

$$N = \in L \ A_a \ S_b \ t$$

where

$\in$ = photoelectron counting efficiency of dissector = .9

L = Sky background illumination level

A_a = Aperture Area = $61.85 \times 10^{-4} \ cm^2$

S_b = Quantum efficiency of photocathode at spectral content of background photons = $1.79 \times 10^{15} \dfrac{elec.}{lum-sec.}$

t = dwell time = 7.8 ms

-10-

$$G = \frac{(30.5)^2}{(1.8)^2} \times 1 = 28.7$$

$$L = 1\times10^{-7} \frac{l}{cm^2} \times 28.7 = 2.87\times10^{-6} \frac{l}{cm^2}$$

$$2.87\times10^{-6} \frac{l}{cm^2} \times \frac{930 cm^2}{ft^2} = 2.67\times10^{-3} \frac{l}{ft^2} = 2.67\times10^{-3} \text{ ft candles}$$

$$L' = 1 \times 10^{-3} \ \frac{\ell}{m^2} = 1 \times \frac{10^{-7}}{\ell/cm^2}$$

$$L = L'G$$

Where the optical gain of the telescope, G, is found as follows:

$$G = \frac{R^2 \ optics}{R^2 \ image} \ \tau_o$$

where τ_o = transmission efficiency = 10%

$$G = \frac{(30.5 \ cm)^2}{(.355 \ cm)^2} \times 10\% = \frac{930}{12.6 \times 10^{-2}} \times .1 = 7.38 \times 10^2$$

$$L = 1 \times 10^{-7} \ \frac{\ell}{cm^2} \times 7.38 \times 10^2 = 7.38 \times 10^{-5} \ \frac{\ell}{cm^2}$$

$$N = .9 \times 7.38 \times 10^{-5} \ \frac{\ell}{cm^2} \times 61.85 \times 10^{-4} cm^2 \times 1.79 \times \frac{10^{15} elec}{l-sec}$$

$$\times 7.8 \times 10^{-3} \ sec$$

$$N = 5.74 \times 10^6 \ electrons$$

$$\sqrt{N} = 2400$$

Star flux generated electrons, N_s, is calculated as follows:

$$N_s = \in W \, Q_s \, t$$

where $W = A_s E_s$

E_s = star flux = 6.1×10^{-5} ft candles

A_s = Star image area = $2.46 \times 10^{-4} cm^2$

$Q_s = 1.1 \times 10^{15} \ \frac{electrons}{lumen-sec}$

-11-

$$\sqrt{N} = 500$$

$$Ns = 1.95 \times \frac{77 \times 10^{-3}}{122 \times 10^{-6}} = 1230$$

$$\frac{N}{s} = 2.46$$

for 3mm equivalent aperture

$$E_s = 6.1 \times 10^{-5} \text{ ft cd} \times 10.764 \times 10^{-4} = 6.566 \times 10^{-8} \text{ phots } (\frac{\ell}{\text{cm}^2})$$

$$N_s = .9 \times 6.566 \times 10^{-8} \frac{\ell}{\text{cm}^2} \times 2.46 \times 10^{-4} \text{cm}^2 \times 1.1 \times \frac{10^{15} \text{elec}}{\text{l - sec}} \times 7.8 \times 10^{-3} \text{ sec.}$$

$$N_s = 125 \text{ electrons}$$

$$S/N = \frac{N_s}{\sqrt{N}} = \frac{125}{2400} = 0.052$$

In the acquisition mode, the FOV and image sizes and stellar magnetudes involved preclude successful utilization of an image dissector.

5.2   Track Mode

While the image dissector does not compare favorably with the vidicon tracker for single frame acquisition, the tracking mode, which allows greater image dwell time, has possibilities. Assuming that the satellite position rate of change is identical to earth rotation angular displacement, the rate of tracking must be at least $7.27 \times 10^{-5} \frac{\text{rad}}{\text{sec}}$. Using a circular electronic aperature, it can be shown that at least 13 samples/frame of data must be taken to ensure target acquisition. (Various scanning patterns such as a rosette, cross, circle, spiral or box may be used with variously resulting data rates.) This implies that the maximum dwell time to be achieved is $\frac{1}{13}$ or 77 milliseconds/ sample. Substitution of this dwell time into the equations of section 5.1 yields a S/N ratio of 1.3. This is an increase of some 25 times in S/N ratio. This ratio, however, is still unusable in this application.

5.3   Image Dissector Summary

The primary difficulty may be seen as the high ambient background starlight illumination level present. If this could be reduced, or a brighter source found for tracking, an adequate S/N ratio could be obtained. It should

-12-

be pointed out that the S/N ratio of the image dissector device itself, i.e., without the background illumination "noise" contribution is far higher.

In the acquisition mode, this may be computed as follows:

$$S/N \cong 1.2 \times 10^9 \sqrt{\frac{Ja}{f}}$$

where

$J = S E_s$

S = photocathode sensitivity = $150 \times 10^{-6} \frac{A}{lum}$

E_s = Star illuminance = 6.1×10^{-5} ft candles (lum/sq. ft.)

a = Electronic aperture = 6.65×10^{-6} sq. ft.

$f = \dfrac{1}{2\Delta t}$ = video bandwidth = 4.1×10^3 hz
(in acquisition mode)

$$S/N \cong 1.2 \times 10^9 \left(\frac{6.1 \times 10^{-5} \times 150 \times 10^{-6} \times 6.65 \times 10^{-6}}{4.1 \times 10^3} \right)^{\frac{1}{2}} = 4.62$$

This is the best case S/N ratio obtainable and indicates that acquisition could occur and tracking in the absence of background illumination would be entirely feasible. Greater magnitude tracking stars would yield the same result.

-13-

6.0 CONCLUSION

Section 4.0 described the S/N ratio required to track an optical image. The S/N ratio of 5:1 using the television approach represents a tracking capability far superior to the image dissector with a S/N of 0.1635.

It is therefore our conclusion that the system best suited for tracking a $+9^m$ star is the Image Isocon Sensor and a centroid TV tracker.

-14-

APPENDIX E

AUTOMATIC TRACKING CONCEPT FOR NASA MOBILE SATELLITE

PHOTOMETRIC OBSERVATORY

AUTOMATIC TRACKING CONCEPT FOR NASA MOBILE SATELLITE
PHOTOMETRIC OBSERVATORY

AUTOMATIC TRACKING is a firm requirement when it is desired to maximize the data obtained from satellite observation opportunities. A system is proposed which can be implimented in the observatory which takes advantage of existing capability and which can be implimented without extensive modification. The components of the system are:

1. A stable quadrature oscillator which permits the telescope to be conically scanned where the field of the telescope is pointed slightly off center from the target and rotated about the boresight, keeping the angle offset constant.

2. Quadrature resolver and summer amplifiers which detect when the target is off center from the boresight and which generate control signals to the declination and polar summer amplifiers providing the required control for automatic tracking.

3. A modified optical assembly in the instrumentation lead which uses the reflected light from the interfaces filters which select the ozone spectrum or the comparison spectrum. A field stop smaller than that used for signal detection is used for tracking to prevent signal dropout during track. This may be accomplished at the impage plane in a relay lens assembly used to transmit light out to the tracking detector.

It is anticipated that these modifications meet the objective of minimum modification to the observatory electro optical system.

Interference
Filter Designed
for 45° Incidence

Collected
Light

Narrow Band
Light Detector
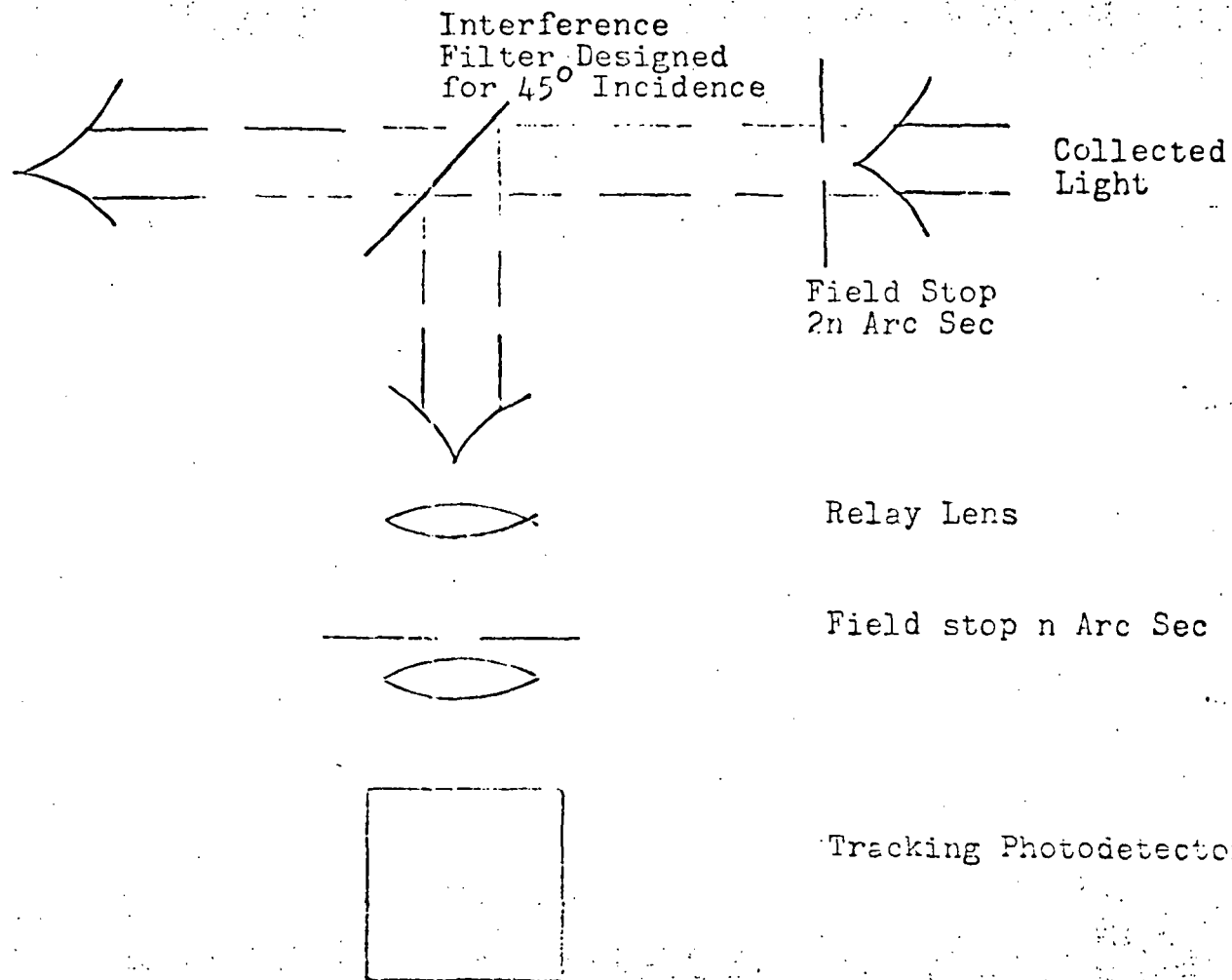
Field Stop
2n Arc Sec

Relay Lens

Field stop n Arc Sec

Tracking Photodetector

SK 9673-1
Optical Modification
for
Automatic Tracking

Quadrature
Oscillator

Declination Control
Summing Amplifier

SIN wt

SIN (wt + 90°)

Comparator

Polar Control Summing
Amplifier

Tracking
Photodetector

Electrometer

Gate

SK 9673-2
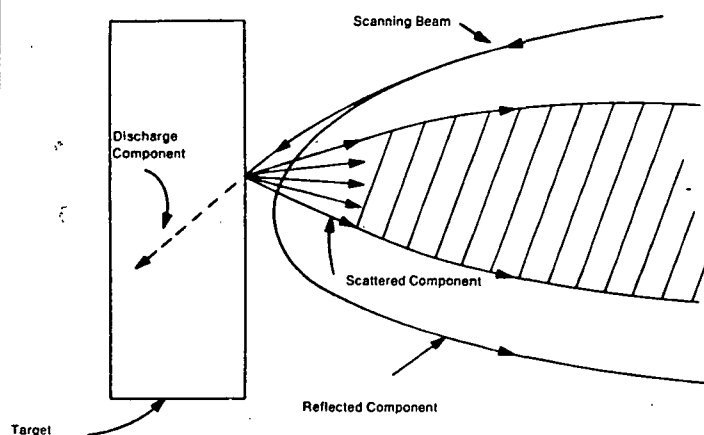Schematic
Electronic Tracker
Satellite Photometric Observatory

120

APPENDIX F
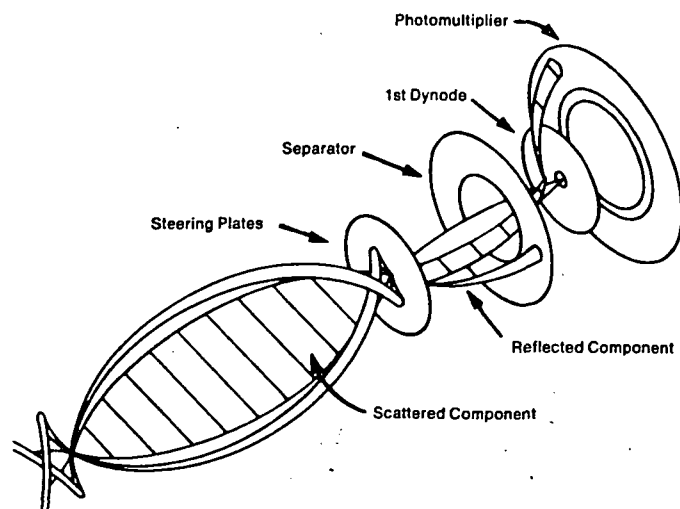

IMAGE ISOCON CHARACTERISTICS
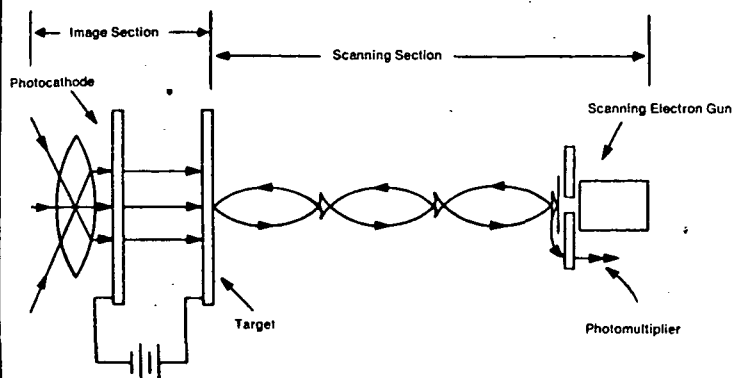
GENERALIZED SCHEMATIC OF ORTHICON/ISOCON TUBES

RETURN BEAM COMPONENTS

ISOCON BEAM SEPARATION

INTRODUCTION

For certain low light level applications, existing Orthicon imaging systems are limited by the amount of noise present in the output signal, particularly in the black portions of the picture. Although Isocon readout greatly reduces this and other problems characteristic of using the Orthicon in such applications, only recently have systems been perfected that offer comparable stability, ease of operation, and set up. Specifically, MTI's Image Isocon Camera exhibits significant improvements in sensitivity, noise, and dynamic range while retaining the packaging and operational advantages of the Orthicon.

The imaging technique used in both systems is similar; photo-electrons from the photocathode positively charge the target which is in turn discharged from the reverse side by the scanning electron gun. It is in the scanning method and processing of the output signal that the two differ.

SCANNING TECHNIQUES

Orthicon scanning produces a negatively modulated signal. The scanning beam lands only on positively charged portions of the target (picture whites), and is totally reflected from the blacks. Output current is therefore a maximum for picture blacks and a minimum for the whites. Since the maximum current represents a totally reflected portion of the input beam, it retains the shot noise inherent in that beam. Further, at low light levels the noise in the beam current needed to discharge picture highlights will eliminate much of the detail in the darker areas.

There are actually two return beams in both the Orthicon and Isocon modes; the reflected beam containing the high shot noise, and a scattered beam which is directly proportional to that part of the original beam actually landing at the target and carries only picture information. The Isocon separates the two and discards the specularly reflected component allowing only the scattered component to enter the electron multiplier from which a video signal is obtained.

ISOCON BEAM SEPARATION

In the Isocon, the scanning beam is emitted from an aperture in the first dynode, passes through an aperture in the separator and between steering plates. These introduce a transverse component of velocity causing the beam as a whole to spiral in the magnetic field and approach the target at a low angle of incidence. The beam, on reaching the target, becomes split into three components.

SPECULARLY REFLECTED COMPONENT — That part of the beam specularly reflected in front of the target returns on a helix of the same pitch as the incident beam and passes between the steering plates. Here it

gains further transverse velocity, increasing the diameter of the helix which then becomes sufficiently large for it to be intercepted by the edge of the separator aperture and discarded.

DISCHARGE COMPONENT—Some of the beam lands on the target and neutralizes positive charge built up by exposure to light.

SCATTERED COMPONENT—Positive charges on the target, corresponding to the incident image, cause part of the beam to be scattered. The Isocon retains this beam since its magnitude is proportional to the positive potential on the target at any given point in the picture and it is free from shot noise. The helical motion of the incident beam is not transferred to this component, which returns towards the multiplier and passes between the steering plates. Here a transverse component of velocity is imparted to it causing it to spiral in a helix tight enough to pass through the aperture in the separator and strike the first dynode. The output signal is then obtained from the anode of the multiplier.

The Isocon Camera therefore produces a positively modulated signal; return beam current is small for small signals and the signal-to-noise ratio is maintained to very low light levels. As a consequence, beam current may be set to discharge highlights without materially affecting low light performance. The camera can therefore be operated over a very wide dynamic range, yet the beam setting remains non-critical.

DESIGN FEATURES

The Isocon tube target is designed for a low storage capacity so that even with very low photocathode currents, it will give an appreciable voltage swing at the target, allowing good landing by the readout beam and minimizing lag. The target is made from E.E.V.'s Electronically Conducting Glass which has a resistivity selected to permit tube operation in a storage mode with an interrupted readout , or in a continuous mode without "after images" becoming apparent on a moving scene. Two additional multiplier stages are incorporated in the tube to make up for the inherent lower current density of the Isocon scan compared with Orthicon.

With static illumination at very low light levels, additional sensitivity may be realized by integrating charge build-up over longer periods of time. In the integrating mode the scanning beam is cut off and the target charge accumulated. The amount of integration time is determined digitally by counting vertical sync pulses and can vary from one to several frames. Also, for such low light levels, a tube with a fiber-optic face plate is available for coupling to an image intensifier.
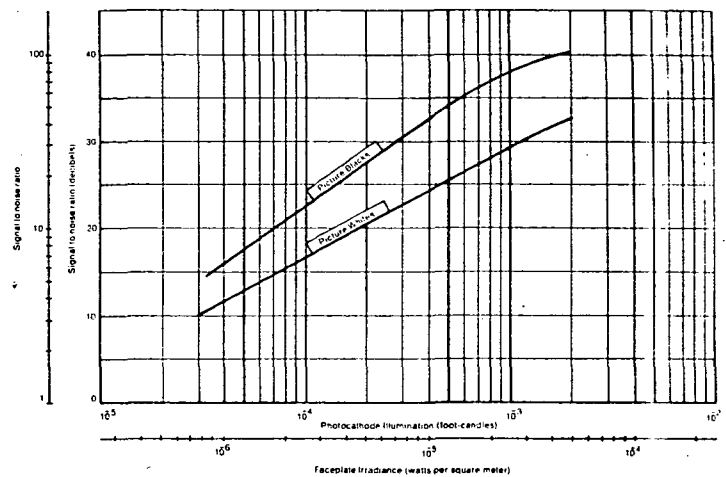
SIGNAL-TO-NOISE RATIO
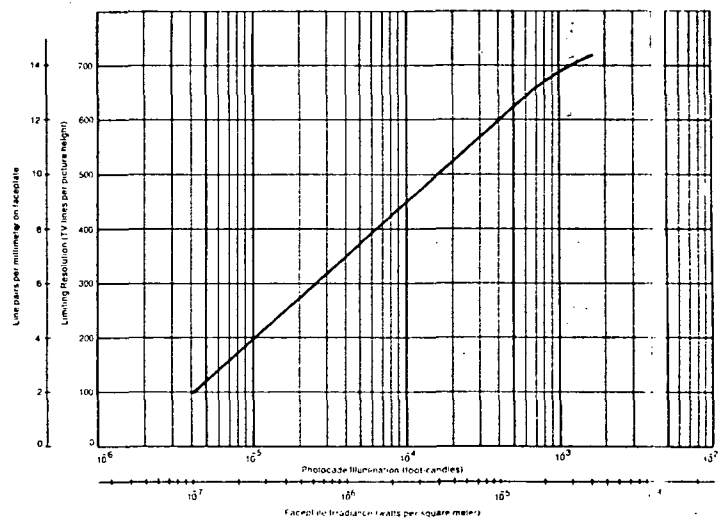
TYPICAL LIMITING RESOLUTION
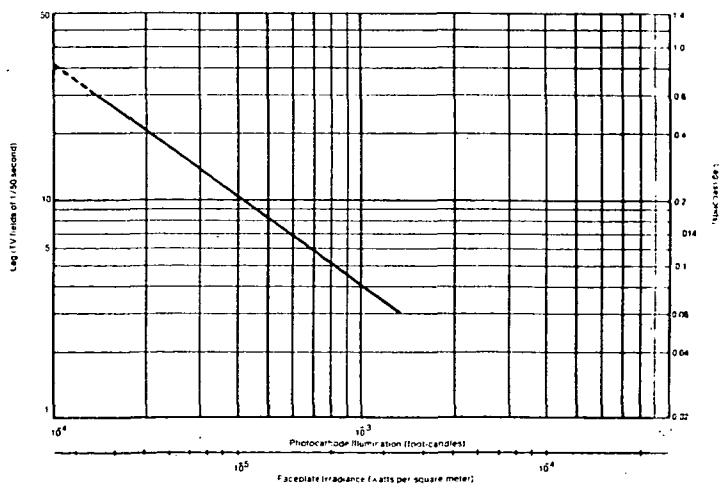
LAG (TIME TO REACH 5% OF INITIAL LEVEL)

ELECTRICAL

HORIZONTAL RESOLUTION:
700 lines @ 10^{-3}f.c.

SENSITIVITY:
Useable picture at 10^{-6}f.c. photocathode illumination

SIGNAL-TO-NOISE RATIO:
42db in blacks, 33db in whites

DYNAMIC RANGE:
300 typical

BANDWIDTH:
10MHz (20MHz available)

GRAY SCALE:
Will display 10 shades of gray

HORIZONTAL SCANNING RATE:
525 line (875, 1023 available)

VERTICAL SCANNING RATE:
60Hz, 2:1 interlace; sequential option

SYNCHRONIZATION:
Internally generated industrial sync
(EIA external available)

LINEARITY:
2% or better over entire image area

VIDEO OUTPUT:
Black negative, 1.0V at 75 ohms

INPUT POWER:
107-127 VAC, 60 Hz, 185 watts, plus 7 watts for camera cooling

REGULATION:
±1% on all power supplies

OPERATING TEMPERATURE:
0 to 50°C

IMAGE TUBE:
EEV P880 Image Isocon w/s-20 photocathode (fiber-optic faceplate and other photocathode surfaces available)

WARRANTY (Isocon Tubes):
180 hrs. Full
1800 hrs. Pro-Rated

MECHANICAL

SIZE:
Camera: 7½ x 23⁵⁄₁₆ x 5½
Camera Control Unit: 17¾ x 11 x 7 Cabinet Style
19 x 7 x 9¼ Rack Style

FINISH:
Camera: Case—Black anodized
Camera Control Unit: Front Panel—Gold anodized.
Cover—Dark brown baked enamel

WEIGHT:
Camera: 25 lbs.
Camera Control Unit: 28 lbs.

MOUNTING:
Camera: (2) ¼" x 20, (1) ½" x 20 threaded tripod mounts
Camera Control Unit: 19" rack or cabinet style

CONTROL CABLE CONNECTOR:
Camera: MS2102A36-15P
Camera Control Unit: MS3102A36-15S

VIDEO OUTPUT CONNECTOR:
BNC

SYNC CONNECTOR:
BNC

m ti ®

VISUAL EDUCOM INCORPORATED
4333 S. Ohio St., Michigan City, Ind. 46360
Telephone: 219 879-8311

124

REFERENCES

1. "Inadvertent Climate Modification," MIT Press, 1971.

2. Nicolet, M.: "Nitrogen Oxides in the Chemosphere;"
J. Geophysical Research, Volume 70, pages 679-689, 1965

3. Bates, D. R., and Nicolet, M.: "Photochemistry of Atmospheric
Water Vapor;" J. Geophysical Research, Volume 55, pages 301-327,
1950.

4. Chapman, S.: "Photochemistry of Atmospheric Oxygen;" Reprots of
Progress in Physics, Volume 9, page 92, 1973.

5. Crutzen, P. J.: "The Influence of Nitrogen Oxides on the
Atmospheric Ozone Content;" Quarterly Journal of the Royal
Meteorological Society, Volume 96, pages 320-325, 1970.

6. Johnston, H.: "Reduction of Stratospheric Ozone by Nitrogen
Oxide Catalysts from SST Exhaust;" Science, Volume 173,
pages 517-522, 1971.

7. Langley, K. F. and McGrath, W. D.: "The Ultra-Violet Photolysis
of Ozone in the Presence of Water Vapor;" Planetary and Space
Science, Volume 19, pages 413-416, 1971.

8. Valley, Shea L.: "Handbook of Geophysics and Space Environments;"
McGraw Hill Book Company, Inc., New York, New York.

9. Mateer, C. L., and Godson, W. L.: "The Vertical Distribution of
Atmospheric Ozone Over Canadian Stations from Unkehr Observations;"
Quarterly J. Royal Meteorological Society; Volume 86, pages 512-518,
1960.

10. Gotz, F. W. P; Meetham, A. R., and Dobson, G. M. B.: "The Vertical
Distribution of Ozone in the Atmosphere;" Proc. Royal Society,
Volume A 145, pages 416-446, 1934.

11. Regener, V.: "Vertical Distribution of Atmospheric Ozone;"
Nature, Volume 167, pages 276-277, 1951.

12. Normand, C.: "Some Recent Work on Ozone;" Quarterly J. Royal
Meteorological Society, Volume 77, pages 474-478, 1951.

13. Venkateswaran, S. N.; Moore, J. G. and Arlen, A. J.: "Determination
of the Vertical Distribution of Ozone by Satellite Photometry;"
J. Geophysical Research, Volume 66, No. 6, page 1751, June 1961.

14. Moore, J. G., and Elliott, S. D.: "A Multicolor Photoelectric
Photometer for Artificial Satellite Observation;" Applied Optics,
Volume 2 No. 6, page 625, June 1963.

15. Link, F.: "Space Research II, North Holland Publishing Company,
Amsterdam, 1961.

125

16. Fesenkov, V. G.: "A Satellite Technique for Sounding the Optical Properties of the Atmosphere;" Soviet Astronomy, Volume 11, No. 1, page 1, January-February 1967.

17. Preski, R. J.: "Determination of Ozone Distribution by Photometric Observations of Artificial Satellites in Eclipse;" Goodyear Aerospace Corporation, SP-6809, January 3, 1969.

18. Lee, R. B., III, and McDougal, D. S.: "Vertical Ozone Profiles from Observations of Eclipsing Satellites;" NASA Langley Research Center, Cospar Papre No. e.28, June 1973.

19. Vigroux, E.: Ann. Physics, 1953, Volume 8, pages 709-762: "Contribution a 1 etude Experimentale de 1' Absorption de 1' Ozone."

20. Taba, H.: "Ozone Observations and Their Meteorological Applications;" WMO Technical Note No. 36, 1961.

21. Mateer, C. L.: "On the Information Content of Umkehr Observations;" J. Atmospheric Sciences, Volume 22, pages 370-381, 1965.

22. Walton, G. F.: "The Calculation of the Vertical Distribution of Ozone by the Gotz Umkehr-Effect;" Ann IGY Volume 5, pages 9-27, 1957.

23. Craig, R. A.; DeLuise, J. J. and Stuetzer, I.: "Comparison of Chemiluminescent and Umkehr Observations of Ozone;" J. Geophysical Research, Volume 72, No. 6, pages 1667-1671, 1967.

24. Mateer, C. L., and Dutsch, H. W.: "Uniform Evaluation of Umkehr Observations from the World Ozone Network, 1, Proposed Standard Umkehr Evaluation Technique;" NCAR, Boulder, Colorado, 1964.

25. Johnson, H. L.; Mitchell, R. I., and Latham, A. S.: "Eight-Color Narrow-Band Photometry of 985 Bright Stars;" Communications of the Lunar and Planetary Laboratory, No. 92, University of Arizona Press, 1967.

26. Mitchell, R. T. and Johnson, H. L.: "Thirteen-Color Narrow-Band Photometry of One Thousand Bright Stars;" Communications of the Lunar and Planetary Laboratory, No. 132, University of Arizona Press, 1969.

27. ANON: "Operation and Maintenance Instructions for NASA Satellite Photometric Observatory;" Prepared for NASA-LRC by Goodyear Aerospace Corporation, GER-12896, Revision A, April 1, 1968.

28. Duardo, J. A., et al: "Study to Develop a Technique for Measurement of High Altitude Ozone Parameters, N-69-19889, November 12, 1968.

29. Hiltner, W. A.: "Astronomical Techniques;" University of Chicago Press, Chicago, Illinois, 1962.